Lille University Of Technology, Lille, France
CRISTAL - Center for Research in Computer Science, Signal and Automatic, Lille, France
Doctoral school Sciences Pour l'Ingénieur

PhD thesis

Passivity-based modeling and power routing of a multi-source power cell for hydrogen production

Submitted in partial fulfillment of
the requirements for the award of the degree of

Doctor of Philosophy in Automatics and Industrial Computer science

Submitted and defended by

Solène Houria CHAABNA

On 30^{th} November 2020

Under the supervision of:

Associate professor: Jean-Yves DIEULOT

Referees:

- Dominique SAUTER, Professor at Université de Lorraine
- Kamal MEDJAHER, Professor at Ecole Nationale d'Ingénieur de Tarbes

Examiners:

- Pierre-Jean BARRE, Professor at Université de Nice Sophia Antipolis, **Jury president**
- Frédéric COLAS, Research engineer at Arts et Métiers, ParisTech
- Anne-Lise GEHIN, Associate Professor at Université de Lille

Université de Lille, France
CRISTAL - Centre de Recherche en Informatique, Signal, et Automatique de Lille, France
Doctoral school Sciences Pour l'Ingénieur

Thèse de doctorat

Modélisation et contrôle dynamique d'échange passif d'une cellule de puissance multi-sources pour la productiond'hydrogène

Soumise dans le cadre des exigences
pour l'obtention du grade de :

Docteur en génie informatique, automatique et traitement du signal

Soumise et présentée par

Solène Houria CHAABNA

Le 30 Novembre 2020

Sous la direction de :

Maître de conférence HDR : Jean-Yves DIEULOT

Rapporteurs :

- Dominique SAUTER, Professeur à l'Université de Lorraine
- Kamal MEDJAHER, Professeur à l'Ecole Nationale d'Ingénieur de Tarbes

Examinateurs:

- Pierre-Jean BARRE, Professeur à l'Université de Nice Sophia Antipolis, **Président du jury**
- Frédéric COLAS, Ingénieur de recherche aux Arts et Métiers, ParisTech
- Anne-Lise GEHIN, Maître de conférence à l'Université de Lille

Acknowledgments

Ce manuscrit est le résultat de mes travaux de recherche effectués dans le cadre de ma thèse de doctorat, dans l'équipe Méthodes & Outils pour la Conception Intégrée des Systèmes (MOCIS), au Centre de Recherche en Informatique, Signal et Automatique de Lille (CRIStAL).

A cette occasion, je tiens à remercier, mon directeur de thèse, Monsieur Jean-Yves DIEULOT, qui m'a accueillie au sein de son équipe de recherche et m'a offert la possibilité d'évoluer. Je le remercie pour ses encouragements, sa patience et sa disponibilité durant toutes ces années, sans oublier ses valeurs humaines et sa bonne humeur qui font de chaque rencontre des moments agréables.

Je remercie particulièrement, Monsieur Pierre-Jean BARRE, Directeur de l'Institut Méditerranéen du Risque, de l'Environnement et du Développement Durable et Professeur à l'université Nice Sophia Antipolis, pour avoir accepté de faire partie de mon jury de thèse et de m'avoir fait l'honneur de le présider.

J'adresse toute ma reconnaissance à Monsieur Kamal MEDJAHER, Professeur à l'Ecole Nationale d'Ingénieurs de Tarbes et à Monsieur Dominique SAUTER, Professeur à l'Université de Lorraine, pour avoir accepté d'être rapporteur sur mes travaux. Je les remercie vivement de leur lecture approfondie et de leurs remarques enrichissantes et constructives.

J'exprime ma profonde gratitude à Madame Anne-lise GEHIN, Maître de Conférences à l'Université de Lille et à Monsieur Fréderic COLAS, Ingénieur de recherche aux Arts et Métiers, ParisTech, pour leur lecture minutieuse et leurs remarques pertinentes.

J'ai été très honorée de présenter mes travaux de thèse devant un jury de cette envergure. Je vous remercie infiniment.

Je remercie également mes collègues au laboratoire : Sumit, Boussad, Man-

arsh, Riad, Ismail, IMENE, Fatiha, Adel, Steeve, Mahdi ainsi que mes amis de France et d'Algérie : Ryma, Lyes, Tony, Mahieddine, Maya, Ouali, Nadia, pour l'ambiance conviviale qu'ils ont su entretenir et les bons et joyeux moments passés ensemble.

Je remercie toute ma famille, ma soeur Zahra, grâce à qui j'ai été scolarisée à l'âge de 5 ans, ma sœur Ounissa qui m'a inscrite au Handball et ma soeur Kamir qui m'a appris à bouquiner et à écouter du Matoub, mon frère Boudjemaa qui a toujours cru en mes capacités et m'a encouragée à entreprendre des études doctorales et à voyager pour poursuivre mes études et réaliser mes rêves, ma belle-sœur Kahina et mon beau-frère Fares qui m'ont toujours soutenue aussi et finalement, je remercie ma mère Hayat et ma tante Fadila pour leur encadrement et leurs sacrifices pour nous voir réussir.

Enfin, je dédie ce travail à la mémoire de mon défunt père Mohand-chérif, à ma famille et à toutes les personnes qui m'ont soutenue de près ou de loin.

Solène Houria CHAABNA

Université de Lille, France

Laboratoire CRIStAL

30 Novembre 2020

Abstract

Green hydrogen is emerging as a powerful solution for the storage of surplus electricity which is generated through renewable energy sources. However, a green hydrogen power cell involves multi-physics phenomena as electrical, fluidic, thermal, etc. and the representation of dynamical power flows therein is quite complex. Furthermore, the power exchange between the different components of the cell (Fuel cell, Electrolyzer, storage units, renewable sources) needs to be thought in terms of global performance while taking care of the energy reserves.

This thesis proposes a Bond Graph derived port-Hamiltonian representation of all the components of a green hydrogen power cell. From this representation, it is possible to design passivity-based control algorithms. The notion of passivity margin is introduced to account for the robustness with respect to modeling uncertainties or known disturbances. For each component, the excess or shortage of power feeds an Energy Tank, which behaves as a virtual storage unit. Hence, the set of Energy Tanks is an image of the power reserves in the power cell. Instead of using conventional power routing between the components, we propose to manage power flows between the Energy Tanks, which allows to control not only the power intensity, but also the level of energy within these tanks. Hence, the methodology enables to control both power and energy at the same time, paving the way to Operating Mode Management triggered by energy levels. An application is given on a platform including a fuel cell, renewable energy sources, and a conventional storage unit.

Keywords: Port-Hamiltonian, passivity margins, Bond graph, Energy Tanks, Hybrid Renewable Energy Systems, Operating mode management, Energy management, power routing.

Résumé

L'hydrogène propre est une solution d'avenir pour le stockage d'électricité renouvelable. Cependant, une cellule multi-sources pour la production d'hydrogène présente de multiples phénomènes physiques, par exemple électriques, électrochimiques, thermiques, fluidiques, etc. et la représentation des flux d'énergie y est très complexe. De plus, les échanges de puissance entre les composants de la cellule (sources renouvelables, pile à combustible, électrolyseurs, batteries) doivent être évalués de manière globale tout en préservant les réserves de puissance de chacun de ces composants.

Cette thèse propose une représentation d'état port-Hamiltonienne, dérivée d'un bond-graph, de chacun des composants d'une cellule de puissance pour la production d'hydrogène. A partir de cette représentation et des propriétés de passivité, il est possible de concevoir des algorithmes de commande. La notion de marge de passivité est introduite pour évaluer la robustesse par rapport aux incertitudes paramétriques ou aux perturbations connues. Pour chaque composant, la variation de puissance alimente un réservoir virtuel d'énergie. L'ensemble des réservoirs constitue ainsi une image des réserves de puissance du système. Au lieu d'utiliser un échange direct de puissance entre les composants et le réseau, nous proposons de gérer les flux de puissance entre les réservoirs, ce qui permet également de contrôler leurs niveaux d'énergie. La méthodologie permet de superviser en même temps la puissance et l'énergie, ce qui conduira à terme à gérer les modes opératoires de la cellule à partir des niveaux d'énergie. La méthodologie est appliquée à une plate-forme comportant des sources renouvelables, une pile à combustible et une batterie conventionnelle.

Mots-clés: systèmes hybrides avec énergies renouvelables, systèmes port-Hamiltoniens, hydrogène, échange de puissance, réservoirs d'énergie, marge de passivité

Nomenclature

a, a_0, b Tafel constants (V/K), V, (V/K)

E_0 Reference potential at standard operating conditions (V)

I Stack current (A)

I_L Limiting current (A)

P_{H_2} Partial pressure of hydrogen (Bar)

P_{O_2} Partial pressure of oxygen (Bar)

u_{Fc} Output voltage of the PE fuel cell (V)

V_{Act} Activation voltage loss (V)

V_{Conc} Concentration voltage loss (V)

BG Bond Graph

CJV Controlled Junctions Vector

DES Discrete Event System

EDHBG Event-Driven Hybrid Bond Graph

EL Electrolyser

ELZ Electrolyzer

FC Fuel Cell

HA Hybrid Automaton

HBG Hybrid Bond Graph

HDS Hybrid Dynamical Systems

HPN Hybrid Petri Net

HRES Hybrid Renewable Energy Systems

MPN Mixed Petri Net

MPPT Maximum Power Point Tracking

OM Operating Mode

OMM Operating Mode Management

PH Port-Hamiltonian

PMG Permanent Magnet Generator

PV Solar Photovoltaic Panels

SSE State-Space Equations

STC Standard Test Conditions

UG Utility Grid

VPP Virtual Power Plant

WT Wind Turbine

Contents

List of Figures

List of Tables

General introduction

Thesis framework

This PhD thesis has been conducted under the supervision of the Associate Professor Jean-Yves DIEULOT in the MOCIS (Méthodes et Outils Pour la Conception Intégrée des Systèmes) team of the CI2S (Conception Intégrée de Systèmes Sûrs) group, within CRIStAL (Centre de Recherche en Informatique, Signal et Automatique de Lille) CNRS (centre National de la Recherche Scientifique) UMR (Unité Mixte de Recherche) 9189, laboratory of the University of Lille, as part of the team's research activities related to hydrogen.

The general theme of the MOCIS team is the integrated design of multi-physical energy systems, which consists of simultaneously and coherently addressing the different aspects of the design of automated systems such as modeling, analysis, control and monitoring as well that the computerization of these procedures. The methodology is based on two complementary approaches, namely, the bond graph methodology for its capacities to model with a unified and energetic tool the systems implementing several fields of physics and the Systems of Systems concept for its ability to model complex systems showing several hierarchical levels.

The MOCIS team in involved in several Hydrogen-based engineering projects and collaborations. First, the thesis of Pierre OLIVIER in 2016 on "Modeling and analysis of the dynamic behavior of a PEM electrolysis system subjected to intermittent stresses: Bond Graph approach", prepared in collaboration between the CEA research center in Grenoble and the CRIStAL laboratory, under the supervision of Professor Belkacem OULD-BOUAMAMA and Cyril BOURASSEAU, respectively. Then, the ANR PROPICE project which included the PhD thesis of Mathieu BRESSEL, under the theme "Graphic modeling for the robust prognosis of a proton exchange membrane fuel cell." in 2016, under the supervision of the Professor Daniel HISSEL from the University of Bourgogne Franche-Comté and the Professor Belkacem OULD-BOUAMAMA from the University of Lille. Finally, the PhD thesis of Ibrahim ABDALLAH in 2017 entitled "Event-Driven Hybrid Bond Graph . Application: Hybrid renewable energy system for

hydrogen production" under the supervision of the Professor Belkacem OULD-BOUAMAMA and Doctor Anne-Lise GEHIN supported by the University of Lille, the school Polytech Lille and the region Hauts-De-France under the project MODIS-H2 (Modélisation et diagnostic des systèmes multi-sources pour la production et le stockage d'hydrogène).

Since 2018, the MOCIS team is part of the E2C (Electrons to high value Chemical products) Interreg 2 Seas European project under the responsibility of the Professor Belkacem OULD-BOUAMAMA. The overall objective of the project is to stimulate investment and implementation of Power-to-X technologies by developing innovative direct and indirect conversion processes for the chemical industry towards higher TRL's, while making use of renewable electricity and lowering the carbon footprint. In the framework of this project a PhD thesis research work is ongoing at the MOCIS group by the PhD student Sumit SOOD supervised by the Professor Belkacem OULD-BOUAMAMA, Associate Professor Jean-Yves DIEULOT and Dr. Mathieu BRESSEL.

General context

Wind turbine and solar energies are the most abundant renewable energy sources on earth. The optimal exploitation of these resources for electrical energy production and distribution can ensure permanent availability of power all over the world and replace the other polluting sources.

Today, one of the major elements which prevents the generalization of these means of production comes from their intermittent production over the day and the year and their dependence on the weather conditions. To improve the efficiency of these sources, two choices are possible, namely, the use of storage units and the combination of these sources for simultaneous operation.

There are several storage units (batteries, capacitors, ultra-capacitors) which are classified according to their energy and power capacities. Indeed, the energy capacity represents the quantity of energy that a system is able to store. The most efficient means of storage so far is the batteries. The power capacity represents the speed at which the stored energy can be supplied by the storage system, for which the capacitors display the best performance. The choice of a storage mode depends on the using context. The batteries are the most widespread to support production systems with renewable energies. However, this kind of power storage remains limited and expensive, its long-term yield is average, because the

chemical aspect of the storage induces energy losses.

One of the promising alternatives to replace batteries is the storage under the form of hydrogen. This new mode of energy storage is said to be clean when produced by clean power, because the process of production, storage and transformation of energy is respectful of the environment and the waste is only water and oxygen, unlike CO2 emissions, in the other cases of energy storage and production. Then, hydrogen can be used in different way, namely, to generate electricity, generate mechanical work or used in several chemical applications.

Hydrogen production is achieved by water electrolysis in an electrolyser, and the reverse generation of electricity using hydrogen is done thanks to a fuel cell. These process are slow but flexible and cleaner than batteries. In this thesis research work, both batteries and hydrogen storage means are used with multi-source renewable energy systems to improve the efficiency and the reliability of the system.

Such a combination of storage and production units is called a Hybrid Renewable Energy System (HRES), that is a system for producing electrical energy from several renewable energy sources. Means for storing and recovering electrical energy are included. The operation of this type of system induces multiple operating modes (OM) which correspond for example to the connection and disconnection of a component. For example, a fuel cell and an electrolyzer will not share common operating modes since it is not efficient to produce electrical energy from the fuel cell and to store hydrogen using the electrolyser at the same time.
In a HRES, the power routing is an important step which consists of delivering the necessary power rate for all the components. The power routing strategy makes it possible to manage the power flows from renewable sources to the various storage and processing units to ensure the power balance but also a global efficiency of the system. The presence of different operating modes implies the development of different power management strategies.

Problematic

The major questions that we have tried to answer in this research work concern the routing of power in a power cell based on intermittent renewable sources with a control of the energy reserves. Our problem is thus a matter of modeling and power routing.

Hydrogen-based power cell modeling

The challenging problem when dealing with hydrogen-based systems is the multi-physics aspect. In addition to mechanics e.g. (wind turbine), power electronics, we end up with thermodynamics, electro-chemistry and fluid mechanics (fuel cell, electrolyzer). These systems become complex and not easy to interconnect, while their modeling needs a deep physical knowledge of the different domains.

The different modeling tools of HRES use multi-model or/and heterogeneous graphical-analytical approaches, namely, Hybrid Automaton [9, 10], Mixed Petri Net (MPN), Hybrid Petri Net (HPN) [11, 12] or Hybrid Bond Graph (HBG) [13], where the discrete and continuous behaviors of the system are described. However, the complexity of the systems makes it difficult to obtain an accurate representation and often the models do not really reflect the real behavior of the systems in addition to the simulations which are time consuming.

The main issue is to obtain models that are both able to represent power flows in a HRES and tailored to control design. For example, a Hybrid Bond Graph is a tool that is able to represent multi-physics systems in a graphical way which captures the power flows between sub-components through ports called bonds. They are able to study causality, that is the way that variables influence each other. HBGs offer a powerful framework for power exchange between subsystems but do not manage explicitly the level of energy. The energy and power efficiency and the application of other model-based tasks (control, diagnosis, sizing ...etc) for HRES is closely connected to the accuracy and reliability of the dynamical models describing the systems.

A generic way to use state space representations based on energetic considerations is to use the concept of passivity. Passive systems are physical systems that do not generate energy and whose variation in internal energy is less than the external power received, thus, passivity is an energetic method of ensuring the stability of a system. The port-Hamiltonian formalism is a good candidate for the modeling and control of a HRES. A port-Hamiltonian model is a passive state space representation which stems directly from a multi-physics Bond-Graph. While it is complicated to capture the causality with a PH representation, it allows to design in a generic fashion control structures by shaping the global energy of the system. In this framework, the Duindam Stramiglioli energy router enables to control the direction and magnitude of the energy flow, released by a nonlinear transformation that instantaneously transfers energy among the multiports of a

system. However, it does not manage explicitly energy. We will use another tool called "Energy Tanks" which can be adapted to ensure power routing and energy management.

Therefore, our goal will be to guarantee a passivity margin for interconnected systems. It will be shown that this approach will be able to compensate known disturbances resulting from modeling errors and the intermittency of renewable sources.

Power routing and energy management

Power routing dispatches the power requests over the different components and helps to track a load power reference, ensure power balance and a common bus voltage stability, respect the components power limits , the storage capacities and possibly minimize a performance criterion. The different operating modes can be triggered with an internal or an external variable.

The literature is quite extensive regarding power routing parameters. We find works using Model Predictive Control, which is based on the minimization of a criterion common to the different elements (an economic criterion for example) as in the works in [14, 15].

It is interesting to remark that, in the literature, a microgrid or a sub-part of a power system is often enforced as an equivalent generator. In [16] an improved version of a microgrid supervisor is presented, where the quadratic error between the SOC targets and the real SOC and the cost of starting a gen-set are minimized, while the optimization problem considers the microgrid network model and the constraints related to voltage and frequency. In [17], a new external droop algorithm has been proposed to achieve the primary control of networked multi-microgrids with multiple distributed energy resources, based on voltage and frequency controllers.

Another energy management system called virtual power plant (VPP) [18, 19] is defined as a low voltage distribution network that participates competitively in active network management of smart grids, namely, in the electricity market and in the optimization of the relation between generation and demand. The VPP are used in the framework of micro-grids as small-scale power sources to support specific groups of electrical loads with effective results.

These approaches do not consider the passivity or control explicitly all the

physical power flows in a power system. Model Predictive Control, for example, uses criteria that are not always related directly to power and considering power flows and energy limitations is done by introducing constraints in the optimal problem.

Finally, our problematic is to use tools related to port-Hamiltonian systems, to achieve power routing by guaranteeing passivity levels and/or energy reserves. The idea, contrary to viewing subsystems as equivalent generators, is to equip them with a virtual storage unit, which accounts for their power reserves. For this, we consider that each system is equipped with an Energy Tank, with States Of Charge equivalent to a battery, thanks to which we can achieve an indirect power routing between these different systems.

Scientific contributions

In this thesis research work, the main scientific achievements can be summarized in the following points:

1. Port-Hamiltonian modeling of a multi-source renewable energy platform for hydrogen production.
2. Estimation of the passivity margins of passive systems using the Energy Tanks concept.
3. Exploitation of the Energy Tanks concept in the framework of the power exchange between several interconnected systems.
4. Application of the passivity margin estimation and power routing concepts using Energy Tanks for the multi-source renewable energy platform for hydrogen production.

Publications

1. Bond Graph Modeling and Energetic Control of a PEM Electrolyzer. S.H. CHAABNA, J.-Y. DIEULOT, ICBGM International Conference on Bond Graph Modelling, 2018, Bordeaux, France
2. Port-Hamiltonian Formulation of the Bond Graph Model of a Hybrid Renewable Energy System. S.H. CHAABNA, J.-Y. DIEULOT, ICBGM International Conference on Bond Graph Modelling, 2018, Bordeaux, France
3. Port-Hamiltonian control and modeling using Energy Tanks. S.H. CHAABNA, J-Y. DIEULOT. 6^{eme} Journée Régionale des Doctorants en Automatique (JRDA), July 2019, HEI, Lille, France. Best Poster Award.

4. Estimation of passivity margins of hydrogen-based hybrid renewable energy systems via Energy Tanks. S.H. CHAABNA, J-Y. DIEULOT, S. SOOD, Mediterranean Conference on Control and Automation, 2020, Saint-Raphael, France.

Thesis structure

The thesis manuscript in composed of four chapters in addition to a general introduction and conclusion. We have chosen to present the tools related to modeling and passivity, with a direct application to the multi-source renewable energy platform. Then, we addressed the routing problem by exchange between Energy Tanks, with at the end the application on the platform.
The first chapter represents the first part of the bibliography related to the thesis work. In addition to the presentation of the main energetic representations and control algorithms for multiphysical systems, the concept of passivity is presented with an insight into passivity margins. The second chapter represents an application to the concepts developed in the first chapter to a hydrogen-based HRES, that is the MODIS-H2 platform. The port-Hamiltonian models of the different components of a multi-source renewable energy platform for hydrogen production are presented, along with simulations. The third chapter starts by exploring the bibliography related to power and energy exchange strategies in the passivity framework. The Duindam-Stramiglioli energy router and the Energy Tank concept are presented. In this chapter a new strategy which uses the virtual Energy Tanks for power and energy controlled routing in multi-physics systems is presented. Impartial and preferential energy distributions strategies are designed as an example of power routing laws. The fourth chapter, displays an application of the concepts presented in the first and the third chapter to a subsystem of the MODIS-H2 HRES. Hence, in this chapter the simulation results of the preferential energy distribution between two virtual Energy Tanks, attached to a fuel cell and a wind turbine and a real battery are shown.
Finally, in the general conclusion, the main results of the thesis work are discussed along with future research perspectives.

Chapter 1

Passivity-based modeling and control applied to HRES

1.1 Introduction

A Hybrid Renewable Energy System (HRES) is a system that combines one, two or more renewable energy sources (photovoltaic solar panels, wind turbine, watermill) and other power systems to deliver higher system effectiveness and higher energy supply equilibrium. There are two main structures of these systems [20]:

1. Grid connected system structure: this structure of the energy system implies a connection to the utility grid which is a flexible solution that allows a continuous supply of energy between renewable energy resources and the utility grid. Despite the many advantages of this structure, it still expensive. Hence, to transmit safely electricity between the grid and the loads, safety and power quality components are needed in addition to the grid-connection requirements from the power provider.

2. Islanded system structure: this energy system structure concerns the regions that are not closely integrated with a larger mainland or continental systems where a local generation of electrical energy is needed. This structure requires reliable local power storage systems.

Otherwise, the different renewable energy sources and loads are connected to AC or DC buses. In both cases, power converters (Chopper, Inverter, Rectifier) are used to synchronize the different connected components of the system. The setup of DC-coupling is easy and unnecessary for the different sources of synchronization. On the other hand, it results in less efficiency against inverter failures for the AC loads, while the system is more flexible in the AC bus, where it is possible to choose AC voltage and frequency for more efficient power transmission. Other configurations are also possible in addition to the AC and DC buses, namely, AC

high and low frequency, combined DC and AC buses.
The intermittent characteristics of the renewable energy resources and the use of long-term and short-term storage equipment generate different operating modes. It is mandatory that a supervisor controls the switches from one mode to another.Then, in order to manage the transition between the different operating modes and for control design and sizing purposes, a model of the HRES is required.
After a literature review on HRES modelling and control, we notice that, because of the multi-physics characteristics of the combined systems (thermal, chemical, hydraulic, electrical, mechanical), energetic representations (Energetic Macroscopic Representation (EMR) and bond graph (BG), Petri Net) are the most used since energy is the common point between these distinct fields.
Energetic Macroscopic Representation (EMR) is a formalism based on the causal representation of physical systems that makes it possible to model multiphysical systems presenting energetic and/or functional couplings. It is a powerful simulation tool which also offers control laws based on the cascade inversion of the structure of the system. This modeling approach has been widely used for several years and is rapidly expanding for the modeling of transport vehicles (in particular at L2EP in Lille for the rail-wheel-motor link of a rail transport system [21, 22] and hybrid power system [23, 24], EPFL in Switzerland for systems based on supercapacitors [25]), for the modeling of industrial processes (University of Trois-Rivieres in Canada [26]) or for the modeling of fuel cell and electrolyser systems (University of Technology of Belfort-Montbéliard, SeT-FC Lab and University of Franche Comte, FEMTO-ST/FC Lab) [27, 28, 29]. However, the EMR is an approach which does not address the synthesis of controllers and passivity.
The bond graph and the port-Hamiltonian state space representation allow to represent straightforwardly physical phenomena, power flows in a system and to derive subsequent control methods which can be tuned according to the physical dimensions or parameters of the model.
To sum up, in this chapter we discuss the different studies and the evolution of the energetic modeling and control of the HRES using the bond graph and the port-Hamiltonian representation. A reminder of the passivity and dissipativity theory will be presented.

1.2 Bond graph and port-Hamiltonian modeling applied to power and energy systems

1.2.1 Bond graph

Definition

Bond graph formalism is a graphical energy-based modeling tool, introduced by Paynter [30] and developed by Rosenberg and Karnopp [31]. It enables the modeling of multi-physics systems (mechanical, electrical,... etc), linear and nonlinear, without solving any differential equations. It allows the understanding of the power transfers in interconnected systems [1, 32, 33].
A bond-graph enables to derive the state space representation of any system, the transfer function in the case of linear systems and the corresponding block diagram, in an easy way while allowing the identification of analogies between different domains.
A bond-graph consists of a set of bonds (edges) on which we find the variables of flow (f) and effort (e). From this representation, a structural and behavioral approach of the system can be obtained, namely the visualization of the causality properties and the deduction of mathematical models.
The basic elements of the bond graph (see figure (1.2.1)) are:

1. R: Modeling element of a physical phenomenon, linking the effort variable to the flow variable
2. I: Modeling element of a physical phenomenon, linking the flow variable to the generalized time variable
3. C: Modeling element of a physical phenomenon, linking the effort variable to the generalized displacement variable
4. S_e, S_f: Source of effort and source of flow
5. Junction "0" and "1": The Junction "0" includes the elements which are subjected to same effort while the junction "1" encompasses the elements that share the same flow
6. TF: Transformer (Electric transformer, gear train, ...)
7. GY: Gyrator (Electric motor, centrifugal pump, ...etc)

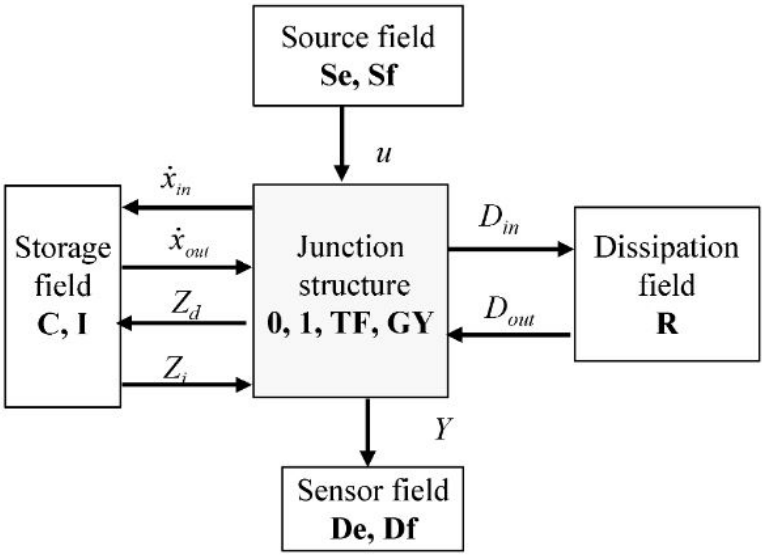

Figure 1.2.1: Bond graph elements [1]

Bond graph and mathematical equations

The graphical representation of multi-physical systems based on bond graphs highlights the links between the sub-systems and specify their nature (electrical, mechanical,...,etc) and the way they are connected together based on the interconnection structure that ensures the exchange of internal and external power. It allows, of course, to display power flow in the whole system.
In what follows we will summarize the steps that allow to derive some mathematical representations of a physical system from a BG model.

1. Differential equations [32, 3]:
   The differential equations stemming from a bond graph can be derived using the causality concept. Indeed, each element of the bond graph has its own equations obtained respecting the causality in the system.

2. State space equations [32, 3]:
   In the bond-graph derived state space model, the state variables of the system are the energy variables contained in the bond graph. These energy variables represent the dynamical elements of energy storage I and C and the dimension of the state vector x corresponds to the number of these elements.
   In this case the state equations are obtained combining both the structure and element's laws with respect to the system causality.

3. Transfer function [32]:
   The transfer function for linear systems relies on Mason's gain formula and

is expressed as follows:

$$G(s) = \frac{Y(s)}{E(s)} = \frac{\sum_{k=1}^{N} G_k(s)\Delta_k(s)}{\Delta(s)} \tag{1.1}$$

with:

$$\Delta = 1 - \sum L_i + \sum L_i L_j - \sum L_i L_j L_k + ... + (-1)^m \sum ... + ... \tag{1.2}$$

where:

(a) $\Delta(s)$: Determinant of the graph

(b) $E(s)$, $Y(s)$: Input and output variable, respectively

(c) $G(s)$: Complete gain between $E(s)$ and $Y(s)$

(d) N: Total number of forward paths between $E(s)$ and $Y(s)$

(e) G_k: Path gain of the k^{th} forward path between $E(s)$ and $Y(s)$

(f) L_i: Loop gain of each loop in the system

(g) L_iL_j: Product of the loop gains of any two non-touching loops (no common nodes)

(h) $L_iL_jL_k$: Product of the loop gains of any three pairwise non-touching loops

(i) Δ_k: The cofactor value of Δ for the k^{th} forward path, with the loops touching the k^{th} forward path removed.

The path represents a set of a continuous branches which are crossed in the direction they are indicating while the path gain represents the gain of the different branches multiplied by each other.
The forward path refers to the path that goes from an input node to an output node crossing each node only once. This is contrary to a loop where the path starts and ends at the same node crossing like in the case of the forward path the different node only once and the product of the gains of all the branches in the loop corresponds to the loop gain. For more details see [32].

Bond graph and HRES modeling

Bond graph modeling of HRES systems that include several multi-physical systems (more than 3 systems) and operating modes has been poorly addressed in the literature. Most of the corresponding studies regarding the complex modeling of a global HRES, whether the authors studied the actual experimental system or used continuous models based on equations, addressed the steady state issue and

less few dealt with the dynamic model.
Table (1.1) summarizes some of the works of the literature in the field of the modeling, control and simulation of hydrogen-based Hybrid Renewable Energy Systems.

HRES components	Modeling	Control	Publication
PV, FC, DC bus	steady state eqautions	Unit Power Control Feeder Flow Control Miwed Control Mode	[34]
PV, FC, Bat, DC bus	State space models	Fuzzy logic control P&O algorithm Imperialist competitive algorithm Particle swarm optimization	[35]
PV, FC, EL, Bat, Review	Steady state equations Chemical equations	Load demand, power best storage and use path	Yilanci et al. [36]
PV, FC, UC EL, Bat, DC bus	Energetic Macroscopic Representation	Maximum Control Structure Power management algorithm	Lu et al. [37]
PV, FC, ELZ, UC Bat, AC/DC bus,Diesel	Steady state equations State state models	Optimal energy flow management	Bajpai et al. [38]
PV, FC, ELZ, UC, DC bus	Steady state equations	Smart energy management algorithm	Nasri et al. [39]
PV, Diesel, FC, Bat, AC/DC bus		Load demand satisfaction with total net present cost (NPC) and levelized cost of energy (LCOE) optimization	Halabi et al. [40]
PV, FC, Bat, DC bus	Steady state equations	Power management system PID algorithm for bus voltage regulation PID compensator and PWM generator	Jiang [41]
PV, FC, ELZ, Bat, DC bus	Steady state equations State space models	Interconnection and damping assignment passivity-based control (IDA-PBC)	[42]
WT, UG, FC, Bat, EZL, SC, DC bus	Eenrgetic Macroscopic Representation. Causal Ordering Graph	Power flow control Electrolyser pressure control Hydrogen flow control	Zhou et al. [43]
PV, WT, FC, ELZ, Bat, H2 Tank, DC bus	Hybrid Bond Graph	Operating mode management Energy management	[5]

Table 1.1: Example of publications related to hydrogen-based HRES

Indeed, BG has been used to describe only the steady state part of the HRES, namely, for wind turbine [44], PV [45, 46], fuel cell [47, 48], electrolyzer [49]. However, in [50, 51] a combination of a WT, PV and a hydrogen fuel cell as the main energy source with batteries through a single bond graph model has been achieved. Nevertheless, the authors didn't consider the connection and disconnection of the component and the switching from an operating mode to another.In [5] an Event-Driven Hybrid BG model (EVH-BG) of a HRES composed of a WT, PV, PEM FC and electrolyzer, battery and hydrogen storage tank has been pro-

posed, where the operating modes are governed by an automaton. Hence, in the presented model, the continuous part of the multi-physical system is modeled using BG while the discrete part is managed by the automaton. The different modes are triggered according to external and internal parameters.

1.2.2 Port-Hamiltonian systems

A port-Hamiltonian system can be represented as in Figure (1.2.2), where the elements "S" and "R" are the internal ports which correspond, respectively, to the energy storage and the dissipation of internal energy and $\mathcal{C}$ and $\mathcal{I}$ are the external ports where $\mathcal{I}$ represents the interaction port, defining the interaction of the system with the rest of its environment and $\mathcal{C}$ is an accessible port (e.g. for controller action) that can also include the sources whenever they exist.
As in the bond-graph [32] theory, the notions of "f" and "e" flow appear in the port-Hamiltonian formalism. Indeed, "R" and "S" elements are linked to a routing structure called "Dirac structure (D)" through effort variables "e" and flow "f". It will be noted that the result of the product "$e^T f$" represents the "*power*" (in bond-graph theory). So if we define the finite-dimensional linear space of the $\mathcal{F}$ flows as well as the *effort* $\mathcal{E}$ space, it becomes easy to see that the set of ports will be $\mathcal{F} \times \mathcal{E}$.

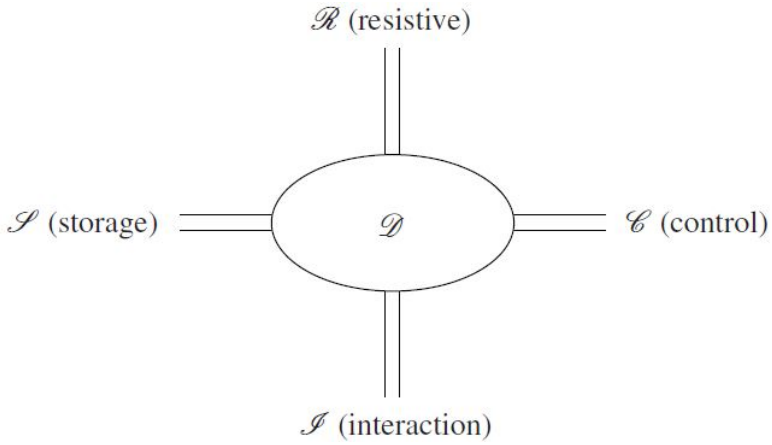

Figure 1.2.2: Port-Hamiltonian system [2]

Definition 1.1 ***Hamiltonian system controlled by ports*** *[52]. Considering the Hamiltonian function $H(x) : \mathbb{R}^n \to \mathbb{R}$, and the following matrices:*

- *$J(x)$ a skew-symmetric matrix of dimensions $(n \times n)$,*
- *Input matrix $g(x)$ of dimension $(n \times m)$ with,*

$$\sum : \begin{cases} \dot{x} &= J(x)\frac{\partial H}{\partial x}(x) + g(x)u, \\ y &= g^T(x)\frac{\partial H}{\partial x}(x). \end{cases} \tag{1.3}$$

The system $\sum$ represents a Hamiltonian system with ports, where $x \in \mathbb{R}^n$ is the state vector combining the energy variables, u and y are the inputs and outputs of the system represented by the power variables of the input/output ports (R).

In the Hamiltonian system described in (1.3), there is no energy dissipation. It is therefore necessary (since all real systems dissipate energy) to rewrite these equations for a dissipative system. The idea would be to connect the dissipative elements with ports.

Definition 1.2 ***Port-controlled Hamiltonian system with dissipation*** *[52]. Considering the following three matrices*

- *$J(x)$ a skew-symmetric matrix of dimensions $(n \times n)$,*
- *Input matrix $g(x)$ of dimension $(n \times m)$,*
- *A symmetric semi-definite positive matrix $R(x)$,*

and the function of the total energy $H(x) : \mathbb{R}^n \to \mathbb{R}$, we can describe a Hamiltonian system with ports with dissipation as follows:

$$\begin{cases} \dot{x} = J(x)\frac{\partial H}{\partial x}(x) + g(x)u + g_R(x)u_R, \\ y = g^T(x)\frac{\partial H}{\partial x}(x), \\ y_R = g_R^T(x)\frac{\partial H}{\partial x}(x), \end{cases} \tag{1.4}$$

with:

$$\begin{bmatrix} g(x) & g_R(x) \end{bmatrix} \begin{bmatrix} u \\ u_R \end{bmatrix} = g(x)u + g_R(x)u_R, \tag{1.5}$$

where u_R and y_R denote the power variables at the ports where the resistive elements are connected.

Definition 1.3 ***Dirac structure*** *[53]. We consider a linear finite element space $\mathcal{F}$ et $\mathcal{E}$ with $\mathcal{F} = \mathcal{E}^*$ a subspace $\mathcal{D} \subset \mathcal{F} \times \mathcal{E}$ and a Dirac structure if:*

- *$< e|f >= 0$, for all $(f, e) \in \mathcal{D}$,*
- *$dim\mathcal{D} = dim\mathcal{F}$.*

where: $< e|f >= e^T f$.
The first property corresponds to power-conservation, and expresses the fact that the total power entering (or leaving) a Dirac structure is zero.
It is therefore possible, using this definition, to identify several structures of Dirac: transformers, gyrators, Kirchhoff's circuit laws, as well as the junctions "1" and "0" in the theory of bond graphs. The following example of a transformer shows

how one can prove that a bond is a Dirac structure.
Consider the following equations which describe the behavior of a transformer:

$$\begin{aligned} f_2 &= \alpha f_1 \\ e_1 &= -\alpha e_2 \end{aligned} \tag{1.6}$$

We get: $e = \begin{bmatrix} e_1 \\ e_2 \end{bmatrix}$ *and* $f = \begin{bmatrix} f_1 \\ f_2 \end{bmatrix}$ *consequently*
$e^T f = e_1 f_1 + e_2 f_2$ *and using the equations* (1.6) *we obtain* $e_1 f_1 + e_2 f_2 = 0$ *which concludes the proof.*

Example 1.2.1 *RLC circuit: influence of the dissipation*
Let's consider the following RLC circuit, figure (1.2.3).

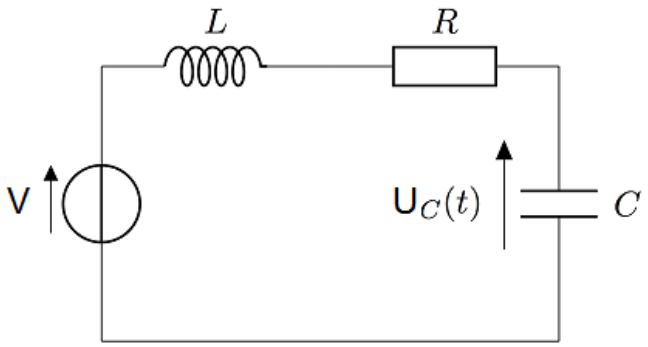

Figure 1.2.3: RLC circuit system

From the circuit we have:

$$V = Ri(t) + L\frac{di(t)}{d(t)} + U_C \tag{1.7}$$

For: $i(t) = \frac{dq(t)}{dt} = C\frac{dU_C(t)}{dt}$

$$V = RC\frac{dU_C(t)}{dt} + LC\frac{d^2U_C(t)}{dt} + U_C \tag{1.8}$$

which is a second order system equivalent to :

$$LC\frac{d^2U_C(t)}{dt} + RC\frac{dU_C(t)}{dt} + U_C = V \tag{1.9}$$

The transfer function of the system is given in following form:

$$H(p) = \frac{U_C(p)}{V(p)} = \frac{1/LC}{p^2 + \frac{R}{L}p + \frac{1}{LC}} \equiv \frac{K\omega_n^2}{p^2 + 2\xi\omega_n p + \omega_n^2} \tag{1.10}$$

where:

$$\begin{cases} \frac{1}{\omega_n^2} = LC \rightarrow \omega_n = \sqrt{\frac{1}{LC}} \quad Frequency \\ \frac{2\xi}{\omega_n} = RC \rightarrow \xi = \frac{R}{2}\sqrt{\frac{C}{L}} \quad Damping \quad of \quad the \quad system \\ K = 1 \quad Gain \quad parameter \end{cases} \tag{1.11}$$

The system can be represented in the linear port-Hamiltonian form as follows:

$$\begin{cases} \dot{x} = [J - R]\, Qx + gu \\ y = g^T Q x \end{cases} \tag{1.12}$$

which is equivalent to:

$$\begin{cases} \begin{bmatrix} \dot{x}_1 = \dot{q} \\ \dot{x}_2 = \dot{\phi} \end{bmatrix} = \left[\underbrace{\begin{pmatrix} 0 & 1 \\ -1 & 0 \end{pmatrix}}_{J} - \underbrace{\begin{pmatrix} 0 & 0 \\ 0 & R \end{pmatrix}}_{R} \right] \underbrace{\begin{bmatrix} 1/C & 0 \\ 0 & 1/L \end{bmatrix}}_{Q} \begin{bmatrix} x_1 \\ x_2 \end{bmatrix} + \begin{bmatrix} 0 \\ 1 \end{bmatrix} V \\ y = \begin{bmatrix} 0 & 1 \end{bmatrix} \begin{bmatrix} 1/C & 0 \\ 0 & 1/L \end{bmatrix} \begin{bmatrix} x_1 \\ x_2 \end{bmatrix} = \frac{x_2}{L} = \frac{\phi}{L} \quad inductance \quad current \end{cases} \tag{1.13}$$

The internal energy of the system is given in equation (1.14).

$$H(\phi, q) = \frac{1}{2L}\phi^2 + \frac{1}{2C}q^2 \tag{1.14}$$

The power of the system is given in equation (1.15):

$$\begin{aligned} \dot{H}(\phi, q) &= \frac{\partial H^T(x)}{\partial x} R(x) \frac{\partial H(x)}{\partial x} + y^T(t)u(t) \\ &= -\begin{bmatrix} \frac{q}{C} & \frac{\phi}{L} \end{bmatrix} \begin{bmatrix} 0 & 0 \\ 0 & R \end{bmatrix} \begin{bmatrix} \frac{q}{C} \\ \frac{\phi}{L} \end{bmatrix} + \frac{\phi}{L} V \\ &= \frac{\phi}{L}(V - R\frac{\phi}{L}) \end{aligned} \tag{1.15}$$

Based on the linear port-Hamiltonian RLC circuit system (1.13) and exploiting the damping expression:

$$\frac{2\xi}{\omega_n} = RC \rightarrow \xi = \frac{R}{2}\sqrt{\frac{C}{L}} \tag{1.16}$$

we notice that the damping parameter ξ is proportional to the resistance (R) of the system and for different values of R in the transfer function with $L = 1$ and $C = 1$, we get the following schemes for a unit step open loop response:

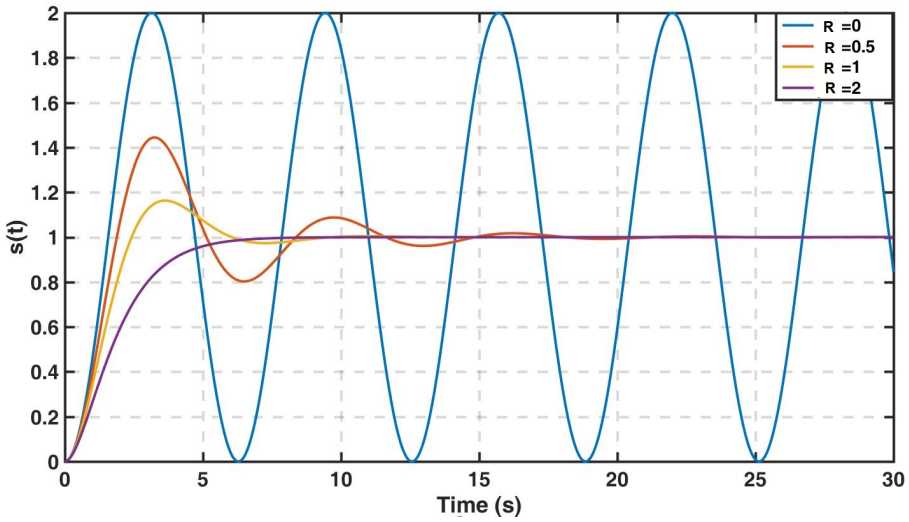

Figure 1.2.4: System step-response

We notice the same behavior of the system when we vary the resistance variable in the linear port-Hamiltonian representation of the system, see figure (1.2.5).

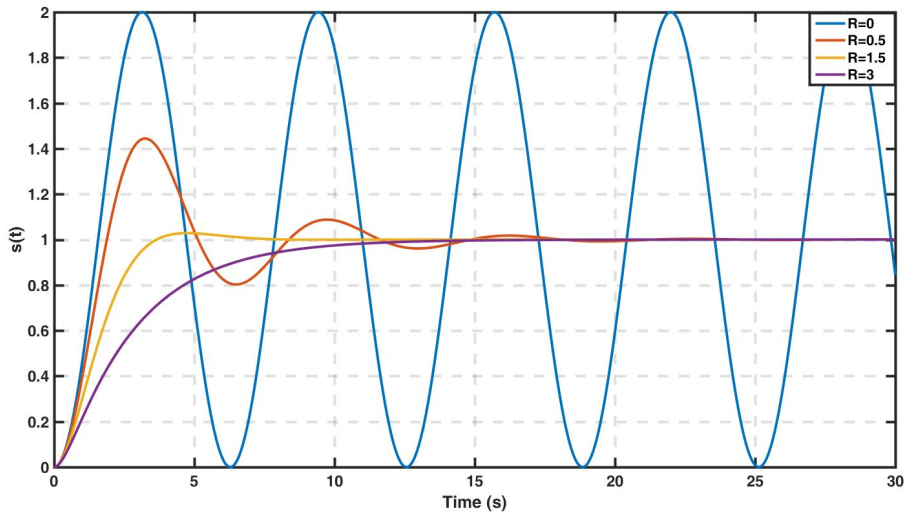

Figure 1.2.5: System step-response

and we get the port-Hamiltonian system output (inductance current) of the system which tends to zero for R>0, see figure (1.2.6)*:*

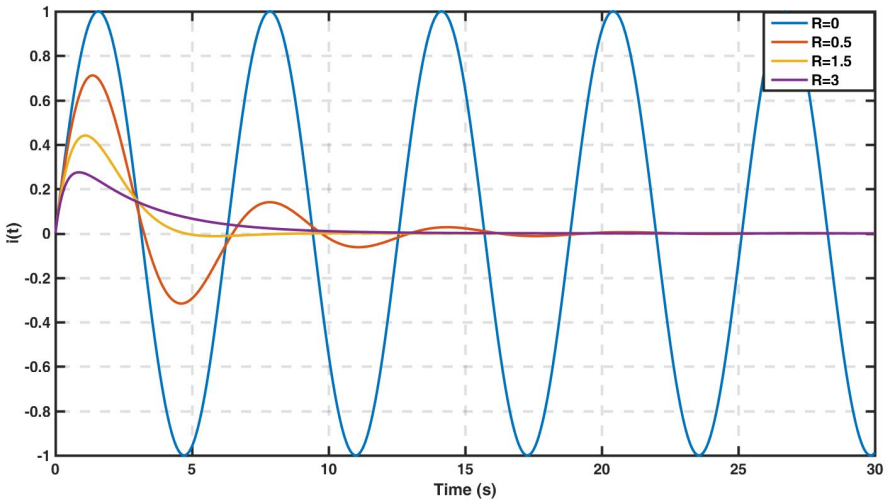

Figure 1.2.6: System output (Inductance current)

For higher value of the Resistance R the transient becomes more damped, which gives a physical interpretation of the dissipation matrix $R(x)$ in the port-Hamiltonian representation.

Example 1.2.2 *Mass-spring system*
Consider the mass-spring system in figure 1.2.7, where the states are q and p that represent, respectively, the displacement of the spring and the momentum of the mass where k is the stiffness of the spring and m its mass [54].
The energy of the system is defined as the sum of the kinetic energy E_c of the mass and the potential energy V of the spring and is given as follows:

$$E = \frac{1}{2m}p^2 + \frac{1}{2}kq^2 \tag{1.17}$$

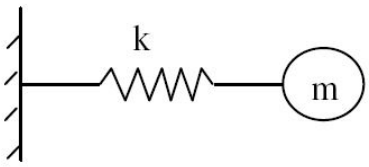

Figure 1.2.7: Representation of the mass-spring system

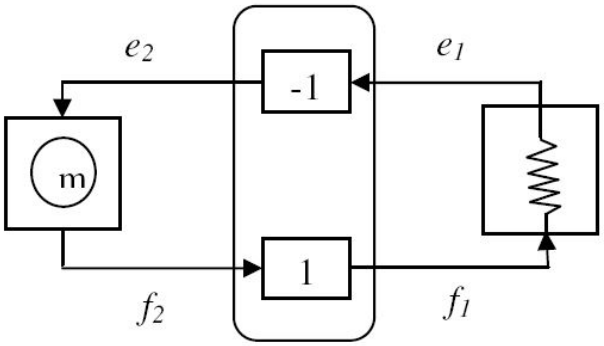

Figure 1.2.8: The interconnection structure of the model

The equations of the system are:

1. *Spring:*

$$\begin{cases} \dot{q} = f_1 \\ e_1 = qk \end{cases} \tag{1.18}$$

2. *Mass:*

$$\begin{cases} \dot{p} = e_2 \\ f_2 = \frac{p}{m} \end{cases} \tag{1.19}$$

From the two equations above we can calculate the quantity of energy extracted from the mass ($\dot{E}_c$) and the spring ($\dot{V}$), as follows:

$$\begin{aligned} \dot{E}_c &= \frac{\partial E_c}{\partial p}\dot{p} = \frac{p}{m}e_2 = f_2 e_2 = P_2 \\ \dot{V} &= \frac{\partial V}{\partial q}\dot{q} = kqf_1 = e_1 f_1 = P_1 \end{aligned} \tag{1.20}$$

The interconnection structure preserves energy, so:

$$P_1 = -P_2 \tag{1.21}$$

and the mathematical expression of the structure can be described as follows:

$$f_1 = f_2, \quad e_1 = e_2 \tag{1.22}$$

From (1.20) and (1.21), we get: $\dot{V} = -\dot{E}_c$, which means that energy is transferred between the two systems. Considering (x) and (p) the stiffness of the spring and the momentum of the mass, respectively. The input u is the force that acts on the mass and the output y the velocity of the mass.
The Hamiltonian function is:

$$H(x,p) = \frac{1}{2m}p^2 + \frac{1}{2}kx^2 \tag{1.23}$$

This allows to write the following port-Hamiltonian representation:

$$\begin{bmatrix} \dot{x} \\ \dot{p} \end{bmatrix} = \begin{bmatrix} 0 & 1 \\ -1 & 0 \end{bmatrix} \begin{bmatrix} \frac{\partial H}{\partial x}(x,p) \\ \frac{\partial H}{\partial p}(x,p) \end{bmatrix} \tag{1.24}$$

$$y = \begin{bmatrix} 0 & 1 \end{bmatrix} \begin{bmatrix} \frac{\partial H}{\partial x} & \frac{\partial H}{\partial p} \end{bmatrix}^T \tag{1.25}$$

with:

$$H(q,p) = \frac{1}{2}kx^2 + \frac{1}{2m}p^2. \tag{1.26}$$

It can be seen through this simple example that the two subsystems (spring and mass) communicate with each other and that there is an exchange of energy between the two components without loss of energy.

1.2.3 From the bond graph to the port-Hamiltonian formalism

Many research works [3, 55, 56, 57] aim to develop methods to derive port-Hamiltonian models from bond graphs, motivated by different interests, namely control and/or simulation [58]. In this section, we will give a scope of the established results supported by examples.

State-Input-Output port-Hamiltonian systems

In [3], the authors have addressed the case of Input-State-Output port-Hamiltonian systems obtained from the causal nonlinear bond graph models. Equivalences between the two domain of modeling have been established especially by comparing the expression of the stored energy and considering the total energy as a common storage function in both formalisms. This procedure leads to define the relations between the key-variables of the two formalisms, and to derive the state space equations in the port-Hamiltonian description as a function of the energy gradient. The description and parameters of the different matrices and the interconnections that govern the port-Hamiltonian representation stem directly from the structure and parameters of the bond graph.
To support the theory, the example of a permanent Magnet Synchronous Motor (PMSM) as well as a linear RLC circuit and a DC-DC converter system were detailed in [3].
As an example, we recall the bond-graph and port-Hamiltonian representation of a series RLC circuit (see Figure (1.2.9)) [3].

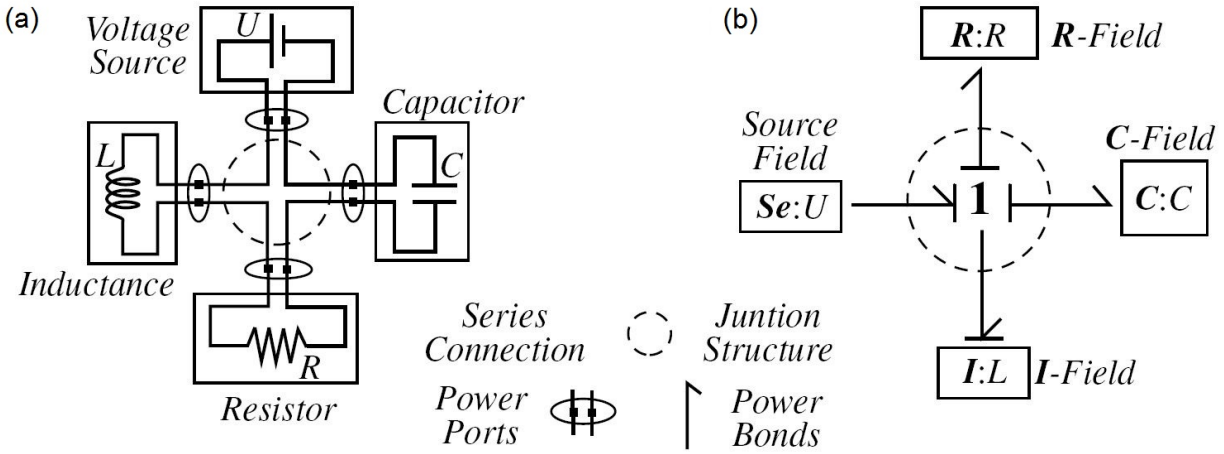

Figure 1.2.9: (a) Series RLC circuit, (b) Bond graph model [3]

From the bond graph (b) of the circuit we first notice that the dimension of the system is equal to 2 which corresponds to the I and C elements of the circuit. The state variables are the same in both formalisms. Then, the Hamiltonian function of the system is defined in (1.27), it is expressed as a function of the inductor flow p_L and the capacitor charge q_C.

$$H(p_L, q_C) = \frac{p_L^2}{2L} + \frac{q_C^2}{2C} \tag{1.27}$$

Finally, we obtain the following expression of the port-Hamiltonian model of the circuit in figure (1.2.9):

$$\begin{cases} \begin{bmatrix} \dot{p}_L \\ \dot{q}_C \end{bmatrix} = \left\{ \begin{bmatrix} 0 & -1 \\ 1 & 0 \end{bmatrix} - \begin{bmatrix} R & 0 \\ 0 & 0 \end{bmatrix} \right\} \begin{bmatrix} \partial H/\partial p_L \\ \partial H/\partial q_C \end{bmatrix} + \begin{bmatrix} 1 \\ 0 \end{bmatrix} u \\ y = \begin{bmatrix} 1 & 0 \end{bmatrix} \begin{bmatrix} \partial H/\partial p_L \\ \partial H/\partial q_C \end{bmatrix} \end{cases} \tag{1.28}$$

Remark 1.1 *The results of the study of the modeling of switching systems, using both approaches, in particular, the port-Hamiltonian and the bond graph structure have shown that port-Hamiltonian modeling is more convenient and better meets the requirements of the designer in term of control design. In the bond graph approach the causalities may be changing along with the mode of the system which is not convenient [59], [60]. However, in the PH formalism we keep the same state variable, the same Hamiltonian function and the same dissipation function, there is no need to reconfigure the system for each mode [61]. Then, with the Hamiltonian form, it's possible overcome the problem of the algebraic constraints (jump rule) that appears in presence of switches and diodes.*

1.3 Passivity and dissipativity

The notion of passivity was first introduced in the field of electricity, that is, the study of electrical circuits. It aims to check whether the energy supplied to a given system at its input will be dissipated or generated by the system seen from its output.
Passivity is considered as a special case of the dissipativity theory [62], which brings us back to present a brief definition of dissipativity, before returning to passivity.

1.3.1 Concept of passive systems

To explain the notion of passivity we first introduce the definition of dissipativity. For this we define the supply rate $w(y,u)$ and the storage function $S(t)$. Let's consider the following non-linear system:

$$\sum : \begin{cases} \dot{x}(t) = f(x,u) \quad with \quad x(t_0) = x_0 \\ y(t) = h(x,u) \end{cases} \tag{1.29}$$

where $x \in X \subset \mathbb{R}^n$, $u \in U \subset \mathbb{R}^m$ and $y \in Y \subset \mathbb{R}^r$ represent respectively the system state variables, its inputs and outputs, with X, U and Y the state, input and output spaces respectively.

Definition 1.4 : The supply rate [62, 63]
The supply rate $w(t)$ is a real-valued function defined in $(U \times Y)$ such that for all $u(t) \in U$, $x_0 \in X$ and $y(t) = h(x,u)$, $w(t)$ satisfies:

$$\int_{t_0}^{t_1} |w(t)|\, d(t) < \infty \tag{1.30}$$

For all: $t_1 \geq t_0 \geq 0$

Definition 1.5 : Dissipative systems [62]
The system (1.29) [62] is said to be dissipative if there exists a non-negative real function $S(x(t)) : X \to \mathbb{R}^+$, called storage function, such that for any $t_1 \geq t_0 \geq 0$, $x_0 \in X$ and $u(t) \in U$, the following dissipation inequality is satisfied:

$$S(x(t_1)) - S(x(t_0)) \leq \int_{t_0}^{t_1} w(u(t), y(t)) d(t) \tag{1.31}$$

Remark 1.2 *: The definition given above allows us to understand from the inequality (1.31) that for a system to be dissipative the energy supplied to the system must be greater than or equal to the energy stored in the system.*

A system is said to be passive when the power withdrawn is achieved at the expense of its internal energy storage. Thus, there can be no internal power generation.

Definition 1.6 *:* **Passive systems [62]**
The system (1.29) is said to be passive if it is dissipative with respect to the supply rate:

$$w(u(t), y(t)) = u^T(t)y(t) \tag{1.32}$$

and the storage function $S(t)$ satisfies $S(0) = 0$.

1.3.2 Stability of passive systems

The concept of passivity implies stability if a positive storage function is used. However, stability is not always ensured by passivity. In this case, additional conditions on zero-state detectability and observability are required:

Definition 1.7 : Zero-state observability and detectability [64, 63]
The system (1.29) is said to be zero detectable state if:

$$y(t) = h(\tau(t, t_0, x, 0)) = 0, \forall t \geq t_0 \geq 0 \rightarrow \lim_{t\to\infty} \tau(t, t_0, x, 0) = 0, \tag{1.33}$$

For all $x \in \mathbb{R}$. where $\tau(.)$ is the solution of $x(t)$.

Starting from the previous definition, one can easily make the link between the passivity and the Lyapunov stability of a system.

Theorem 1.1 *[63] We consider that the system described in the (1.29) equation is passive with a C^1 storage function S. Then the following properties hold:*

1. *If S is positive definite, then the equilibrium $x = 0$ of (1.29) with $u = 0$ is Lyapunov stable*
2. *If (1.29) is ZSD then the equilibrium $x = 0$ of (1.29) with $u = 0$ is stable*
3. *If in addition to either Condition 1 or Condition 2, $S(x)$ is radially unbounded (i.e., $S(x) \rightarrow \infty$ as $\|x\| \rightarrow \infty$), then the equilibrium $x = 0$ in the above conditions is globally stable (GS)*

Remark 1.3 *There are many works in the literature that deal with the stability of passive linear time invariant (LTI) systems. The result was often written in the form of linear matrix inequalities (LMI) See [65] for more details.*

Remark 1.4 *It stems from theorem (1.1) that passivity does not necessarily imply stability.*

1.3.3 Kalman–Yacubovich–Popov property

The following description applies to one of the most essential properties of passive systems:

Definition 1.8 : Kalman–Yacubovich–Popov property [4]
Considering the following affine nonlinear system

$$\mathbb{H}: \begin{cases} \dot{x} &= f(x) + g(x)u, \\ y &= h(x). \end{cases} \tag{1.34}$$

où $x \in \mathbb{R}^n$, $u \in \mathbb{R}^m$, $y \in \mathbb{R}^l$. *Consider also the function* $S(x) : x \to \mathbb{R}$, *with* $S(0) = 0$. *The system* $\mathbb{H}$ *owns the property of Kalman-Yakubovich-Popov (KYP) if:*

$$\begin{aligned} L_f S(x) &= \frac{\partial S(x)}{\partial x} f(x) \leq 0 \\ L_g S(x) &= \frac{\partial S(x)}{\partial x} g(x) = h^T(x) \end{aligned} \tag{1.35}$$

The term $L_f S(x) = \frac{\partial S(x)}{\partial x} f(x)$ *represents the Lie derivative.*

Proposition 1.2 *A system (1.29) which has the KYP property is passive, with a storage function S (x). Conversely, a passive system having a* C^1 *storage function has the KYP property.*

Proposition 1.3 *[53] A port-Hamiltonian system with dissipation is a passive system and the storage function is the Hamiltonian function.*
If $R(x) = 0$, *namely if there is no dissipation in the system, we have*

$$L_{(J(x)-R(x))\frac{\partial H}{\partial x}} H(x) = 0 \tag{1.36}$$

Therefore, a lossless passive system is a port-Hamiltonian system without dissipation. In addition, if R(x) is strictly positive definite, the PH scheme is strictly passive. Thus, losslessness, passivity and a PH system's rigid passivity can be determined by merely inspecting the matrix sign R(x). The following equation explains the role of the dissipation matrix:

$$P = y^T u = \frac{dH}{dt} + \underbrace{\frac{\partial^T H}{\partial x} R(x) \frac{\partial H}{\partial x}}_{P_{diss}} \tag{1.37}$$

The dissipated energy sign depends on R(x). If R(x) is strictly positive definite, $P_{diss} > 0$ *which implies that the system always dissipates some energy and the system is therefore strictly passive. If* $R(x) = 0$ *namely* $P_{diss} = 0$, *this implies that there is no dissipation and the scheme is lossless as a result. If R(x) is negative definite and* $P_{diss} < 0$, *this implies that the system is not passive as there exists an internal energy production.*

1.3.4 Passivity margin of perturbed systems

Let's consider the port-Hamiltonian model with disturbances given in equation (1.38).

$$\begin{cases} \dot{x} = [J(x) - R(x)] \frac{\partial H(x)}{\partial x} + g(x)u + \zeta \\ y = g^T(x) \frac{\partial H(x)}{\partial x} \end{cases} \tag{1.38}$$

where, $x \in \mathbb{R}^n$ is the state, ζ is a bounded disturbance, $J(x) = -J^T(x)$ is a skew-symmetric matrix of dimension $(n \times n)$ and $R(x) \geq 0$ is a positive semi-definite matrix that represent respectively, the internal energetic interconnections and the dissipation of the port-Hamiltonian system. $H(x) : \mathbb{R}^n \to \mathbb{R}$ is a lower bounded Hamiltonian function representing the amount of energy stored in the system. The pair (u, y) is a power port through which the system can exchange energy with external environment and their product gives the amount of power that can be exchanged.
When the disturbance $\zeta = 0$, the passive Hamiltonian system verifies the following condition,

$$\dot{H}(x) + \frac{\partial^T H(x)}{\partial x} R(x) \frac{\partial H(x)}{\partial x} = u^T(t) y(t) \tag{1.39}$$

where $D(x) = \frac{\partial^T H}{\partial x} R(x) \frac{\partial H}{\partial x} \geq 0$ is the power dissipated by the system, which means that the power supplied to the system is either stored or dissipated, see figure (1.3.1).

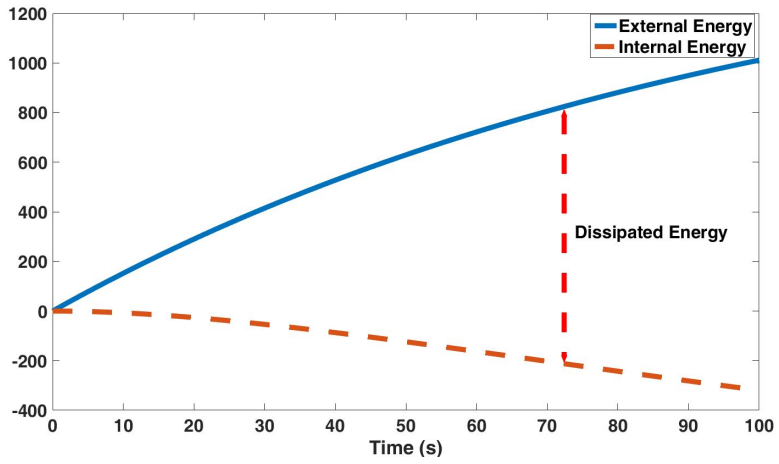

Figure 1.3.1: Energy gap between external and internal energy

The dissipated power $D(x)$ represents a "passivity margin", the greater $D(x)$, more the system will be able to absorb the energy generated by a non-passive behavior (e.g. increasing the rigidity of a viscoelastic coupling) while maintaining its passivity.
When the disturbance ζ in equation (1) is not zero and is either known or esti-

mated [1], then ζ is said to be a "matching disturbance" if there exist a matrix $R_\zeta = diag(r_{\zeta_i})$, $i = 1, ..., dim(R_\zeta)$, such that

$$\zeta = -R_\zeta \frac{\partial H}{\partial x} \tag{1.40}$$

In this case, one can use a new passivity margin for a perturbed PH system. $D_\zeta = \frac{\partial^T H}{\partial x} R(x) \frac{\partial H}{\partial x} + \frac{\partial^T H}{\partial x}\zeta = \frac{\partial^T H}{\partial x}(R(x) - R_\zeta)\frac{\partial H}{\partial x}$ which can be negative or positive depending on the positive definiteness of $(R - R_\zeta)$. Note that this new concept can be extended easily to uncertain PH systems when the uncertainty in $R(x)$ is known or bounded.

Now we define what is a PH system with a guaranteed passivity margin. Let us consider a matrix $R_{min} \geq 0$. Then, we define a modified passivity margin as $D_{min} = \frac{\partial^T H}{\partial x}(R(x) - R_{min})\frac{\partial H}{\partial x} + \frac{\partial^T H}{\partial x}\zeta > 0$, with $R_{min} \geq 0$. If the modified passivity margin $D_{R_{min}}$ is greater that of system with dissipation matrix R_{min}, the power reserve for the system (1.38) which guaranties a minimum passivity margin will be less than for the original passive system. Of course this notion can be extended to the perturbed systems using a $D_{min,\zeta}$.

1.3.5 Interconnection of Passive Systems

Theorem 1.4 :Interconnections of passive systems [4]

Suppose that systems H_1 and H_2 are passive (as shown in Figure (1.3.2)). Then the two systems, one obtained by the parallel interconnection, and the other obtained by feedback interconnection, are both passive. If systems H_1 and H_2 are ZSD and their respective storage functions $S_1(x_1)$ and $S_2(x_2)$ are C^1, then the equilibrium $(x_1, x_2) = (0, 0)$ of both interconnections is stable.

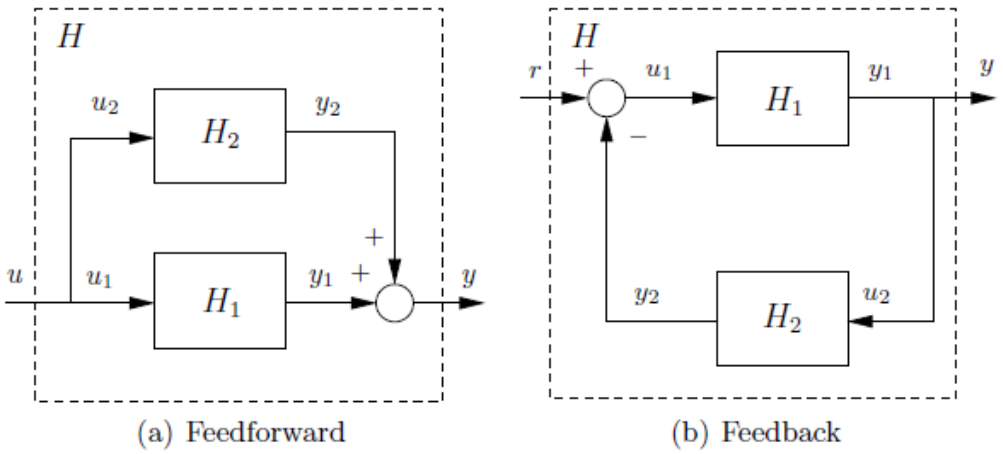

(a) Feedforward (b) Feedback

Figure 1.3.2: Interconnections of passive systems [4]

[1] the estimation of ζ is not in the scope of this thesis and should be the topic of future works

1.4 Port-Hamiltonian control

We have seen in the previous sections that the Hamiltonian representation has several advantages. Indeed, this representation is based on the physics of a real system and the storage of energy is taken explicitly into account. As there exists a bond-graph dual to a port-Hamiltonian representation, one can observe the causality and observability properties on the graph which is much more difficult for a non-physical state-space representation when the order of the model is not small. As the storage function is directly related to the passivity, and hence the stability of a system, it is possible to shape this storage function to obtain a passive closed-loop representation and derive corresponding control laws.
Hence, in this section, we will discuss another great advantage of Hamiltonian systems, namely, their ability to shape energy for control design. We will present some control techniques used in the theory of port-Hamiltonian systems and for HRES control.

1. **Passivity-based control**
   It has been demonstrated that Hamiltonian systems enjoy all the properties of passive systems [53]. We can therefore use the control techniques based on passivity.
   Considering the Hamiltonian system with dissipation represented in (1.4), this system can be stabilized asymptotically if we add an artificial "damping", starting from the following inequality of passivity:

$$\frac{d}{dt}H \leq u^T y, \tag{1.41}$$

   If what follows, "damping" is added by a simple output feedback $u = -y$, we will get:

$$\frac{d}{dt}H \leq -||y||^2. \tag{1.42}$$

   We can therefore prove the asymptotic stability from the result (1.42). However, attention must be paid to the observability condition of the zero state.

Example 1.4.1 *Considering the following Hamiltonian system:*

$$\begin{aligned}
\begin{bmatrix} \dot{p}_1 \\ \dot{p}_2 \\ \dot{p}_3 \end{bmatrix} &= \begin{bmatrix} 0 & -p_3 & p_2 \\ p_3 & 0 & -p_1 \\ -p_2 & p_1 & 0 \end{bmatrix} \begin{bmatrix} \frac{\partial H}{\partial p_1} \\ \frac{\partial H}{\partial p_2} \\ \frac{\partial H}{\partial p_3} \end{bmatrix} + \begin{bmatrix} g_1 \\ g_2 \\ g_3 \end{bmatrix} u, \\
y &= \begin{bmatrix} g_1 & g_2 & g_3 \end{bmatrix} \begin{bmatrix} \frac{\partial H}{\partial p_1} \\ \frac{\partial H}{\partial p_2} \\ \frac{\partial H}{\partial p_3} \end{bmatrix}.
\end{aligned} \tag{1.43}$$

with

$$H(p) = \frac{1}{2}(\frac{p_1^2}{I_1} + \frac{p_2^2}{I_2} + \frac{p_3^2}{I_3}). \tag{1.44}$$

Since $\dot{H} = 0$ *and the minimum of* H *is* $p = 0$ *then the equilibrium is stable. An addition of "damping" is carried out:*

$$u = -y = -g_1\frac{p_1}{I_1} - g_2\frac{p_2}{I_2} - g_3\frac{p_3}{I_3}. \tag{1.45}$$

It has been proved that this feedback makes it possible to have a convergence towards the largest set contained in:

$$\begin{array}{rcl} S: & = & \{p \in \mathbb{R}^3 | \dot{H}(p) = 0\} \\ & = & \{p \in \mathbb{R}^3 | g_1\frac{p_1}{I_1} + g_2\frac{p_2}{I_2} + g_3\frac{p_3}{I_3} = 0\}, \end{array} \tag{1.46}$$

we can prove that the largest set contained in S *is the origin if* $g_i \neq 0$ *for any* $i \in \{1, 2, 3\}$*. In this case we can say that the equilibrium point is asymptotically stable.*

2. **Control by Interconnection and Damping Assignment(IDA-PBC)**
It is possible to store only the energy of the system, i.e to find the control which allows to replace the Hamiltonian H with a new desired Hamiltonian H_d. However, this requires to solve the partial derivative equation,

$$\begin{bmatrix} g^{\perp}(x)[J(x) - R(x)] \\ g^T(x) \end{bmatrix} \frac{\partial H_a}{\partial x}(x) = 0. \tag{1.47}$$

called the "matching equation", which might not have a solution. These equations are subject to the dissipation obstacle [2], that is they might not be feasible when the dissipation matrix is nonzero. This problem can be overcome by the IDA-PBC method where a new junction matrix J_d is proposed. The rest of this part is largely based on the work in [66].

Theorem 1.5 *Consider the system (1.4) and the following closed-loop system*

$$\dot{x} = [J_d(x) - R_d(x)]\frac{\partial H_d}{\partial x}(x), \tag{1.48}$$

with $H_d(x) = H(x) + H_a(x)$*,* $J_d(x) = J(x) + J_a(x)$*,* $R_d(x) = R(x) + R_a(x)$ *where* $J_d(x) = -j_d^T(x)$ *and* $R_d(x) = R_d^T(x)$*. Consider a desired equilibrium point* x^**. We assume that we can find functions* $u(x)$ *and* $H_a(x)$ *and matrices* $J_a(x)$ *and* $R_a(x)$ *that fulfill following conditions:*

- *At the equilibrium point* x^* *we have:*

$$\frac{\partial H_a}{\partial x}(x^*) + \frac{\partial H}{\partial x}(x^*) = 0. \tag{1.49}$$

- *The Hessian of $H_a(x)$ at the equilibrium point x^* satisfies:*

$$\frac{\partial^2 H_a}{\partial x^2}(x^*) + \frac{\partial^2 H}{\partial x^2}(x^*) > 0. \tag{1.50}$$

Then the equilibrium point x^* will be a stable equilibrium of the closed-loop system described in (1.48). It will also have the property of asymptotic (local) stability if the largest invariant set contained in:

$$\{x \in \mathcal{X} \mid \frac{\partial H_d}{\partial x}(x) R_d(x) \frac{\partial H_d}{\partial x}(x) = 0\} \tag{1.51}$$

is equal to x^*.

Remark 1.5 *The difference between the IDA-PBC control and the control by energy-shaping and damping injection is that in the case of control by energy-shaping, we modify the dissipation matrix R(x), while in the IDA-PBC we modify both the resistive matrix R(x) and the interconnection matrix J(x) that link the system to the external environment. Otherwise, in both cases the Hamiltonian $H(x)$ of the system is shaped to the desired value $H_d(x)$.*

Remark 1.6 *The IDA-PBC method has been applied to the control of the PEM electrolyser described in chapter 2 and published in [67].*

1.5 Control of linear port-Hamiltonian systems

Let's consider the following linear port-Hamiltonian system:

$$\begin{cases} \dot{x} = (J - R)\,\bar{Q}x + gu \\ y = g^T \bar{Q} x \end{cases} \tag{1.52}$$

with quadratic storage function:

$$H(x) = \frac{1}{2} x^T \bar{Q} x \tag{1.53}$$

where, $J = -J^T$ is a skew symmetric matrix, $R = R^T \geq 0$, $\bar{Q} \geq 0$ is a symmetric $n \times n$ matrix, referred to as the energy matrix.
For:

$$\begin{cases} gu_d = (J - R)\,\bar{Q}x_d \\ v = u + u_d \end{cases} \tag{1.54}$$

we get, the following port-Hamiltonian system,

$$\begin{cases} \dot{x} = (J - R)\,\bar{Q}(x - x_d) + gv \\ y = g^T \bar{Q}(x - x_d) \end{cases} \tag{1.55}$$

To stabilize the system and ensure tracking control, we use, the following proportional controller:

$$v = -Ky = -Kg^T\bar{Q}(x - x_d) \tag{1.56}$$

by replacing the equation (1.56) in (1.55), we get,

$$\dot{x} = \left(J - R - gKg^T\right)\bar{Q}(x - x_d) \tag{1.57}$$

which is equivalent to,

$$\dot{x} = \left[J - \left(R + gKg^T\right)\right]\bar{Q}(x - x_d) \tag{1.58}$$

for K symmetric positive definite matrix.

The above results may be generalized to systems where $Q(x) = \hat{Q}(x)\bar{Q}$, with:

$$\begin{cases} \dot{x} = (J - R)\,\hat{Q}(x)\bar{Q}x + gu = \left(\hat{J} - \hat{R}\right)\bar{Q}x + gu \\ y = g^T\bar{Q}x \end{cases} \tag{1.59}$$

where:

$$\begin{cases} \hat{J} = J\hat{Q}(x) \\ \hat{R} = R\hat{Q}(x) \end{cases} \tag{1.60}$$

which for

$$\begin{cases} gu_d = \left(\hat{J} - \hat{R}\right)\bar{Q}x \\ v = u + u_d(x) \end{cases} \tag{1.61}$$

we get:

$$\begin{cases} \dot{x} = \left(\hat{J} - \hat{R}\right)\bar{Q}(x - x_d) + gv \\ y = g^T\bar{Q}(x - x_d) \end{cases} \tag{1.62}$$

So for $v = -Ky = -Kg^T\bar{Q}(x - x_d)$, we get:

$$\dot{x} = \left[\hat{J} - \left(\hat{R} + gKg^T\right)\right]\bar{Q}(x - x_d)\ . \tag{1.63}$$

Note that the system (1.63) is port-Hamiltonian if and only if:

$$\begin{cases} \hat{J} = -\hat{J}^T \\ \hat{R} = \hat{R}^T \geq 0 \end{cases} \tag{1.64}$$

The matrices $\tilde{J}$ and $\tilde{R}$ are obtained using a decomposition of a square matrix into symmetric and skew-symmetric matrices. Hence, for a square matrix $C_{n\times n}$, we can write,

$$C = \frac{1}{2}\left(C + C^T\right) + \frac{1}{2}\left(C - C^T\right) = A + B \tag{1.65}$$

where $A = A^T$ is symmetric and $B^T = -B$ is skew symmetric.

1.6 HRES port-Hamiltonian modeling and control

Like for bond graphs, few studies have been devoted to the port-Hamiltonian description of HRES through the literature and they generally consider just a part of the global system. Hence, in [68, 69] a wind turbine port-Hamiltonian model with a PMSG (Permanent Magnet Synchronous Generator) and DFIM (Doubly Fed Induction Motor), respectively, has been presented. In addition to the PH model, an energy shaping control has been applied to the system in [68]. Then, in [70] a PH model and an energetic control using the interconnection and damping assignment passivity based control technique of a hydrogen fuel cell with supercapacitors for applications with high instantaneous dynamic power has been presented. However, the fuel cell model is only static, where the FC voltage is described by a 5^{th} order polynomial function of the stack current. Otherwise, in [57] a PH model of a lift system micro-grid, composed of a solar panel, three-phase electrical network, a battery, a super capacitor, an (AC/DC, DC/DC) converter, a Salient Permanent Magnet Synchronous Machine (SPMSM) and mechanical system for different optimisation objectives in view of an efficient energy management within the microgrid system has been presented.

1.7 Energy routing and operating mode management

Regarding the operational complexity in the HRES that involves different generators and storage units, a global control strategy is needed to manage the power for the various components. The power management at the lower layer of HRES control consists of the collection of continuous control laws applied to each of the system components (power control, MPPT, etc.), in order to guarantee energy balance, voltage and frequency regulation [71] and the healthy operating conditions of the components by respecting the sources and storage system dynamics [72, 73].

There exist different power management strategies for HRES. Hence, in some works only one source is considered as a primary source with an MPPT algorithm while the other sources are controlled. Then, to satisfy the residual load power that corresponds to the difference between the generated power and the load power, Unit Power Control (UPC) and Feeder-Flow Control (FFC) [74] are used. The UPC strategy consists in extracting a constant power from a local storage/source which is usually a limited power source or sensitive for dynamic loads (for example batteries, FC/EL) and at the same time a secondary storage/source such as the grid is used to compensate the rest of the variable load profile which therefore protects and extends the lifetime of the sensitive storage components.

Another power management strategy for HRES, known as peak shaving strategy [75] or frequency based distribution [76], consists in managing the storage components each according to the HRES dynamical behaviour.
Depending on the weather conditions and dynamics of the devices, a HRES operates under different modes. For example, the wind turbine must be stopped at very high wind speed conditions and disconnected from the whole system. Hence, different configurations of the HRES can be considered and for which limitations and structure change. In [5] for example as in many other studies, an automaton is configured in order to manage the switching between the different operating modes of a multi-source platform. The system outputs consists of Boolean values (1/0) sent to the controlled junctions of the Event Driven Hybrid bond graph.

1.8 Conclusion

Multi-sources hydrogen-based HRES are clean and reliable alternative solutions for electrical power production in the future. The weather and seasonal dependency of the resources in addition to the dynamics of the storage devices generate different operating modes and different configurations of the platforms implying a drastic reconfiguration of the models description and control strategies. Hence, there is a need for reliable and flexible power management strategies and operating mode management. It is very important to rely on a model of the system that takes in consideration its multi-disciplinary hybrid aspect, simulates the different modes and allows to build control strategies.
Analytical equations used for the modeling of such systems is time consuming and limited over time because the hybrid physical aspect of the systems. The graphical modeling tools (GB, EMR, ..etc) are the most used tools so far since the models are built based on a common element between these different physical systems which is "Energy". In order to build explicit control laws which can be tuned directly from the systems' parameters, a state space representation of multi-physics systems is required. The port-Hamiltonian formalism is dual to bond-graphs and considers the energy storage of the system, port variables and is strongly related to passive systems.
A brief review of the application of these concepts to HRES has been provided, which shows that while some graphical representations as EMR have been widely used, works on bond-graphs or port-Hamiltonian systems are less widespread. However, the EMR formalism is able to provide only a general control structure while the port-Hamiltonian formalism supplies directly the control law and an insight on the tuning of control parameters. Indeed, it has been recalled that adequate control methods allow to shape the energy function, and change the

equilibrium while keeping the system stable. However, in this chapter, only the passivity property has been introduced, and one can wonder whether power reserves are enough to preserve an adequate behavior of the system with respect to disturbances or parametric uncertainties. This will be the core of our work, shown in chapters 3 and 4.

Chapter 2

Port-Hamiltonian modeling of a multi-source hydrogen platform

2.1 Introduction

In this chapter, the main goal is to elaborate a simplified port-Hamiltonian model of the multi-source renewable energy platform presented in the introduction. To achieve this representation, we first detail the different equipment of the platform, namely, the electrolyser, fuel cell, the renewable energy sources (solar panel, wind turbine), storage elements (battery) and the power converters.
The PH models are derived from the bond graph model for some equipment, based on the work in [5]. The interconnection of the platform's components in the port-Hamiltonian framework is also presented.
The results obtained in this chapter were the subject of two conference papers, where in [77] the port-Hamiltonian representation of the components of the platform has been addressed and in [67] a port-Hamiltonian model of the electrolyzer is presented in addition to a control strategy using the IDA-PBC control technique that is not presented in this thesis.

2.2 Presentation of the platform

The multi source renewable energy platform for hydrogen production and storage, see figure (2.2.1) , consists of the following elements:

1. Sources
   (a) A PMG WT with a DC 24 Volt
   (b) Two PV 200 Watt modules of 54 serial cells each, the two modules are set in parallel electrical configuration. The output of the PV modules is connected to 24 Volt DC bus through a DC/DC converter.
   (c) A PEM-FC of 36 cells generated power up to max 1500 Watt.

2. Storage elements
   (a) A battery bank (110 Ah) with DC 24 Volt.
   (b) Hydrogen storage bottles with max pressure of 11 bars.
3. A resistive load factor allowing load profiles to be modeled.
4. A PLC system which links the various components from the common DC bus and disconnects them.

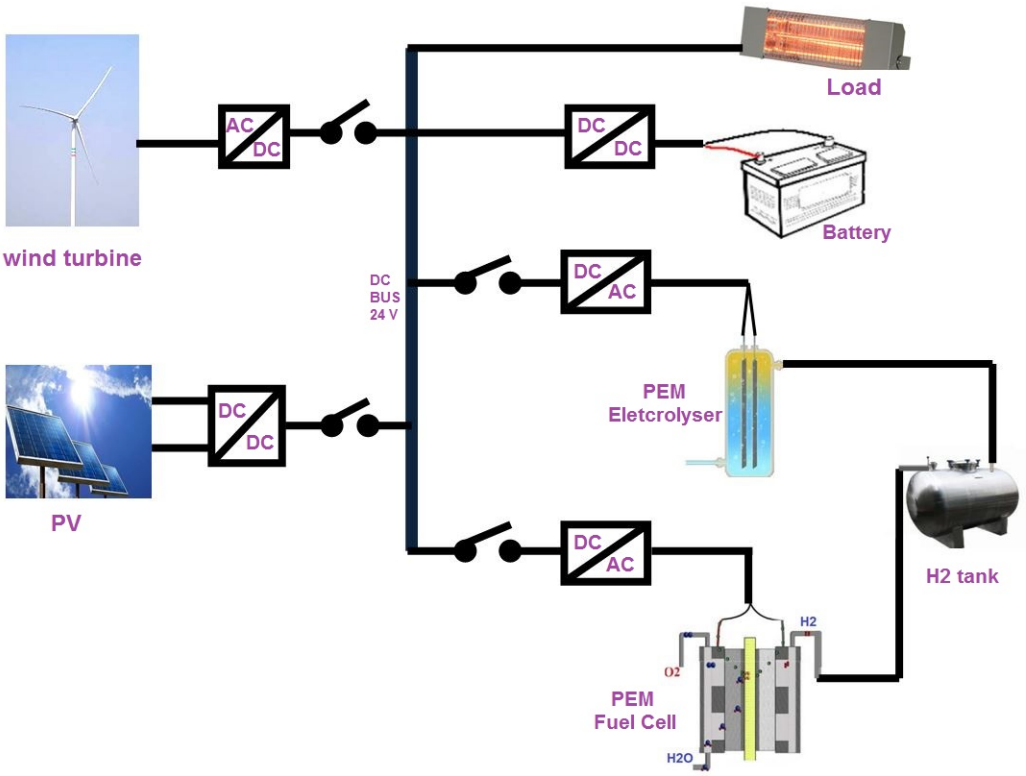

Figure 2.2.1: Multi-source renewable energy platform MODIS-H2

An electrolyzer is used to store the electrical energy excess in the form of hydrogen, in Metal Hydride Storage Canisters (MHS), in addition to the battery, see figure (2.2.2).
Electrical energy is produced by the inverse action of the electrolyzer, through the fuel cell, when there is a shortage of energy from the renewable resources.The intermittence of the renewable sources and the possible appearance of faults generates as many modes of operation which may be predictable or not.

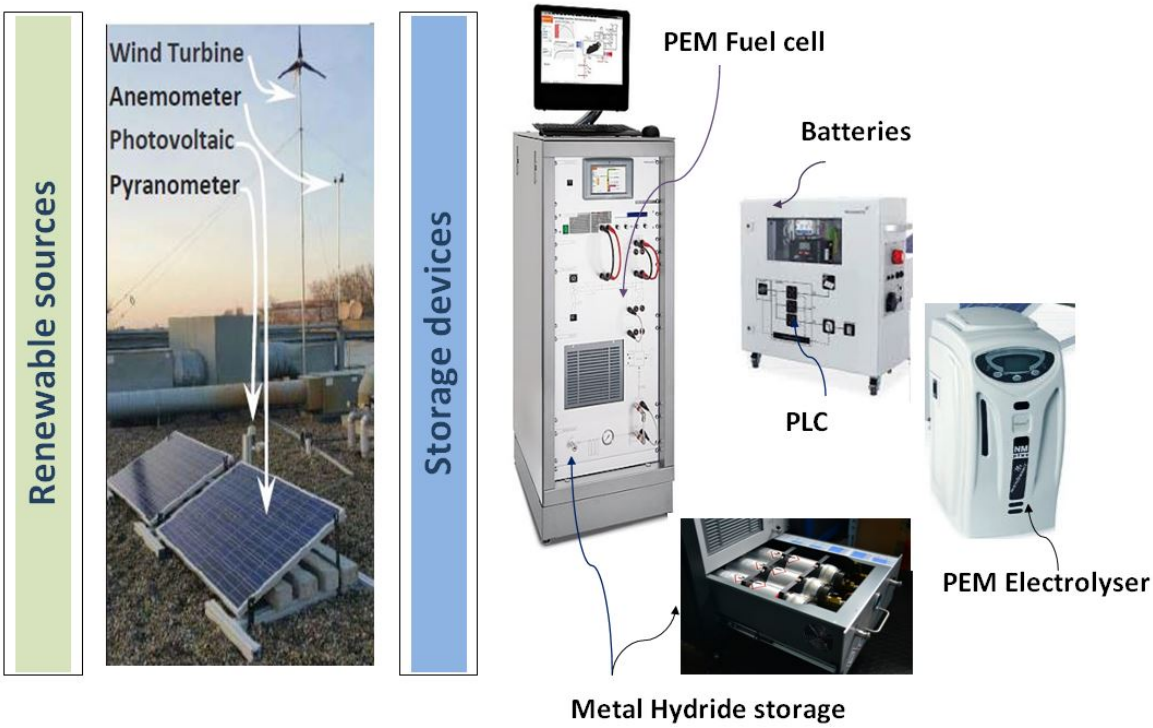

Figure 2.2.2: Platform structure

2.3 Port-Hamiltonian modeling of the hydrogen based-elements

2.3.1 Proton exchange membrane electrolyzer

PEM electrolyzer presentation

An electrolyzer is an apparatus, equipped with an electrolysis cell that allows to carry out chemical reactions in order to convert electrical energy into chemical energy.
The technique of separating the elements of chemical compounds is called **electrolysis** and it is used in different industrial processes, namely, the production of aluminium, electroplating, the production of dihydrogen by electrolysis of water, etc.
The electrolyzer inputs are voltage, temperature, pressure, water quantity and quality. The chemical reaction of the water and the voltage produces oxygen, hydrogen ions and electrons. In fact, the water separation occurs at the anode, such that oxygen gas is produced as well as hydrogen ions and electrons. The hydrogen ions travel to the cathode through the membrane, where they form hydrogen gas combined with the electrons that traveled from the anode through the outer circuit. Figure (2.3.1) summarizes the inputs and the outputs of the electrolyzer.

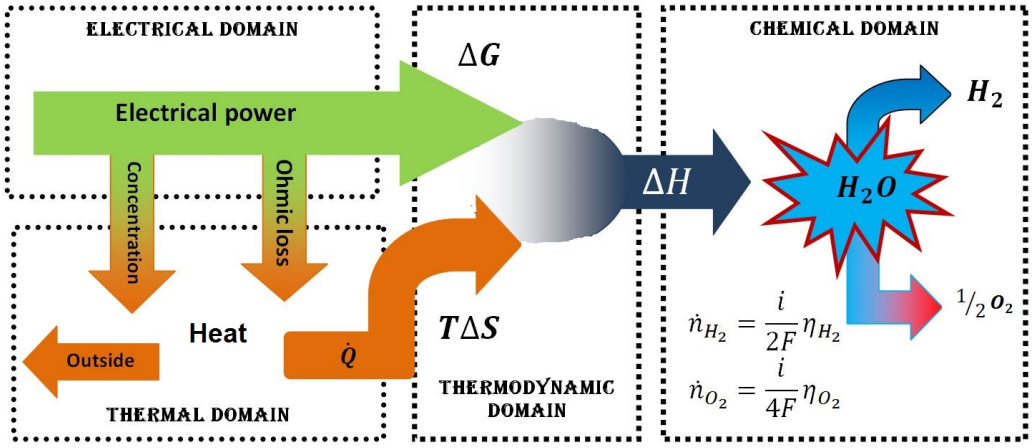

Figure 2.3.1: Electrolyzer inputs and outputs

Thermodynamically, the amount of the energy (per mole) needed for the electrolysis process, at temperature T, is represented by the enthalpy δH^0_T, see (2.3.1). This energy is needed in electrolysis in both electrical and thermal forms.The energy balance is given in the following equation :

$$\Delta \mathrm{H}^0_{(T)} = \Delta G^0_{(T)} + T\Delta S^0_{(T)} \tag{2.1}$$

$\Delta G^0_{(T)}$ is the Gibbs energy that represents the amount of useful reversible energy in a thermo-chemical reaction. In the electrolysis, Gibbs free energy represents the amount of the net electrical energy needed for the chemical process of the electrolysis without counting the losses. $T\Delta S^0_{(T)}$ is the amount of heat (thermal energy) involved in the reaction.$\Delta \mathrm{H}^0_{(T)}$ and $T\Delta S^0_{(T)}$ are temperature and pressure dependent.
In general, both are given in lookup tables in standardized conditions (STP) (1 atm, $25°C$) $\Delta \mathrm{H}^0_{(298)}$, $\Delta S^0_{(298)}$. Eq. (2.2) and Eq. (2.3) represent the temperature-based approximations of $\Delta \mathrm{H}^0$ and ΔS^0 in the neighbourhood of the standard temperature with the thermodynamic parameters defined in Table (2.1).

$$\Delta \mathrm{H}^0_{(T)} = \Delta \mathrm{H}^0_{(298)} + \alpha_{rec}\,(T - 298) + \frac{\beta_{rec}}{2}\left(T^2 - 298^2\right) + \frac{\gamma_{rec}}{3}\left(T^3 - 298^3\right) \tag{2.2}$$

$$\Delta S^0_{(T)} = \Delta S^0_{(298)} + \alpha_{rec} \ln\left(\frac{T}{298}\right) + \beta_{rec}\,(T - 298) + \frac{\gamma_{rec}}{2}\left(T^2 - 298^2\right) \tag{2.3}$$

By replacing the equations (2.2) and (2.3) in (2.1) we obtain the Gibbs free energy $\Delta \mathrm{H}^0_{(T)}$.
The approximation equations (2.2) and (2.3) are given at a fixed standard pressure P_0 (1 atm). Equation (2.4) includes a correction term for the open-current voltage

expression i.e ΔG^0, at any pressure defined as follows:

$$\Delta G^0_{(T,P)} = \Delta G^0_{(T,P_0)} + RT \ln\left(\frac{P_{H_2}}{P_O}\right) + RT \ln\left(\frac{P_{O_2}}{P_O}\right)^{0.5} \tag{2.4}$$

α_{rec}	-11.5575
β_{rec}	$3.9582\times\ 10^{-3}$
γ_{rec}	$3.9582\ \times\ 10^{-6}$

Table 2.1: General enthalpy coefficients [8]

Open-circuit voltage: Dividing by Faraday constant and the reaction involved electron number ($2e^-$), the enthalpy and Gibbs free energy can be written in form of electrical potential as shown in Eq.(2.5). The obtained expressions in Eq. (2.5) represent, respectively, the open-circuit electrical potential associated to the standard-pressure and its correction for any given pressure.

$$E_{rev(T,P)} = \frac{-\Delta G^0_{(T,P)}}{2F} = -\frac{\Delta G^0_{(T,P_0)}}{2F} - \frac{\delta G^0_{(P,P_0)}}{2F} \tag{2.5}$$

$$E_{rev(T,P)} = E_{rev(T,P_0)} + \delta E_{rev(P_0,P)} \tag{2.6}$$

Operating voltage: The reversible power is the net power used directly into the chemical process. In fact, their exist many losses between the electrolysis applied electrical power and the net power involved in the chemical reactions as shown in Fig. (2.3.1) . The losses can be illustrated in form of an increase in the electrolysis electrical potential between the cathode and the anode. Eq. (2.7) shows three types of dissipative phenomena during the electrolysis reactions [78], [79]:

1. The ohmic losses $\eta_{ohm}(i) = R_{ohm}\,|i|$
2. The activation losses $\eta_{act}(i) = \frac{RT}{2\alpha_{elec}} \ln\left(\frac{|i|+|I_n|}{I_0}\right)$
3. The ions transportation losses $\eta_{trans}(i) = \frac{RT}{2\beta_{elec}} \ln\left(1 - \frac{|i|}{I_{\lim}}\right)$

$$U_{EL,cell} = E_{rev(T,P)} + |\eta_{act}(i)| + |\eta_{ohm}(i)| + |\eta_{trans}(i)| \tag{2.7}$$

$\eta_{ohm}(i)$, $\eta_{act}(i)$ and $\eta_{trans}(i)$ represent the dissipated energies in form of heat, i is the current an dP the pressure

In the electrolysis, however, this heat contributes, partially or totally depending

on its amount to the reaction. In case where the generated heat has the same amount that is needed for the electrolysis i.e $|\eta_{act}(i)| + |\eta_{ohm}(i)| + |\eta_{trans}(i)| = T\Delta S^0_{(V)}$, the applied electrical potential is called the thermo-neutral potential $E_{tn_EL[V]} = \Delta G^0_{(V)} + T\Delta S^0_{(V)} = \Delta \mathrm{H}^0_{(V)} \cong 1.48V$.

PEM electrolyzer modeling

In [80, 81], a dynamic bond graph model of the electrolyzer has been supplied considering the different energies interacting in the system, under the hypotheses that the operating temperature and pressure are constant, considering pure gases and no parasitic phenomena except gas permeation (Crossover). Then, in [49], a global dynamic bond graph model of a 27 kW electrolyzer, with 2 stacks of 48 cells was presented. The model incorporates the thermofluidic, electrochimical and thermal domain of the electrolyzer. This is a novelty because other BG models of the electrolyzer represented only the electrochimical part of the stack. To build the model, the authors made some hypotheses, namely, the use of ordinary differential equations with lumped parameters, perfect mass flow sources of the pumps, chillers and fan and finally, an assumption that gases are ideal. In addition, the diffusion losses were not considered since they are occurring for high current density; the stack temperature was assumed to be homogeneous and the chemical reaction in the water electrolysis reaction endothermic.
In [23, 82] a causal ordering graph model of the electrolyzer was presented focusing on the electrical part and the pneumatic phenomenon of the electrolyzer. The model was exploited in the regulation loops of the stack voltage and hydrogen pressure with a real time test with the Hardware-In-The-Loop simulations.
In the framework of the graphical representation of the PEM electrolyzer, several studies have been undertaken using the EMR [27, 83, 23, 82]. In [83], the authors presented a model that includes the electrochimical, thermal, hydraulic and thermodynamic domain of the electrolyzer, imposing the current input of the electrolyzer in order to control the gas flows.
Dynamic and static simulation of the PEM electrolyzer has been the subject of many studies [84, 85, 86, 87, 88]. The first dynamic model has been presented by Gorgun [89], who proposed a representation of a PEM electrolyzer with 3 cells, under atmospheric conditions using Matlab/Simulink. The model has not been validated using a real PEM electrolyzer. In [90] a PEM model of the electrolyzer has been simulated to study the effect of the temperature and pressure variation on the cell performance and polarization.
In [23], an adequate empirical model is used to describe the characteristics of a given electrolyzer.

Bond graph model of a PEM electrolyzer

For our study case, the used electrolyzer is an NMH2 plus 500 model, see table (2). A bond graph model of the system has been elaborated in [5] as given in figure (2.3.2), where the system is supplied by a voltage source (Se:Ac) with a shunt resistance R_{sh_e} in series with an AC/DC converter (TF : ac/dc). X_1 is a controlled junction that receives an external signal and the modulated resistance r_{act} is controlling the input current to the electrolyzer.

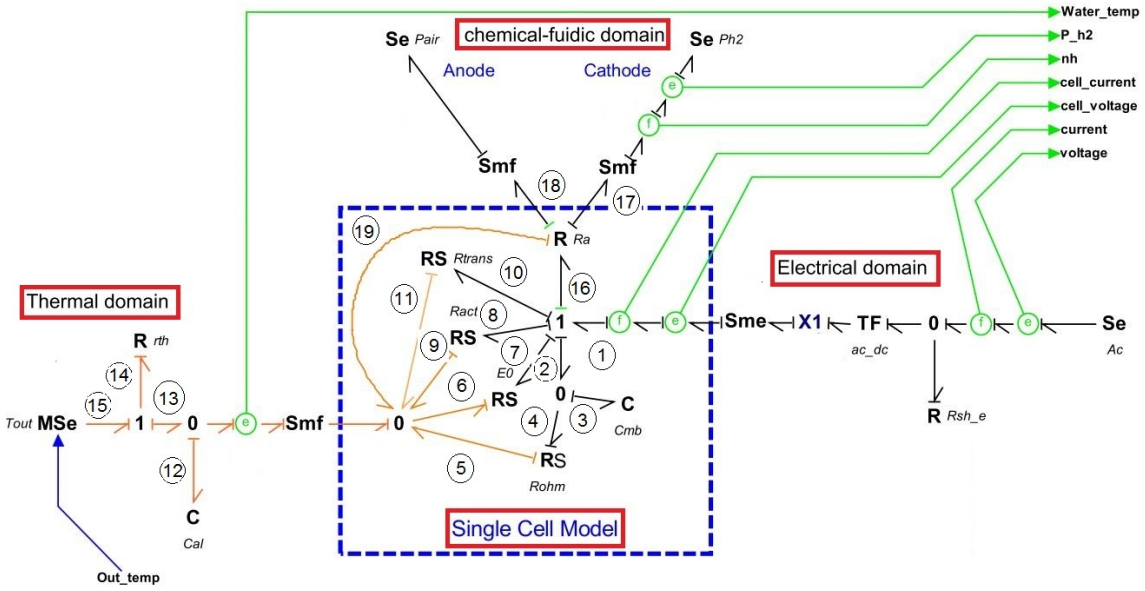

Figure 2.3.2: Bond graph model of the PEM electrolyzer

To take in consideration the electrolyzer's cell number (ns) mounted in series, its electrical voltage input is amplified using the S_{me} port. The S_{mf} ports in the chemical part are also in charge to increase the oxygen and hydrogen flow rates and the heat flow according to the number of cells.
The input power to the electrolyzer is subject to losses, represented by the R_{act}, R_{trans} and R_{ohm} resistances, which makes the net power less than the supplied one.
$R : R_a$ is a 4-port element. It links the chemical model with the electrical and the thermal models. It receives the electrical flow cell current as an input and injects the molar flow rate n_{h2} of the generated hydrogen. Thus, the presented model is a pseudo-BG in the fluidic domain where the product of the flow and effort is not a power.

The thermal dynamic of the EL [91] is represented by Eq.(2.8).

$$C_{cal}\frac{dT}{dt} = \sum_{i=1}^{n} \dot{Q}_i - T\Delta S - \dot{Q}_{ex} \tag{2.8}$$

- C_{cal} represents the global thermal capacity of the cell.
- $\dot{Q}_i$ are the heat fluxes generated by the resistive losses.
- $T\Delta S$ is the heat flux used in the chemical process.
- $\dot{Q}_{ex}$ is the heat flux emitted to the outside medium.

Assuming the temperature of the reaction is homogeneous, a 0 junction is used to collect the heat flows generated from the electrical losses $RS : R_{act}$, $RS : R_{ohm}$ and $RS : R_{trans}$. From this dissipated heat, through its thermal port, $R : E_0$ absorbs (input power bond) the required heat for the chemical process $T\Delta S^0_{(V)}$, see Eq. (2.2). In return, the temperature needed to calculate $\Delta G^0_{(V)}$ is communicated through the thermal port as an effort. The consumed electrical power at R : Ra is injected as flow into the thermal model via its thermal bond. In order to calculate $\delta E_{rev(P_0,P)}$, R : Ra needs the water temperature and both hydrogen and oxygen partial pressures. They are communicated as efforts respectively through the thermal, cathode and anode bonds. C_{mb} represents the double-layer capacity of the proton exchange membrane. X1 represents the controlled junction, it receives an external Xel On/Off signal.

Port-Hamiltonian model of the PEM electrolyzer

Based on the bond graph model of the PEM electrolyzer exposed in figure (2.3.2) and using the integral causality, the following equations which use equations (2.1)-(2.8) are obtained:

1. Thermal balance

$$\begin{aligned}
&e_{15} = T_{out} = MSe : T_{out} \\
&f_{12} = f_{13} + f_{19} + f_{11} + f_9 + f_5 - f_6 \\
&= \frac{1}{R_{th}}(T_{out} - \frac{1}{C_{cal}}q_{cal}) + f_1 + f_1 e_{10} + f_1 e_8 \\
&+ \frac{1}{R_{ohm}}(\frac{1}{C_{mb}}q_{mb} + \frac{1}{C_{cal}}q_{cal}) - f_1 e_7 \\
&f_{13} = f_{14} = \frac{1}{R_{th}}(e_{15} - e_{13}) = \frac{1}{R_{th}}(e_{15} - e_{12}) \\
&= \frac{1}{R_{th}}(T_{out} - \frac{1}{C_{cal}}q_{cal})
\end{aligned} \tag{2.9}$$

2. Electro-chemical domain

$$\begin{aligned} &f_1 = Se : I_{DC} = f_2; e_3 = \tfrac{1}{C_{mb}} q_{mb} \\ &f_4 = \tfrac{1}{R_{ohm}}(e_4 + e_5) = \tfrac{1}{R_{ohm}}(e_3 + e_5) \\ &e_5 = e_6 = e_9 = e_{11} = e_{12} = e_{13} = \tfrac{1}{C_{cal}} q_{cal} \\ &f_4 = \tfrac{1}{R_{ohm}}(e_3 + e_{12}) = \tfrac{1}{R_{ohm}}(\tfrac{1}{C_{mb}} q_{mb} + \tfrac{1}{C_{cal}} q_{cal}) \\ &f_3 = f_2 - f_4 = f_1 + \tfrac{1}{R_{ohm}}(\tfrac{1}{C_{mb}} q_{mb} + \tfrac{1}{C_{cal}} q_{cal}) \end{aligned} \tag{2.10}$$

The combination of the following equations generates the following pseudo PH system:

$$\begin{cases} \dot{q}_{mb} = -\frac{1}{R_{ohm}} \frac{q_{mb}}{C_{mb}} + \frac{1}{R_{ohm}} \frac{q_{cal}}{C_{cal}} + f_1 \\ \dot{q}_{cal} = -\frac{1}{R_{ohm}} \frac{q_{mb}}{C_{mb}} - \left(\frac{1}{R_{ohm}} + \frac{1}{R_{Th}} \right) \frac{q_{cal}}{C_{cal}} + f_1 + \frac{1}{R_{Th}} e_{15} \\ + f_1 e_8 + f_1 e_{10} - f_1 e_7 \\ y = \frac{\partial H}{\partial x} \end{cases} \tag{2.11}$$

where $H = \frac{1}{2} \frac{q_{mb}^2}{C_{mb}} + \frac{1}{2} \frac{q_{cal}^2}{C_{cal}}$ and the inputs are: $u = \begin{bmatrix} f_1 = I_{DC} \\ e_{15} = T_{out} \end{bmatrix}$, with: $e_8 = V_{act}(I_{DC})$, $e_7 = V_{ohm}(I_{DC})$ and $e_{10} = V_{conc}(I_{DC})$. q_{mb} is the electrical charge due to the phenomenon of double layer and $C_{mb} = \varepsilon \frac{S}{d}$ is the electrical capacity, S is the area of the electrodes, d the distance between the two electrodes and ε is a dielectric dependent constant.
Introducing the change of variable $h = f_1 + \frac{1}{R_{Th}} e_{15} + f_1 e_8 + f_1 e_{10} - f_1 e_7$, one obtains a port-Hamiltonian model, with $J = \begin{bmatrix} 0 & 1/R_{th}; & -1/R_{th} & 0 \end{bmatrix}$,
$R = \begin{bmatrix} 1/R_{th} & 0; & 0 & R_{th} + R_{ohm}/R_{th}R_{ohm} \end{bmatrix}$.
One of the main contributions that we published in [67, 77] is that the model is passive and truly port-Hamiltonian with respect to outputs q_{cal} , q_{mb} and inputs I_{DC} and V and Hamiltonian H. We called it pseudo port-Hamiltonian because it is not passive when considering initial inputs I_{DC} and T_{out}.
The PEM electrolyser specifications are given in table (2.2).

PEM Electrolyser	
Hydrogen flow rate STP (20 C, 1 bar)	Model NMH2 Plus 500 0-500 cc/min at STP
Max outlet pressure	11 bar
Power consumption	350 W
Input voltage	110 - 230 V / 50 - 60 Hz Max

Table 2.2: PEM electrolyser specifications

2.3.2 Proton exchange membrane fuel cell

PEM fuel cell presentation

A fuel cell is a voltage generation apparatus which converts chemical energy into electrical energy by oxidation on one electrode of a reducing fuel (for example dihydrogen), coupled to the reduction on the other electrode of an oxidant, such as the oxygen in the air. The oxidation reaction of hydrogen is accelerated by a catalyst which is generally platinum, see Figure (2.3.3).

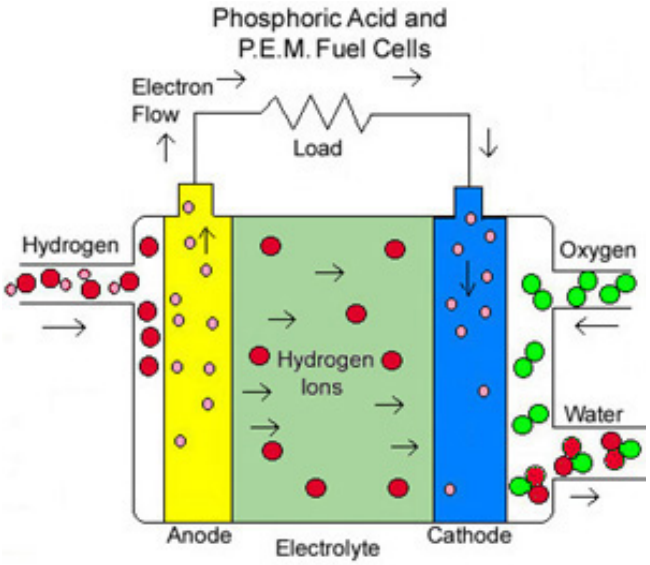

Figure 2.3.3: Operating principle of a fuel cell

The fuel cell reaction is a multi-domain process induced by coupled energetic phenomena including: electrical, chemical, thermodynamic and thermal domains, like the electrolyser system, see Fig (2.3.4).

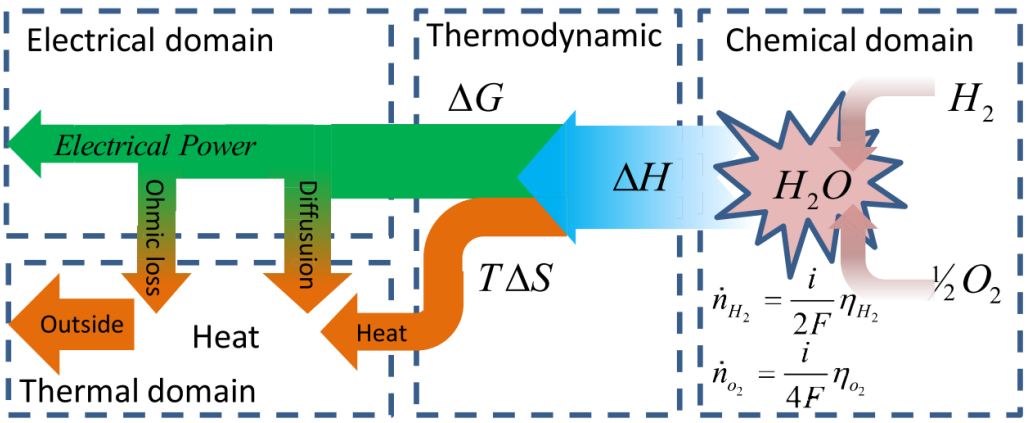

Figure 2.3.4: Fuel cell reaction balance [5]

Thermodynamically, the amount of the energy (per mole) produced in fuel cell, at temperature T, is represented by the enthalpy $\Delta H^0_{(T)}$, see Fig (2.3.4). This

energy is generated in the fuel cell in both electrical and thermal forms. Eq. (2.1) shows this energy balance.
In the fuel cell, Gibbs free energy $\Delta G^0_{(T)}$ represents the amount of the useful reversible energy in a thermo-chemical reaction. It represents the net electrical energy produced before any dissipation. As in the case of the electrolyser, $T\Delta S^0_{(T)}$ is the amount of heat (thermal energy) involved in the reactions.
By analogy to the electrolyser, a higher temperature in a FC means the energy balance showed in Fig. (2.3.4) is shifted to generate more heat, therefore the thermodynamic efficiency of the fuel cell decreases with high temperature.
The reversible power is the net power used directly into the chemical process. But, there are many losses between the extracted electrical power and the net power involved in the chemical reactions as shown in Fig. (2.3.4). The losses can be illustrated in form of a decrease in the fuel cell between the cathode and the anode as follows:

$$U_{FC,cell} = E_{rev(T,P)} - |\eta_{act}(I_{FC})| - |\eta_{ohm}(I_{FC})| - |\eta_{trans}(I_{FC})| \tag{2.12}$$

where, I_{FC} is the fuel cell current, T the temperature and P the pressure Based on the bond graph model of the PEM FC and the existing models in the literature we get the equivalent electrical circuit of the PEMFC of the figure (2.3.5).

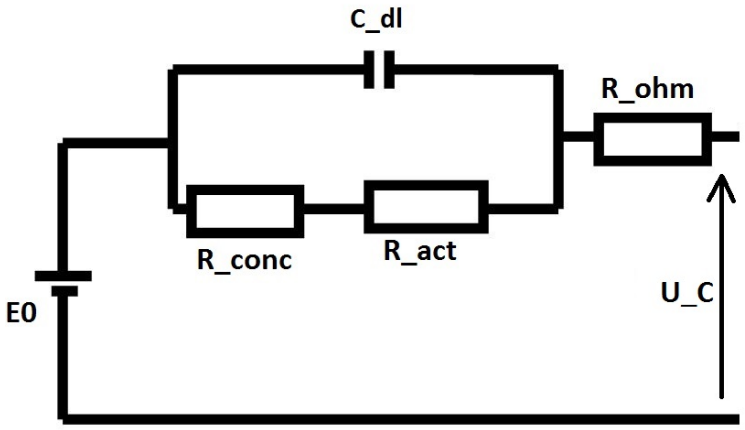

Figure 2.3.5: Equivalent electrical circuit of fuel cell

From the electrical circuit we get the following expressions:

$$U_C = E_0 - U_{conc} - U_{act} - U_{R\_ohm} \tag{2.13}$$

where:

- $E_0 = -\frac{\Delta G}{2F}$ is the reversible potential of cell at temperature T and atmospheric pressure, where ΔG is the Gibbs free energy.
- $U_{ohm} = n_c R_{ohm} I_{FC}$ the ohmic voltage drop caused by the ohmic losses in the

membrane and electrodes, where n is the number of the cells in series and I_{FC} the fuel cell current.

- $\eta_{act}(I_{FC}) = \frac{RT}{2\alpha_{elec}} \ln\left(\frac{|I_{FC}|+|I_n|}{I_0}\right)$ voltage drop of the activation losses, a phenomenon which is due to the kinetic reaction, where n_c is the number of the cells placed in series, A_{Taf} the Tafel constant, T the temperature and I_0 the exchange current and I_{FC} the current delivered by the fuel cell.
- $\eta_{conc}(I_{FC}) = \frac{RT}{2\beta_{elec}} \ln\left(1 - \frac{|I_{FC}|}{I_{\lim}}\right)$ the voltage drop of the concentration losses which are due to a loss of partial pressure as the species are consumed, a phenomenon that happens at high current, where n_c is the number of the cells in series, B the concentration constant, T the temperature and I_L the maximum current to consider.

Port-Hamiltonian model of PEM fuel cell

Fuel cell system performs the reverse function of the electrolyzer, see figure (2.3.6). The system is supplied by the hydrogen ($Se : P_{h_2}$) and oxygen ($Se : P_{O_2}$) pressure sources with a fixed cell-current for the thermal and electrical energy at the cell level, which is required to start the chemical reaction. The FC model considered in our study is a Nexa 1.2 KW, see Table (2).
In addition to the input parameter differences the $RS : E0$ element in the fuel cell is in charge of the injection of the generated thermochemical heat to the thermal sub-model.

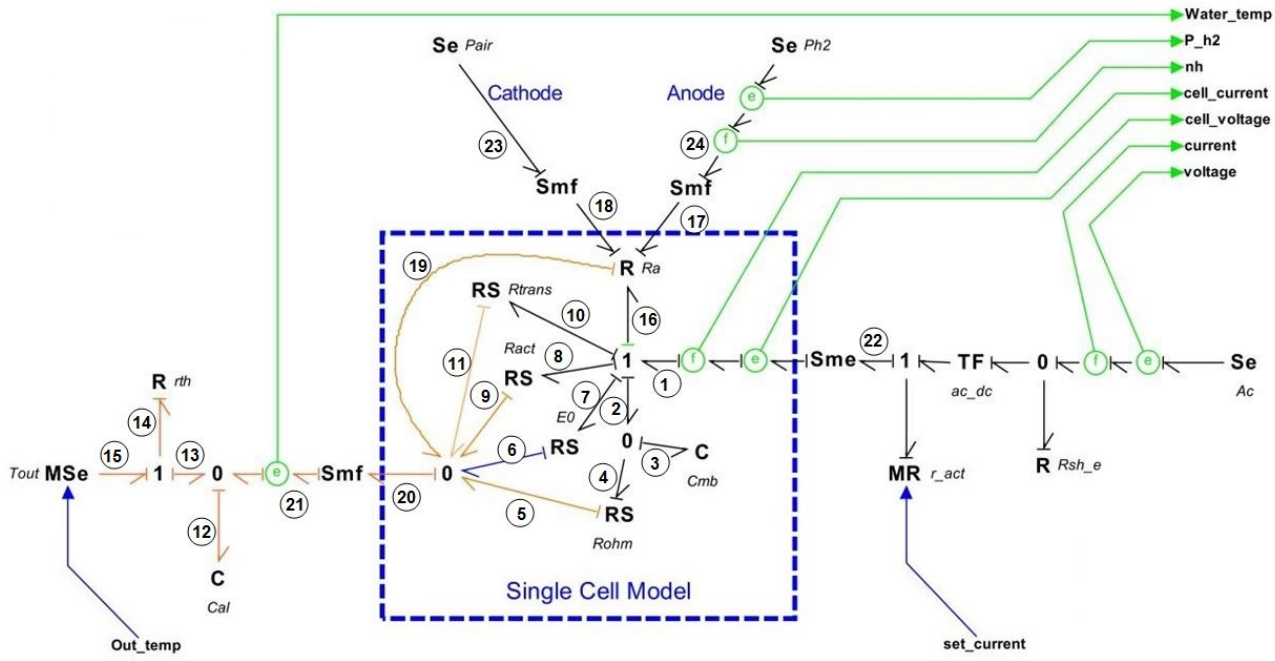

Figure 2.3.6: Bond graph model of the fuel cell [5]

Based on the bond graph model of the fuel cell as reported in figure (2.3.6), we derive the following equations description of the dynamic of the system.

$$
\begin{aligned}
&f_{13} = f_{14} = f_{15} = \tfrac{1}{R_{th}}\left(e_{15} - e_{12}\right) = \tfrac{1}{R_{th}}\left(T_{out} - \tfrac{q_{cal}}{C_{cal}}\right)\\
&n_s f_{20} = n_s(f_5 + f_6 + f_9 + f_{11} + f_{19}) = f_{21}\\
&f_{19} = \tfrac{1}{R_a} e_{12} = \tfrac{1}{R_a}\tfrac{q_{cal}}{C_{cal}}\\
&f_4 = \tfrac{1}{R_{ohm}}\left(e_3 - e_5\right) = \tfrac{1}{R_{ohm}}\left(\tfrac{q_{mb}}{C_{mb}} - \tfrac{q_{cal}}{C_{cal}}\right)\\
&f_5 = f_4 e_4 = \tfrac{1}{R_{ohm}}\left(\tfrac{q_{mb}}{C_{mb}} - \tfrac{q_{cal}}{C_{cal}}\right)\tfrac{q_{mb}}{C_{mb}}\\
&f_3 = f_2 - f_4 = I_{FC} - \tfrac{1}{R_{ohm}}\left(\tfrac{q_{mb}}{C_{mb}} - \tfrac{q_{cal}}{C_{cal}}\right)\\
&f_6 = \tfrac{e_7}{e_6} f_7 = \tfrac{E_0}{q_{cal}/C_{cal}} I_{FC}\\
&f_9 = \tfrac{e_8}{e_9} f_8 = \tfrac{V_{act}}{q_{cal}/C_{cal}} I_{FC}\\
&f_{11} = \tfrac{e_{10}}{e_{11}} f_{10} = \tfrac{V_{conc}}{q_{cal}/C_{cal}} I_{FC}\\
&f_1 = f_2 = f_7 = f_8 = f_{10} = f_{16} = I_{FC}\\
&e_{16} = e_{18} + e_{17} + e_{19} = P_{H_2} + P_{O_2} + \tfrac{q_{cal}}{C_{cal}}\\
&e_2 = e_3 = \tfrac{q_{mb}}{C_{mb}}\\
&u_{FC} = e_1 = e_{16} + e_{110} + e_8 + e_7 + e_3 = P_{H_2} + P_{O_2} + \tfrac{q_{cal}}{C_{cal}} + \tfrac{q_{mb}}{C_{mb}} + V_{act} + V_{conc} + E_0
\end{aligned}
\tag{2.14}
$$

u_{Fc} represents the output voltage of the fuel cell. the inputs vector is:

$$
U = \begin{bmatrix} e_1 = I_{FC} \\ e_{15} = T_{out} \\ e_{18} = P_{O_2} \\ e_{17} = P_{H_2} \end{bmatrix} \tag{2.15}
$$

and:

$$
\begin{aligned}
E_0 &= n_s\left(\tfrac{-\Delta G^0}{2F}\right)\\
V_{act} &= a_0 + Ta + Tb\ln(I_{FC})
\end{aligned}
$$

then, we have:

$$
V_{conc} = -\frac{RT}{eF}\ln\left(1 - \frac{I_{FC}}{I_L}\right)
$$

From the equations above, we deduce the following port-Hamiltonian representation of the PEM FC system:

$$
\begin{bmatrix} \dot{q}_{mb} \\ \dot{q}_{cal} \end{bmatrix} = \begin{bmatrix} -\frac{1}{\mathrm{R_{ohm}}} & 0 \\ 0 & \frac{1}{\mathrm{R_{th}}} \end{bmatrix} \begin{bmatrix} \frac{\mathrm{q_{mb}}}{\mathrm{C_{mb}}} \\ \frac{\mathrm{q_{cal}}}{\mathrm{C_{cal}}} \end{bmatrix} + \begin{bmatrix} 1 & 0 \\ h & \frac{1}{\mathrm{R_{th}}} \end{bmatrix} \begin{bmatrix} I_{FC} \\ T \end{bmatrix} \tag{2.16}
$$

where, I_{FC} the load electrical current, q_{mb} (C) the system state that represents the electrical charge relative to the phenomenon of double layer, that can be observed during transients, due to the accumulation of electrons on the electrodes, q_{cal} the

second state of the system that represents the thermal energy quantity (J), C_{mb} is an electrical capacitor (F), C_{cal} a thermal capacity $(J/K.Kg)$, R_{th} a thermal resistance (K/W), R_{ohm} the membrane resistance (ohm) , $h = f_1 + \frac{1}{R_{Th}}e_{15} + f_1e_8 + f_1e_{10} - f_1e_7$ represents the sum of the entropy at the zero junction that links the electrical, thermal and fluidic domains.
The FC model specifications are given in table (2.3).

PEM Fuel Cell	
FC model	Nexa 1.2 kW
H_2 pressure	0.3 - 0.5 bar
Power	1200 W
Output voltage	40-20 V/DC

Table 2.3: Fuel Cell model specifications

2.3.3 Hydrogen storage tank

Hydrogen tank's definition

A hydrogen tank, also called cartridge or canister is a metal container used to store hydrogen for portable applications, in-house and in-board storage, see figure (2.3.7). The main materials used inside the container are the aluminum alloy or stainless steel, depending on the hydrogen storage form, namely, gaseous, liquid or solid form, knowing that the hydrogen gaseous storage form at high pressure is a mature technique which is the most used to store hydrogen nowadays. It is more and more adopted by industrial, especially when hydrogen is transported.
The metal tank for the hydrogen storage must satisfy some criteria, namely, the density of storage, that must be as high as possible, the quick locking of the tanks, flexibility in the tank size and the capacity of storing at low temperature.

Figure 2.3.7: Metal Hydride Storage Canisters

The gaseous form of the hydrogen has to be extracted from the molecules that contain it, such as water and organic compounds.

Hydrogen storage tank modeling

In our research work, we are interested in the metal hydride storage form of the hydrogen and the used metal hydride storage canisters are with a hydrogen capacity storage of 800 NI ($20°C$ and 25 bar), from Heliocentris Academia GmbH, that allow safe and compact storage of relatively large amounts of hydrogen at low pressures. Heliocentris' metal hydride storage canisters can store a multiple amount of hydrogen in comparison to a pressure storage at low pressure [92], see figure (2.3.7).
The mathematical description of the hydrogen storage tanks, under different assumptions, have been the subject of several studies [93, 94, 95, 96], considering one [97, 98], two [99] and three [100] dimensional models. The gas motion and the initial parameters which are the initial temperature and pressure have been considered in experimental studies to determine the effective thermal conductivity and the conductance inside the reactor, see [101, 102, 103, 104].
In [105] a review on the metal hydride description has been presented. Based on this study, there are two methods to hydride a metal, the direct dissociative chemisorption and the electrochemical splitting of water, under the following reaction:

$$\begin{aligned} M + \tfrac{x}{2} H_2 &\leftrightarrow MH_x \\ M + \tfrac{x}{2} H_2O + \tfrac{x}{2} e^- &\leftrightarrow MH_x + \tfrac{x}{2} OH^- \end{aligned} \tag{2.17}$$

where M is the metal.

Bond graph modeling the metal hydride

The bond graph modeling of the metal hydride, under a low pressure, has not been widely addressed in the literature. A simplified bond graph model of the hydrogen tank under a maximum pressure of 10 bar has been presented in [5], see figure (2.3.8). The model considers the tank's storing capacity $C : ch_2$ which depends on the tank Volume (V) and temperature (T) with the hydrogen molar flow $f_{H_2} = \dot{n}_{H_2}$ as the input to the system and the storage pressure P_{H_2} as the output . The model considers the leak resistance, present in the bottles which is represented by $R : rv$.
In order to get the output storage pressure in bars, the recovered storage pressure in the atmospheric pressure is multiplied by the gain K.

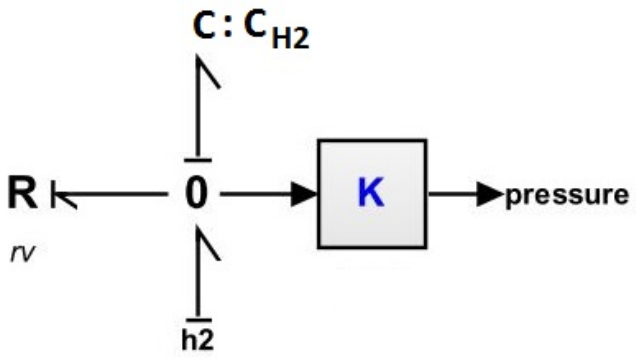

Figure 2.3.8: Bond graph model of the hydrogen storage tanks[5]

Port-Hamiltonian model of the hydrogen storage tank

Based on the bond graph model of the hydrogen tank given in figure (2.3.8), we deduce the following port-Hamiltonian representation of the system,

$$\begin{cases} \dot{q}_{C_{H2}} = \left[-\frac{1}{r_v}\right] \frac{q_{C_{H2}}}{C_{H2}} + N_{H2} \\ y = \frac{q_{C_{H2}}}{C_{H2}} \end{cases} \tag{2.18}$$

where, qc_{h2} is the state that represents the hydrogen molar flow, $C_{H2} = V_{tank}/(RT_{tank})$ is the storage capacity that depends on the volume and temperature of the hydrogen tank, N_{H2} is the input which represents the hydrogen molecular flow, r_v is the leak of resistance. The Hamiltonian $H = \frac{1}{2}\frac{q^2_{C_{H2}}}{C_{H2}}$ represents the chemical energy of the tank system.

2.4 Port-Hamiltonian modeling of the power sources and storage elements

2.4.1 Photovoltaic

Solar panel's definition

A solar panel is a device designed to transform solar radiation into heat or electrical energy using solar energy based on solar thermal collectors or photovoltaic, see figure (2.4.1). The solar panels are classified according to their rated power output in Watts which corresponds to the amount of power the solar panel would be expected to produce in 1 peak sun hour.

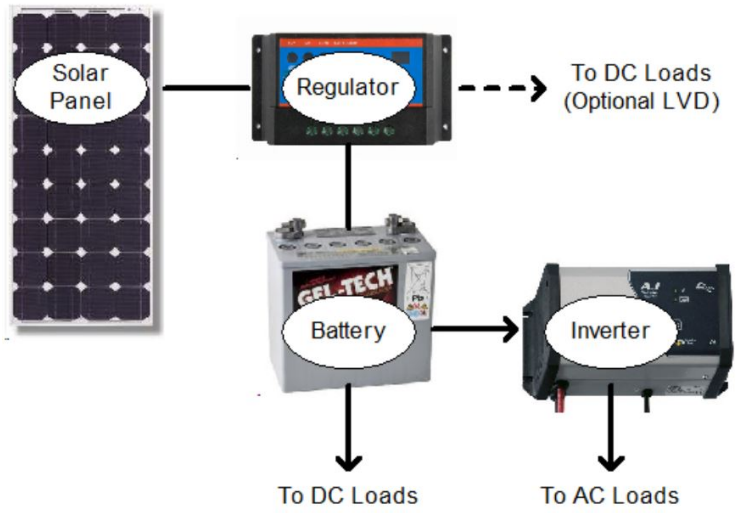

Figure 2.4.1: Solar panel

Solar panels can be wired in series or in parallel to increase voltage or current respectively. Their output changes with the cell operating temperature. Panels are rated at a nominal temperature of $25°C$. The output power of a typical solar panel can be expected to vary by 2.5% for every $5°C$ variation in temperature. As the temperature increases, the output power decreases.

Solar panel regulator and inverter

Solar regulators or charge controllers as they are also called are used to regulate the current from the solar panels to prevent the batteries from overcharging that causes gassing and loss of electrolyte resulting in damage to the batteries. They are rated by the amount of current they can receive from the solar panels
Most solar regulators also include a Low Voltage Disconnect feature, which switches off the supply to the load if the battery voltage falls below the cut-off voltage, see figure (2.4.1). This prevents the battery from permanent damage and reduced life

expectancy. In the other side, an inverter is a device that converts the DC power in a battery to AC electricity. Inverters come in two basic output designs, pure sine wave and modified sine wave (square wave). They are generally rated by the amount of AC power they can supply continuously.

Solar panel modeling

The literature is rich of studies devoted to the photovoltaic solar panels [106, 107, 108] and the most widespread equivalent electrical circuit of the panel solar is reported in the figure (2.4.2).

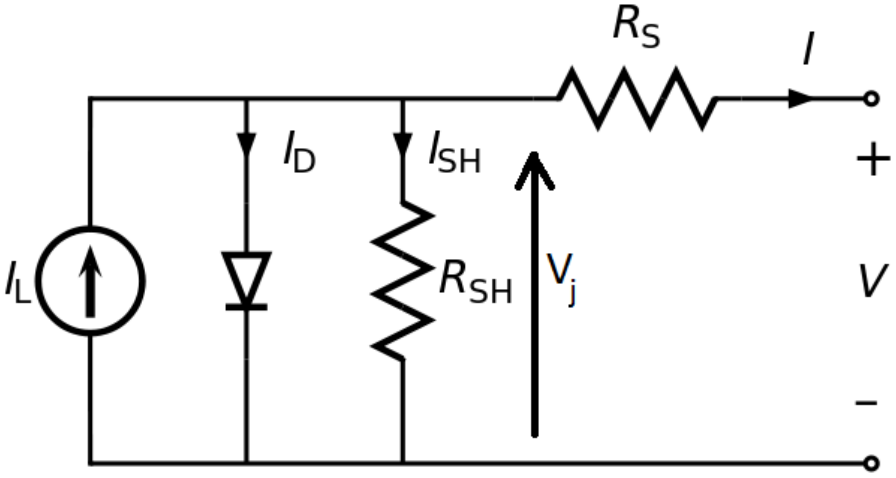

Figure 2.4.2: Basic equivalent electrical circuit of the PV

From the electrical circuit we get the following equations that describe the phenomena inside the system. To begin with the output current of the panel (I) equals the photogenerated current I_L to which we subtract the current that goes through the diode I_D and the current going through the shunt resistor (I_{sh}), expressed as follows:

$$I = I_L - (I_D + I_{sh}) \tag{2.19}$$

The diode current is given by the Shockley diode equation:

$$I_D = I_0 \left[\exp \left[\frac{V_j}{nV_T} \right] - 1 \right] \tag{2.20}$$

where: I_0 is the reserve saturation current, n the diode ideality factor which is equal to 1 is the ideal case, q the elementary charge, k the Boltzmann's constant, T the absolute temperature and $V_T = kT/q$ the thermal voltage which equals 0.0259 for $T = 25°C$ and the current resistance is given by:

$$I_{SH} = \frac{V_j}{R_{SH}} \tag{2.21}$$

where R_{SH} is the shunt resistance and v_j is the voltage across the diode, given by the equation:

$$V_j = V + IR_S \tag{2.22}$$

with V_j the voltage across the diode and resistor, V the voltage across the output terminals, I the output current and R_S the series resistance.
By combining the equations above, we get the characteristic equation of a solar cell that incorporates the solar cell parameters, the output current and voltage, as follows:

$$I = I_L - I_0 \left[exp \left[\frac{V + IR_S}{nV_T} \right] - 1 \right] - \frac{V + IR_S}{R_{SH}} \tag{2.23}$$

There are different methods to solve the equation (2.23) resulting in different approximation mathematical models. Hence, the above characteristic equation is commonly used in nonlinear regression to measure the I_0, n, T_S and R_{SH} parameters since they can not be measured directly [109].

Solar panel bond graph modeling

Among the different bond graph models of the solar panel that exist in the literature, we exploited the model developed in [5]. The model represents a polycrystalline NeMo solar panel from Heckert Solar, composed of 54 cells in series. The model consists of a photo-current source I_{ph} in parallel with a diode d and a shunt resistance R_{sh}, the whole in series with a resistance R_S. The bond graph model is given in figure (2.4.3), where only one single cell connected to a DC/DC converter via a 54 amplification factor is represented. The effort amplifier Sme is used to simulate the 54 cells in series.

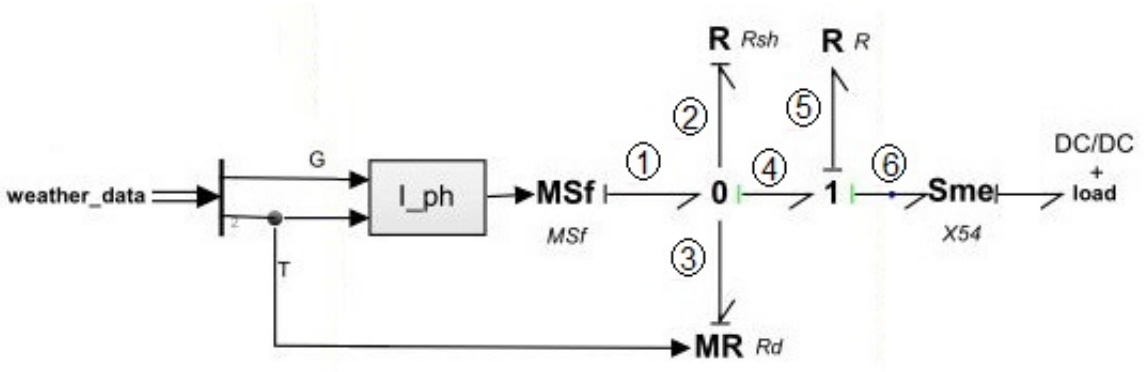

Figure 2.4.3: Bond graph model of the solar panel[5]

The PV model specifications are given in table (2.4) and its polarization curve in figure (2.4.4).

Heckert Solar	Polycrystalline	Nemo54P220 7
STC 1000 W/m^2, 25 C °, 1.5 AM	U_{OC}	33.77 V
P_{MPP} 220 W p (±2.5 W p)	I_{SC}	8.62 A
U_{MPP} 27.54 V	δI_{SC} 0.05 %/°K	4.335 10{-3} V/°K
I_{MPP} 8.08 A	δU_{OC} - 0.32 %/°K	0.108 V/°K

Table 2.4: PV specifications

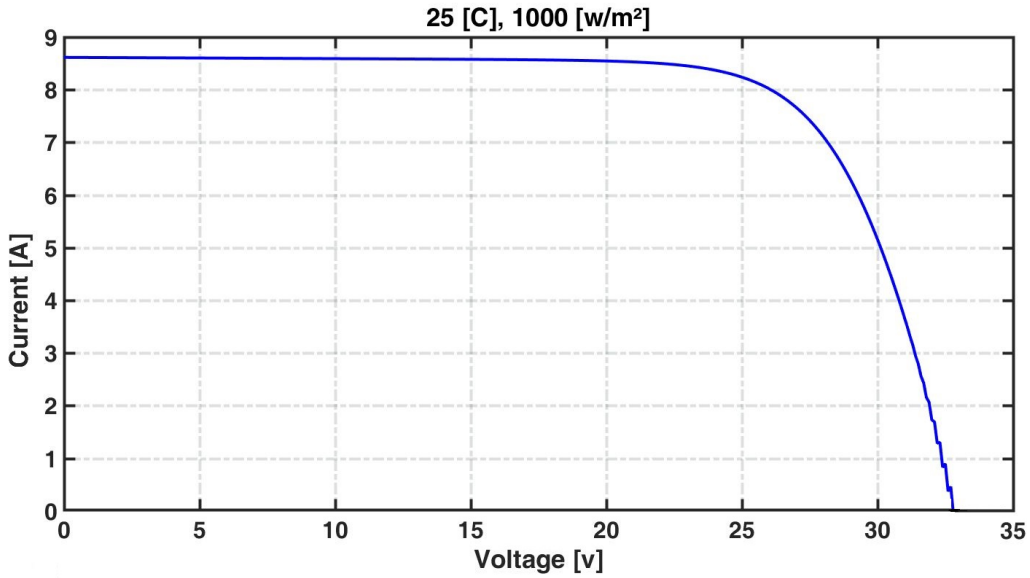

Figure 2.4.4: PV polarization curve

The output of the system which is the cell current is given in the following form:

$$f_6 = I_{Cell} = I_{Ph} - I_{sat}\left(\exp^{\frac{V_{Cell}+R_S I_{Cell}}{V_{Th}}}\right) - \frac{V_{Cell}+R_S I_{Cell}}{R_{Sh}} \tag{2.24}$$

For the PV model we only used a static representation of the system and not a port-Hamiltonian representation.

2.4.2 Wind turbine

Wind turbine definition

A wind turbine is a mechanical system that converts a part of the captured kinetic energy of the wind into a torque that ensures the rotation of the rotor blades, see figure (2.4.5). One can not extract all the power from the wind. Hence, the power obtained from a WT is always restricted by a theoretical peak limit of 59% (Betz limit). The aerodynamic efficiency coefficient C_p often refers to this power extraction effectiveness between the wind kinetic energy and the extracted mechanical power. This latter primarily relies on the aerodynamic characteristics, the airfoil

and the ratio of the incident wind speed V_w to the WT blade rotation speed.

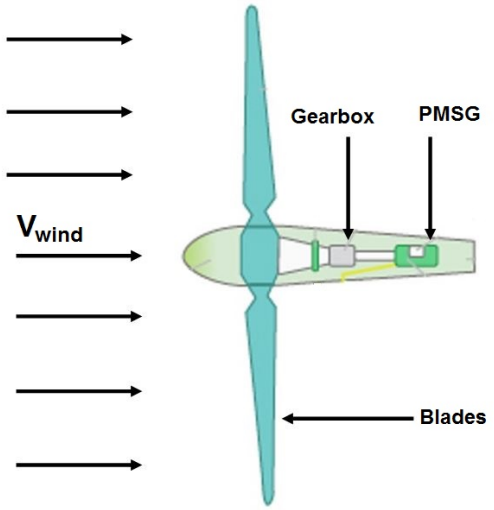

Figure 2.4.5: Wind turbine with a PMSG

Different kinds of generators can be combined with a turbine, generally a double fed induction generator (DFIG); for a small system as the turbine in our platform, a permanent magnet synchronous generator (PMSG) can be enough.
The mechanical transmission modeling between the wind turbine and the PMSG as described in figure (2.4.6) can be obtained by applying the fundamental principle of the dynamics of a system in rotation,

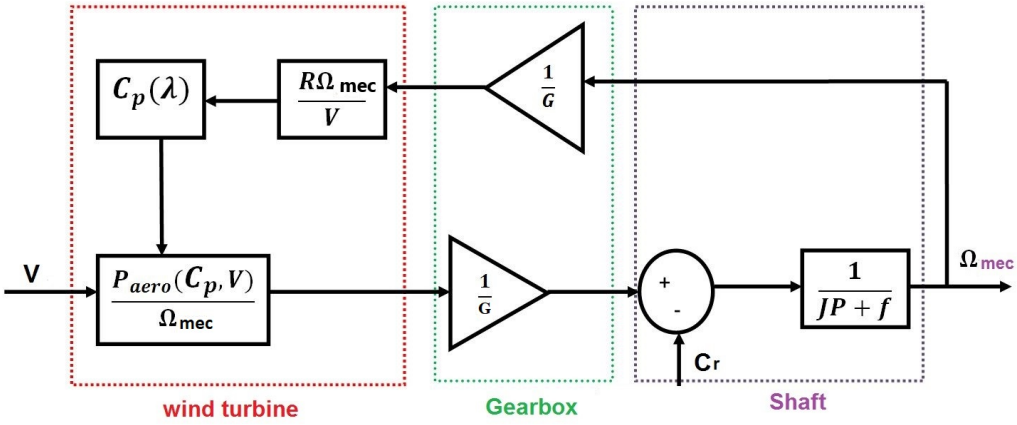

Figure 2.4.6: Block diagram of the wind turbine transmission system

$$J\frac{d\Omega_{mec}}{dt} = C_{aero} - C_r - C_{vis} \tag{2.25}$$

where, V is the wind speed, R the radius, $C_p(\lambda)$ the power coefficient, λ is the tip speed ratio, Ω_{mec} is the wind turbine rotation speed $[rad/s]$, C_{aero}, C_r $[N.m]$ and $C_{vis} = f\Omega_{mec}$ are respectively the aerodynamic torque from the wind turbine,

resistive torque or the machine and the viscous torque. $J = \frac{J_{mec}}{G^2} + J_{mec}$ is the total inertia of the wind turbine and the generator rotor.

$$P_{aero} = \frac{1}{2} C_p(\lambda) \rho \pi R^2 V^3 \tag{2.26}$$

$$C_{aero} = \frac{P_{aero}}{\Omega_{mec}} = \frac{C_p(\lambda) \rho \pi R^2 V^3}{2\Omega_{mec}} \tag{2.27}$$

$$\begin{aligned} C_p = {} & 7.9563 * 10^{-5} * \lambda^5 - 17.375 * 10^{-4} * \lambda^4 + 9.86 * 10^{-4} * \lambda^4 + \\ & 9.86 * 10^{-3} * \lambda^3 - 9.4 * 10^{-3} * \lambda^2 + 6.38 * 10^{-2} * \lambda + 10^{-3} \end{aligned} \tag{2.28}$$

Bond graph model of PMSG Wind turbine

The wind turbine is assumed to display a direct connection between the wind turbine and the $PMSG$ (Permanent Magnet Synchronous Generator), see figure (2.4.7).

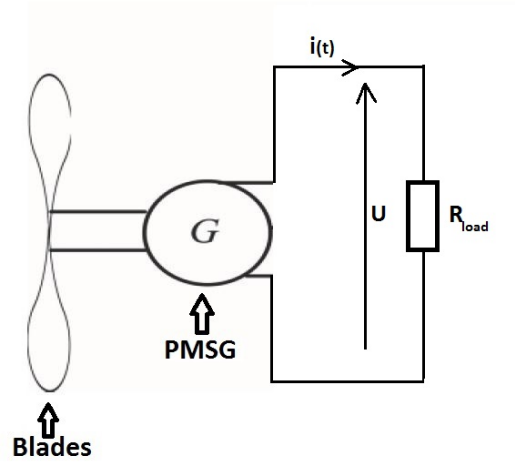

Figure 2.4.7: Equivalent electrical circuit of the wind turbine proposed model

The bond graph model of a wind turbine with a PMSG as given in figure (2.4.8) is developed in [5], where the input of the system is the incident wind velocity ($MSf : v_m$). The wind speed is transformed into a mechanical torque $T_{mech} = r_{GY}.f_{wind}$, using a gyrator which transforms flow into effort according to $r_{GY} = C_p.P_{wind}/v_w$. The inertia of the system, the friction viscosity of the bearings and the stator resistance are respectively presented by $I : m_r$, $R : f_r$ and $R : d$. the disconnection of the turbine from the DC bus is released using its generator which plays the role of an electromagnetic brake by reducing the rotation speed.

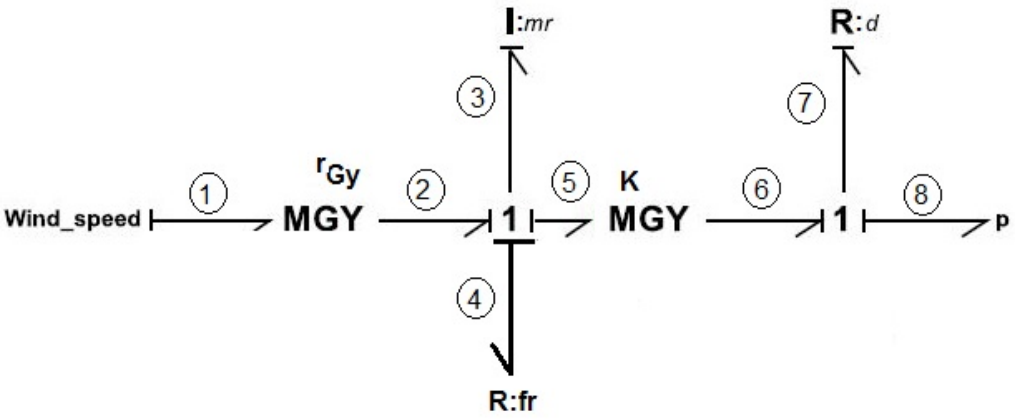

Figure 2.4.8: Bond graph model of the wind turbine [5]

The studied wind turbine model specifications are given in table (2.5) and the the parameter C_p for the MPPT controller is given in figure (2.4.9).

Primus	Air 40 24 $[V]$
Rotor Diameter	1.17 $[m]$
Wind speed	3.1 - 22 $[m/s]$
Alternator	PM brush-less
Startup Wind Speed	3.1 $[m/s]$
Voltage	24 $[VDC]$

Table 2.5: Wind turbine specifications

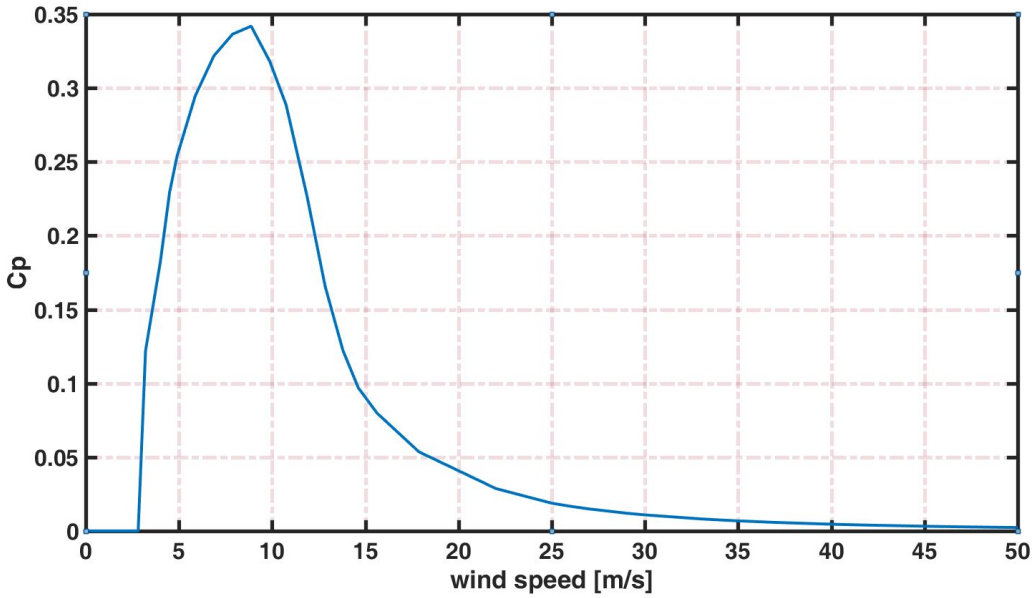

Figure 2.4.9: Wind turbine Cp in function of the wind speed

Port-Hamiltonian model of PMSG Wind turbine

From the bond graph model of the wind turbine reported in figure (2.4.8), we can write the following equations:

$$\begin{array}{l} f_1 = V_w \\ e_1 = r_{Gy} f_3, e_2 = r_{Gy} V_w, e_4 = f_r f_3, e_5 = K f_6 = K f_7 \\ e_3 = e_2 - e_4 - e_5 = r_{Gy} V_w - f_r f_3 - K f_7, e_7 = e_6 - e_8 = K f_3 - U_{bat} \\ f_7 = \frac{1}{d} e_7 = \frac{K}{d} f_3 - \frac{1}{d} U_{bat} \end{array} \tag{2.29}$$

Finally we get

$$\begin{array}{l} e_3 = -\left(f_r + \frac{K^2}{d}\right) f_3 + r_{Gy} V_w + \frac{K}{d} U_{bat} \\ f_3 = \frac{1}{m_r} \int e_3 dt \end{array} \tag{2.30}$$

and the dynamic port-Hamiltonian model extracted from the bond graph model through the given equations is given in the following form:

$$\left\{ \begin{array}{c} \dot{p} = -\left(f_r + \frac{K^2}{d}\right) \frac{p}{m_r} + r_{Gy} v_w + \frac{K}{d} U_{bat} \\ y = r_{Gy} \frac{p}{m_r} \end{array} \right. \tag{2.31}$$

where, the angular momentum p relative to the inertia $I : m_r$ is the state, m_r, f_r and d, represents respectively, the inertia of the system, the friction viscosity of the bearings and the stator resistance, $r_{GY} = C_p.P_{wind}/v_w$ is the gyrator which transforms flow into effort, v_w is the wind speed, P_{wind} the wind power, C_p is the ratio between the extracted power to the incident wind kinetic power and K is the DC generator transformation. $H = \frac{1}{2}\frac{p^2}{m_r}$ represents the Hamiltonian of the system which is its kinetic energy of rotation. U_{bat} is the voltage imposed by the bus (24V);

2.4.3 Battery

Lead-acid battery

The most commonly used storage technology in HRES and Hybrid Electrical Vehicles (HEV) are the conventional lead-acid batteries, with a gradual improvement in batteries based on lithium. Batteries are a short-term storage device with mild weight-to-weight capability.
The lead acid batteries (see figure (2.4.10)) consist of flat lead plates immersed in a pool of electrolyte. They are composed of several single cells connected in series. Each battery cell consists of two lead plates a positive plate covered with a paste of lead dioxide and a negative made of sponge lead, with an insulating material (separator) in between. The plates are enclosed in a plastic battery case and then submersed in an electrolyte consisting of water and sulfuric acid, [6, 110].

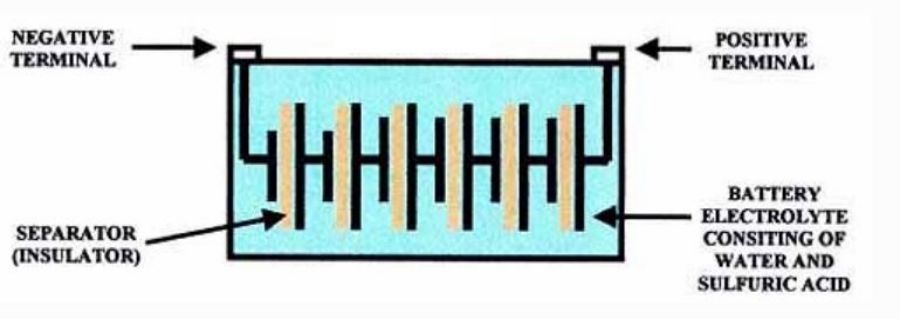

Figure 2.4.10: Six single cells connected in series, lead-Acid battery [6]

Bond graph model of a Lead-acid battery

The sub-models, PV, WT, EL, FC and hydrogen storage tanks are linked to the common bus DC defined by the central 0-junction. Based on the causalities, the voltage effort is given by the batteries effort source Se: U_{bat} and transmitted to the other components via the DC common bus. Constant U_{bat} voltage is considered for batteries.
Through integrating the output current signal of the batteries, the SoC charging status is determined according to the following equation,

$$SoC = SoC_0 - \frac{100}{C_{bat}} \int_{t_0}^{t} idt \tag{2.32}$$

where SoC_0 is the initial state of charge (32%), and C_{bat} is the battery capacity (5Ah).
The bond graph model of the battery is given in figure (2.4.11).

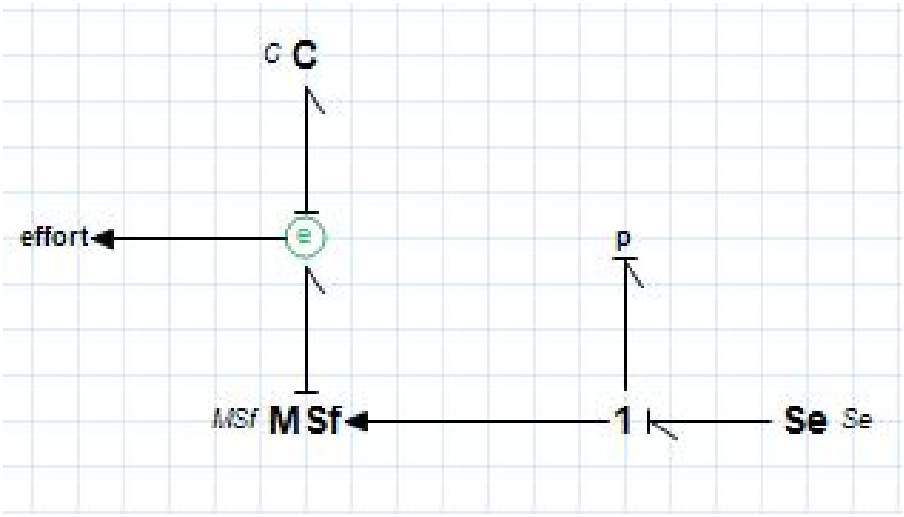

Figure 2.4.11: Bond graph model of the battery [5]

where C is the battery capacity (55Ah), $Se : se$ is the constant voltage source (24 V). For our study, we consider the linear operating part of the battery.

2.5 Interconnection of the platform components

2.5.1 Common voltage junction

The platform's components are connected to a common bus, see figure (2.5.1). In the bond-graph formalism, this corresponds to a 0-junction, with common voltage. The battery enforces and stabilizes the value of the voltage by controlling its current. It is thus necessary to have an additional battery if one wants one additional current source (a physical Energy tank as will be discussed next chapter).

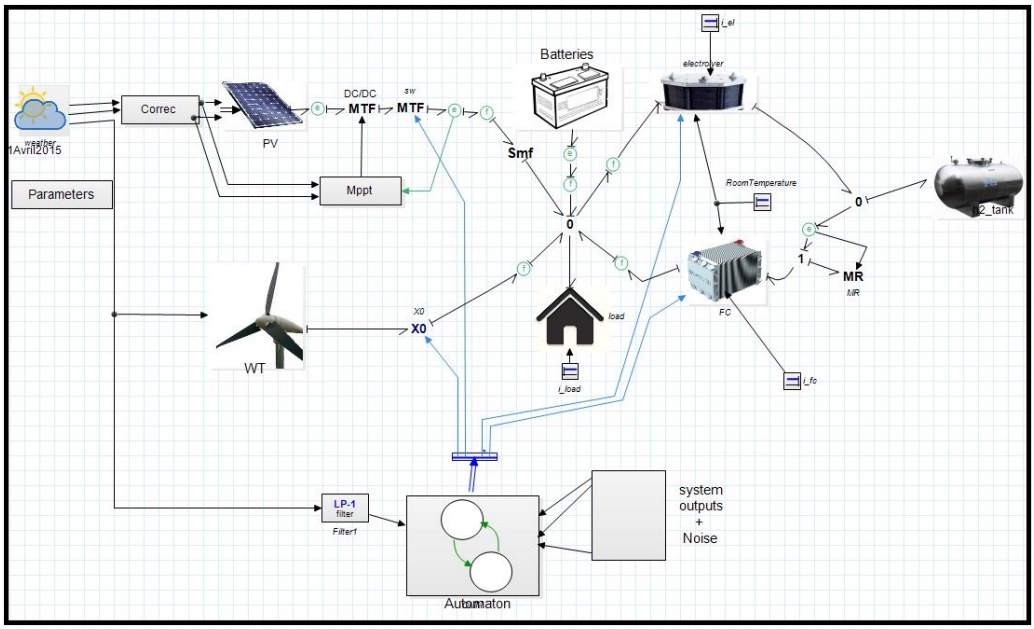

Figure 2.5.1: Bond graph model of a multi-source renewable energy platform [5]

In the port-Hamiltonian framework, one can connect the different subsystems through their ports. For simulation purposes, it seemed to us more simple to use the power balance at the bus stage.
A possibility to handle the connection and disconnection of the different elements would be to consider each device as an agent. Hence, the different sub-systems (solar panel, wind turbine, PEM electrolyzer, PEM fuel cell, battery and load) are individually described in the port-Hamiltonian framework, as explained in the previous parts of the chapter.
The multi-agent system configuration is well suited when dealing with multi-physical systems, which is the case of the multi-source renewable platform, where several systems are working together despite their physical domain and dynamics differences. This allows to design decentralized controllers.

2.5.2 Implementation and simulation results

The multi-source renewable energy system is implemented using Matlab/Simulink, see figure (2.5.2).

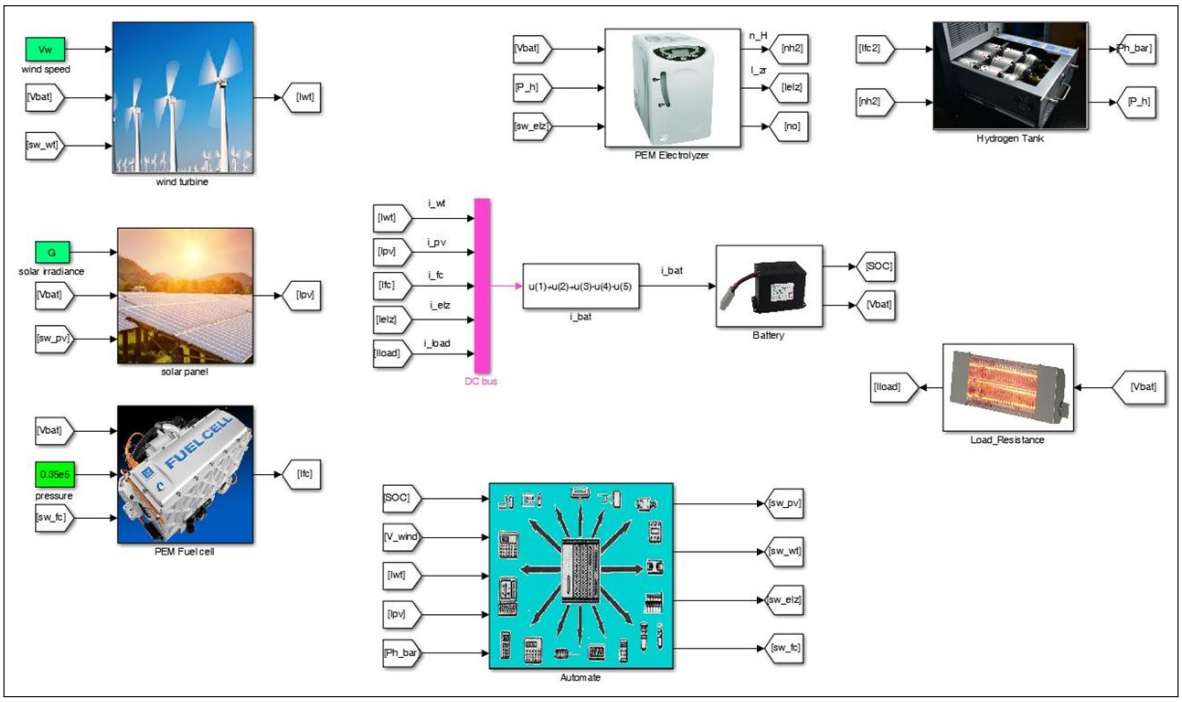

Figure 2.5.2: Multi-source renewable energy platform in Matlab/Simulink

The sub-systems of the platform are linked to a common bus of 24 V imposed by the battery, which receives in return the current (A), see figure (2.5.3).

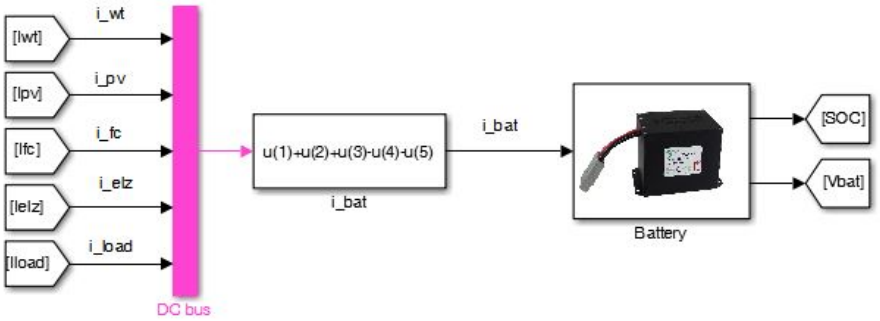

Figure 2.5.3: DC-bus

The wind turbine and solar panel are respectively equipped with an MPPT controller that optimizes the extraction of energy from the two devices. Then, (AC/DC, DC/DC,DC/AC) power converters are integrated in the models to adapt the inputs and outputs to the DC bus and from the renewable sources and storage components and consumption.
The platform consists of a PEM electrolyser and a PEM fuel cell that operate

alternately. Hence, to prevent the simultaneous production and consumption of hydrogen, which is not an effective nor profitable operating mode, an automaton that receives the state of charge of the battery, current from the wind turbine, current from solar panels, wind speed, state of charge of the battery and hydrogen storage pressure, is designed to control the switches between the different operating modes of the platform, see figure (2.5.4). In addition, to ensure an alternative operating mode of the PEM electrolyser and fuel cell, the automaton is in charge of turning the wind turbine on or off for security reasons under high wind speed.

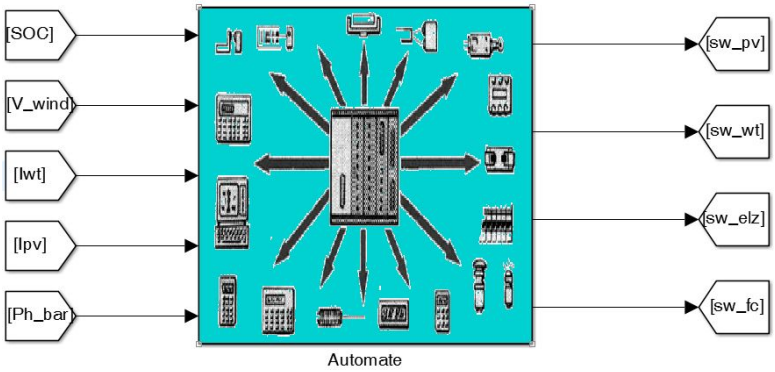

Figure 2.5.4: Automaton for operating mode management (OMM)

For simulation, 24h weather data of the solar irradiance (G) and wind speed (V) are collected using the two PV and PMS wind turbine, see figure (2.5.5) where the simulations are done using the PH model of the platform..

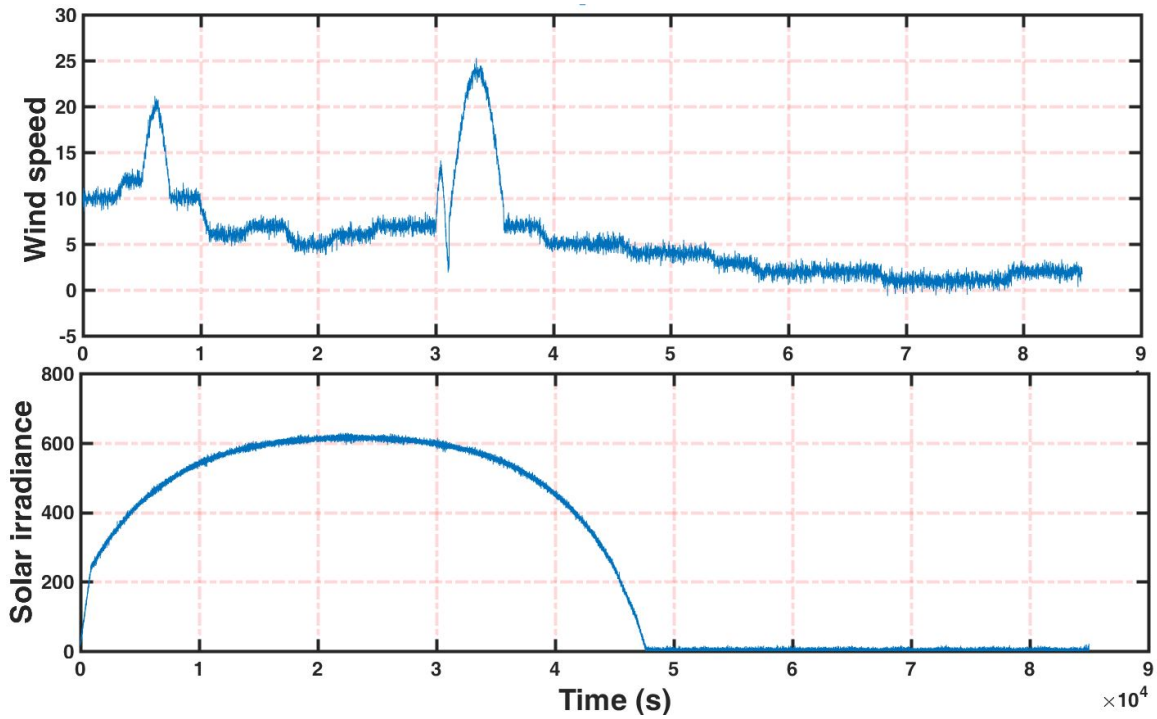

Figure 2.5.5: Wind speed $[m/s]$ and solar irradiance$[W/m^2]$

For the given weather data, we obtain the following current profile from the wind turbine and solar panels.

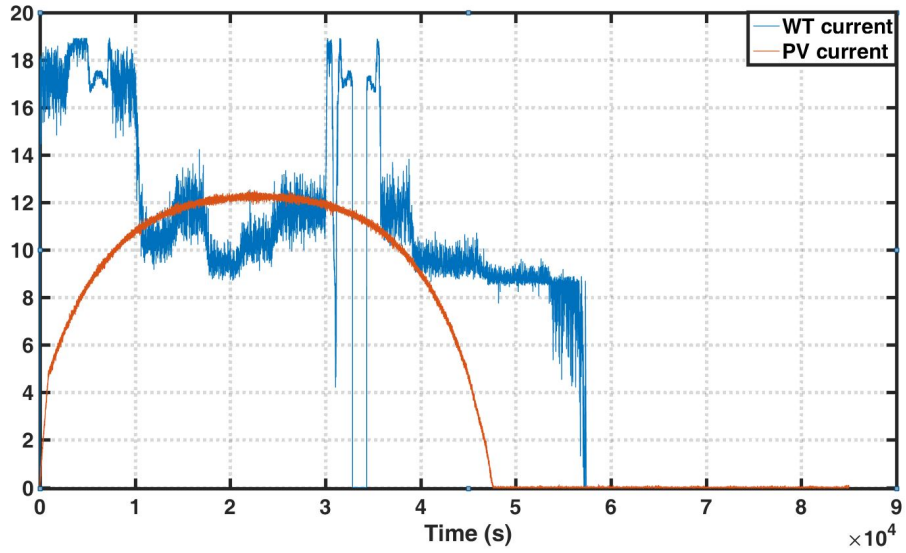

Figure 2.5.6: PV and WT current (A)

In figure (2.5.7) the generated current by the fuel cell and the transformed current by the electrolyser are exposed showing the alternative operating of the PEM electrolyser and fuel cell.

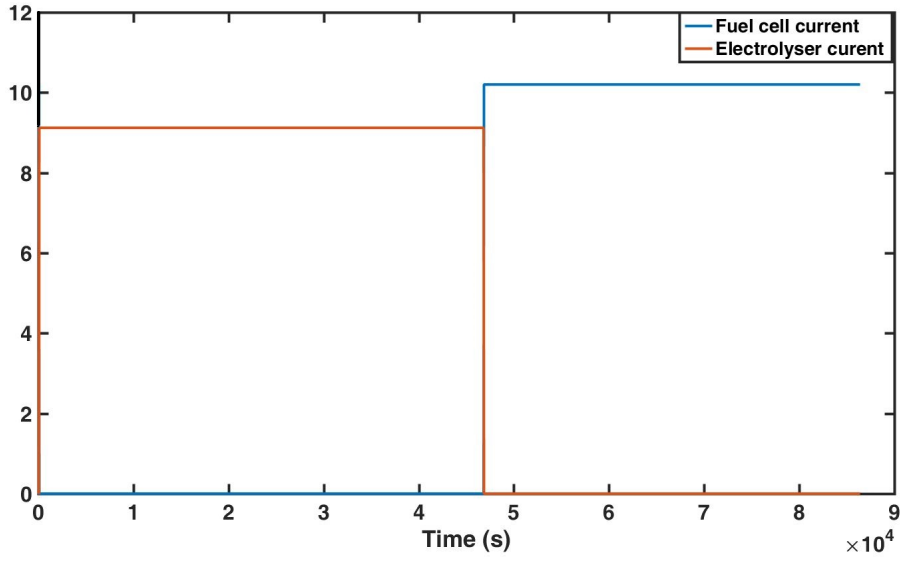

Figure 2.5.7: PEM electrolyser and fuel cell current (A)

2.6 Conclusion

In this chapter, a simplified port-Hamiltonian representation of the components of a multi-source renewable energy platform, composed of two solar panels, PMG wind turbine, PEM electrolyser, hydrogen storage tank, PEM fuel cell, resistive

load and battery, based on their bond graph representation has been presented. The different elements of the platform have been interconnected. The simulation of the platform was achieved under Matlab/Simulink.
The interest of this representation is that every component can be controlled individually, but power exchanges can also be enforced in such a way that one component helps another to meet its specifications, or to allow the whole platform to reach a global control objective. The main problem is that the power exchanges should take care of the limitations of the different devices, their power reserves which as it will be seen in next chapter can be achieved in the port-Hamiltonian framework with the introduction of Energy Tanks.

Chapter 3

Passivity margins estimation and power exchange via Energy Tanks

3.1 Introduction

In this chapter, the Energy Tank concept is presented, supported by different illustrative examples (electrical and robotic fields). The dissipated energy recovered through the Energy Tanks machinery can be used to implement control actions on the port-Hamiltonian systems while respecting the passivity constraints.
The virtual Energy Tanks perform the same tasks than the usual storage batteries. They are in charge to store energy and in the same time, inform about the maximum and minimum power flow and the available quantity of energy ready to be transferred to the other systems.
In the framework of interconnected systems endowed with Energy Tanks, energy can be exchanged between two or more systems to guarantee the passivity margins of the subsystems and the passivity of the whole system. Moreover, different energy exchange strategies (impartial, preferential) could be considered while exchanging energy between the tanks, depending on the expected results.
Software-in-the-loop and Hardware-in-the-loop simulation are the commonly used tools in power distribution and storage since more piece of product hardware/software are used in industry. Regarding, the virtual Energy Tank the system behaves as a physical storage battery and by exploiting its SOC the energy transfer between systems can be released without any hardware/software product.

3.2 The Duindam-Stramigioli energy router

3.2.1 Introduction

The electrical energy transfer between the subsystems of a multidomain platform is commonly achieved under a steady state operation of the platform system. Indeed, the platform system transforms the power demand of the subsystems into

current or voltage references and a proportional and integral controller is usually used to track these references.
The steady-state approach is practically not quite efficient. Hence, it can only approximately achieve the desired objective of the energy transfer and slow-versus-fast discrimination of the power demand, especially, during the transients or when fast dynamic response is required. Indeed, we notice that the delivery of required power in response to current and voltage references and the time response action of the filters may be far from satisfactory, in this situation. Moreover, it is desirable that, when several passive systems exchange power, the whole system remains passive.
To solve this problem a dynamic power flow controller based on port-Hamiltonian representations, called " Dynamic Energy Router (DER)" is presented in [7] and we will recall its principle, advantages and drawbacks in what follows.

3.2.2 DS-DER algorithm

To explain the Duindam-Stramigioli dynamic energy router (DS-DER) concept, we consider the case of two interconnected multiports systems, see figure (3.2.1) [7]. For the energy management application purposes, energy dissipation in the two systems is neglected. Then, at time $t \geq 0$ we instantaneously transfer energy from system 2 to system 1 without losses, namely:

$$v_1^T(t)i_1(t) + v_2^T(t)i_2(t) = 0 \tag{3.1}$$

and:

$$\begin{aligned} \dot{H}_1(t) &= v_1^T(t)i_1(t) > 0 \\ \dot{H}_2(t) &= v_2^T(t)i_2(t) < 0 \end{aligned} \tag{3.2}$$

To achieve the energy transfer objective, the two systems are linked through

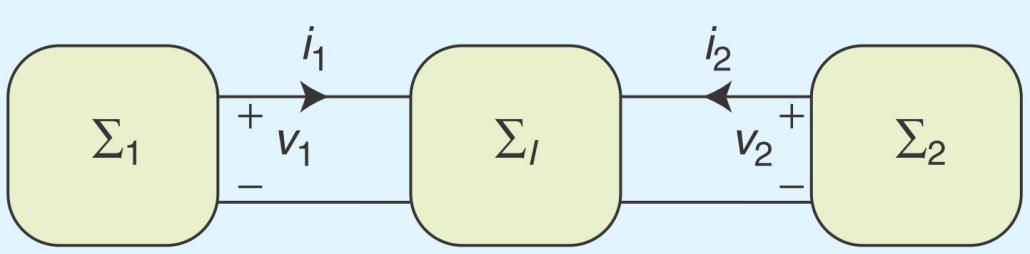

Figure 3.2.1: Two interconnected systems [7]

another multi-port system as illustrated in figure (3.2.1). To satisfy the constraint (3.1), the coupling system must be lossless.
A lossless interconnection that satisfies (3.2) is the DSER defined by:

$$\Sigma_I = \begin{bmatrix} 0 & \alpha v_1(t)v_2^T(t) \\ -\alpha v_2(t)v_1^T(t) & 0 \end{bmatrix} \tag{3.3}$$

The relation between the port variables is thus:

$$\begin{bmatrix} i_1(t) \\ i_2(t) \end{bmatrix} = \begin{bmatrix} 0 & \alpha v_1(t) v_2^T(t) \\ -\alpha v_2(t) v_1^T(t) & 0 \end{bmatrix} \begin{bmatrix} v_1(t) \\ v_2(t) \end{bmatrix} \tag{3.4}$$

where α is a designer possibly time-varying chosen parameter that controls the direction and rate of change of the energy flow.

Remark 3.1 *The DSER defined in (3.4) is a current-tracking multi-port. Hence, given the voltages $v_1(t)$ and $v_2(t)$ the system (3.4) defines the desired values to be imposed on the multi-port currents. a dual, voltage-current tracking DSER can be defined as:*

$$\begin{bmatrix} v_1(t) \\ v_2(t) \end{bmatrix} = \begin{bmatrix} 0 & \alpha i_1(t) i_2^T(t) \\ -\alpha i_2(t) i_1^T(t) & 0 \end{bmatrix} \begin{bmatrix} i_1(t) \\ i_2(t) \end{bmatrix} \tag{3.5}$$

Example 3.2.1 *Let's consider two interconnected electrical systems as reported in figure (3.2.2) [7], The dynamic of the two systems is described in the following*

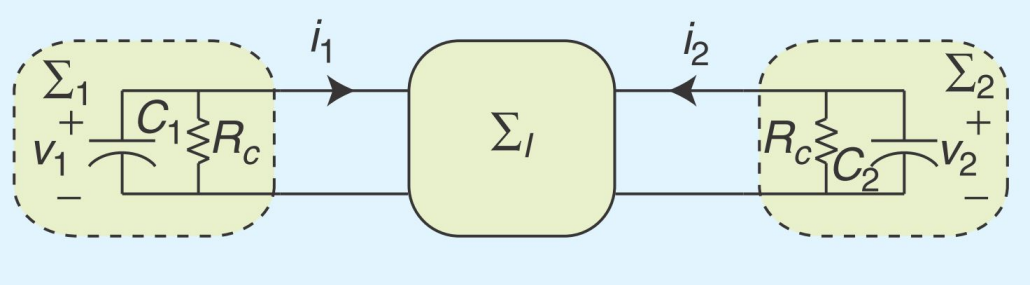

Figure 3.2.2: Interconnection of linear capacitors, chosen as subsystems

equations :

$$\begin{cases} C_1 \dot{v}_1(t) = i_1(t) - \frac{1}{R_C} v_1(t) \\ C_2 \dot{v}_2(t) = i_2(t) - \frac{1}{R_C} v_2(t) \end{cases} \tag{3.6}$$

Each capacitor model contains a parallel resistance R_C, which are not considered in the model simulation because of its high value. The capacitance of each capacitor is 250 F, which corresponds to a super-capacitor. This amplitude is linked to the storage capacity and to the voltage variation, and only slight variations in the voltages $v_1(t)$ and $v_2(t)$ are therefore expected. Capacities on the order of hundreds or thousands of μF are normally used for voltage regulation, while, capacities of the order of hundreds of F are used for the storage elements.
The two systems are interconnected through a bidirectional energy exchange static converter, exposed in figure (3.2.3)

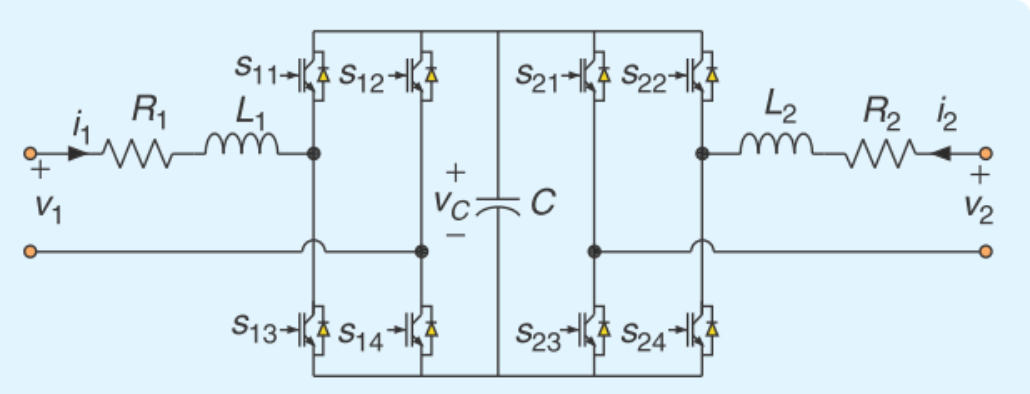

Figure 3.2.3: Static converter used to implement the energy router

where its dynamic is described by the following equations,

$$\begin{cases} L_1 \frac{di_1(t)}{dt} = -R_1 i_1(t) - \alpha_1(t) v_C(t) + v_1(t) \\ L_2 \frac{di_2(t)}{dt} = -R_2 i_2(t) - \alpha_2(t) v_C(t) + v_2(t) \\ C_C \frac{dv_C(t)}{dt} = \alpha_1(t) i_1(t) + \alpha_2(t) i_2(t) \end{cases} \tag{3.7}$$

The relation between the port variables is thus

$$\begin{bmatrix} i_1(t) \\ i_2(t) \end{bmatrix} = \begin{bmatrix} \alpha v_1(t) v_2^T(t) v_2(t) \\ -\alpha v_2(t) v_1^T(t) v_1(t) \end{bmatrix} \tag{3.8}$$

The parameter $\alpha(t)$ that controls the direction and rate of change of the energy flow is given in figure (3.2.4).

The simulation of the system generates the power curves in figure (3.2.5).

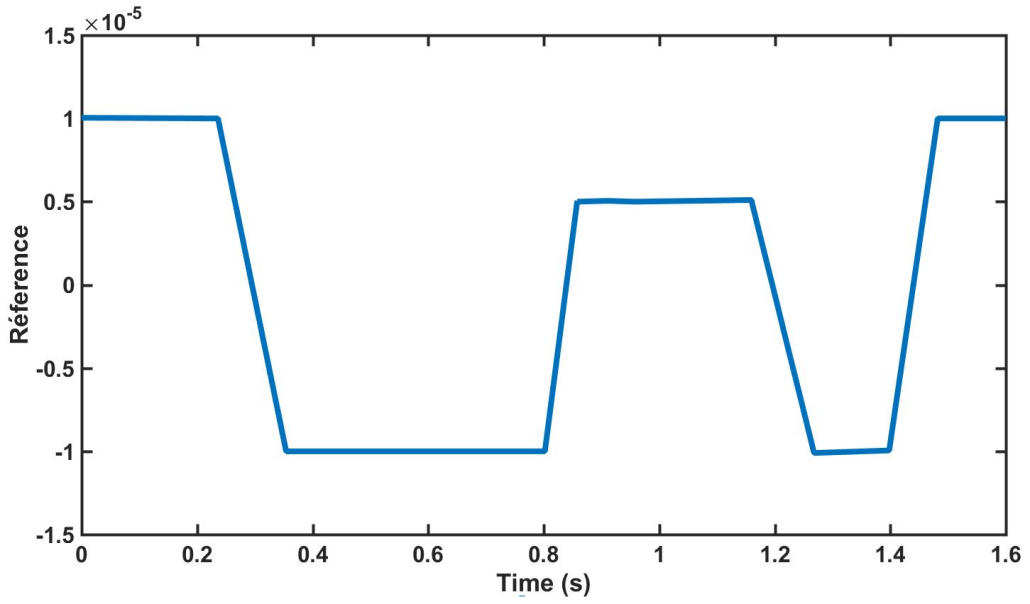

Figure 3.2.4: Time evolution of the parameter $\alpha(t)$

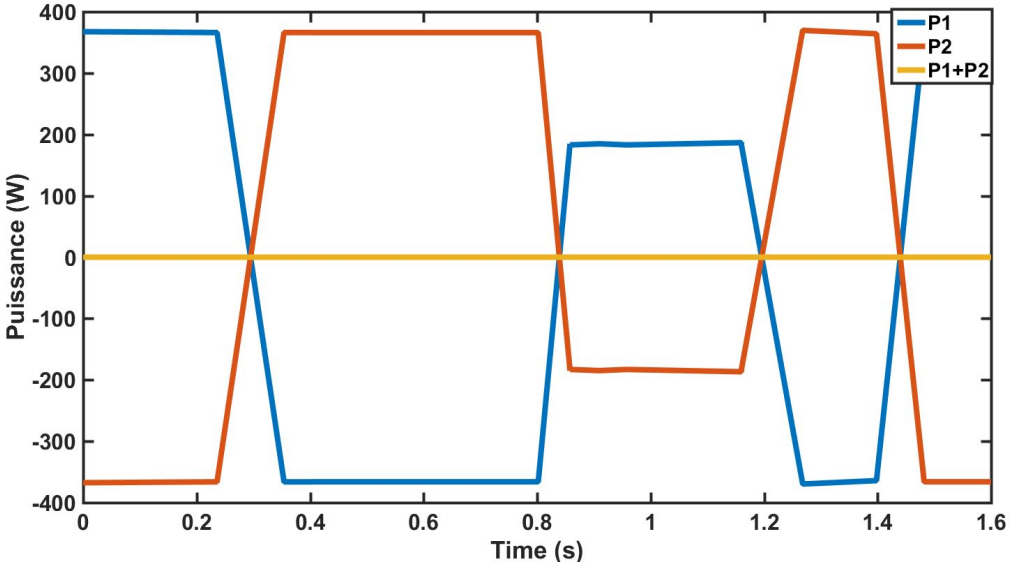

Figure 3.2.5: Power curves in system 1 and 2

The energy in system 1 and 2 are given in the figure (3.2.6).

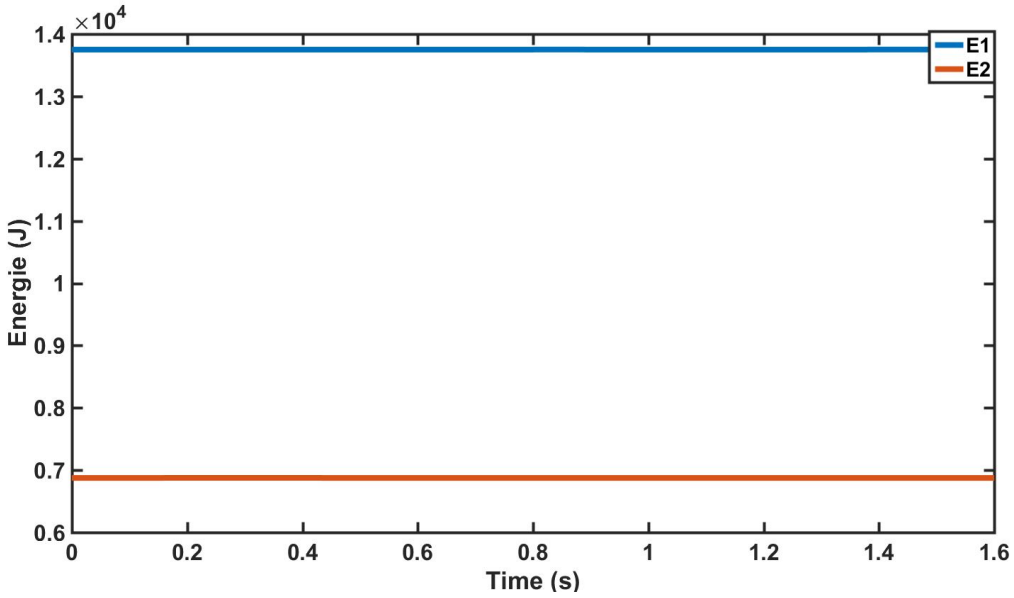

Figure 3.2.6: Energy curves in system 1 and 2

For a different $\alpha(t)$ *curve, as reported in the figure* (3.2.7) *where only the amplitude of* $\alpha(t)$ *changed,*

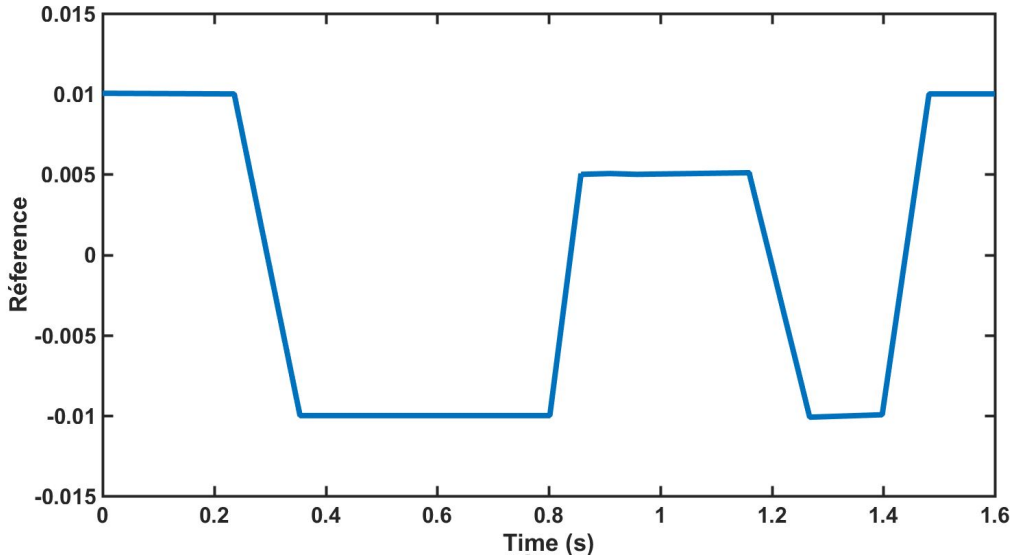

Figure 3.2.7: New shape of $\alpha(t)$

we obtain the energy exchange between the system and system 2 as in the figure (3.2.8).

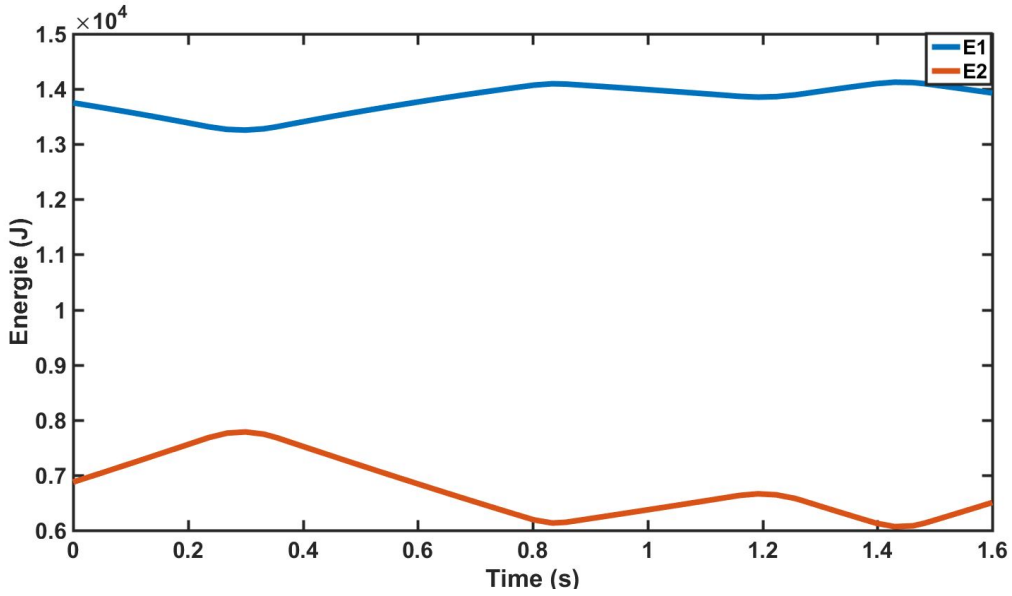

Figure 3.2.8: Energy curves in system 1 and 2

3.2.3 Discussion

The Duindam-Stramigioli dynamic energy router (DS-DER) is a switching electrical circuit, namely, a power converter system (Σ_I) that ensures energy transfer between electrical multi-ports in the desired direction and magnitude, based on parameters that come directly from the power port considerations (α). The advantage of monitoring the energy flow in microgrids directly is due to the ability

to monitor stocks, as well as the energy consumption in the system's various storage and source devices. For example, when applying energy transfer involving batteries, it is important to be aware of the energy level of the batteries before making decisions on the appropriate energy control policy.
Despite the dynamic control aspect of the energy flow that the DS-DER offers, the correct operation of the system is based on a crucial assumption, namely that the multi-port and the DER itself are optimal, loss-free machines which is clearly not the case in practical implementations, where the energy of the DER decreases monotonously in the presence of dissipation, leading to inappropriate actions and ultimately to a complete DS-DER dysfunction. To fix this problem the authors in [111] proposed to add an external battery to compensate for the losses in the DER, which effectively solved the problem, but its realization is restricted to the specific implementation of the DER proposed in the paper and questions arise about its robustness to the uncertainties in the dissipation functions, in addition to its physical implementation.
To summarize, the problem of the DS DR Energy router is that it links physically the two systems. Whereas the power exchange can be controlled, the desired total amount of energy is not monitored, which is a drawback for power systems. Also, in practice, the solution appears under the form of an analog system, whereas flexible power sharing should better be achieved with a numerical procedure.
In the next section, an alternative proposition to the DS-DER, called "Virtual Energy Tank" which is available in the case of dissipative systems, will be presented.

3.3 Virtual Energy Tanks concept

The Energy Tank concept is widely used in the field of robotics, namely, in the variable impedance controller of a multi-DOF robot [112, 113, 114, 115], where the Energy Tanks are used to ensure the overall passivity of the robot and consequently its stability both in free motion and in the case of interaction with the external world, through energy and power limitations.
The machinery of the Energy Tank concept is inspired by the energy dissipated through the dissipative elements (Electrical resistance, dry and viscous friction, hydraulic restriction). Hence, physical systems with dissipative elements are considered as passive systems which are a class of processes that dissipate certain types of physical or virtual energy (see figure (3.3.1)), described by Lyapunov-like

functions, that satisfies the following energy-balance equation:

$$\underbrace{H(x(t)) - H(x(0))}_{stored\ \ energy} = \underbrace{\int_0^t u^T(s)y(s)ds}_{supplied\ \ energy} - \underbrace{d(t)}_{dissipated\ \ energy} \tag{3.9}$$

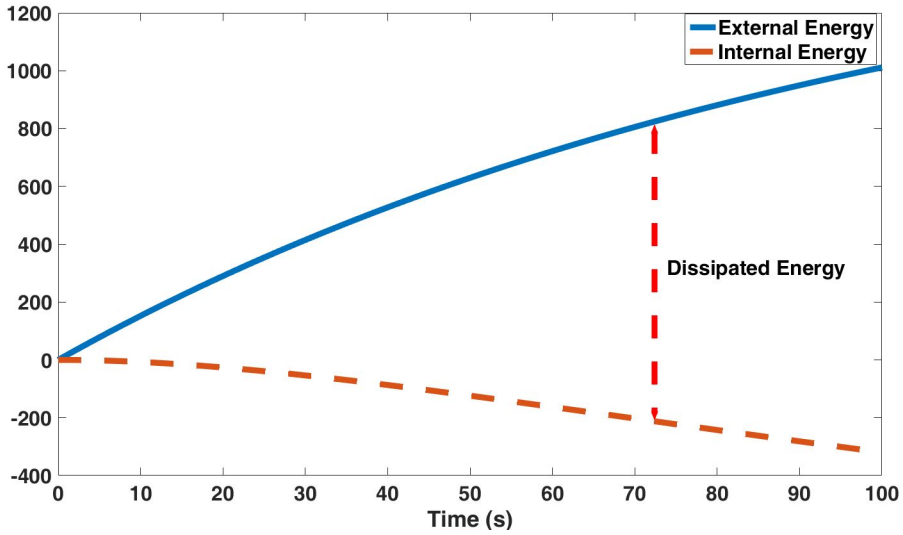

Figure 3.3.1: Energy system

According to the energy balance equation, the stored energy in passive systems is less than the supplied energy because of the dissipated energy:

$$D(x) = \frac{\partial^T H}{\partial x} R(x) \frac{\partial H}{\partial x} \geq 0 \tag{3.10}$$

Consequently, if the dissipated energy is recovered we can make good use of it and in the framework of automatic control, we can use the recovered energy to implement passive desired control actions and ensure the stability of the system as explained in chapter 1.
The dynamical port-Hamiltonian system with an Energy Tank is given in equation (3.11) [112].

$$\begin{cases} \dot{x} = [J(x) - R(x)] \frac{\partial H}{\partial x} + g(x)u \\ \dot{x}_t = \frac{\sigma}{x_t} D(x) + \frac{1}{x_t}(\sigma P_{in} - P_{out}) + u_t \\ Y = \begin{pmatrix} y \\ y_t \end{pmatrix} \end{cases} \tag{3.11}$$

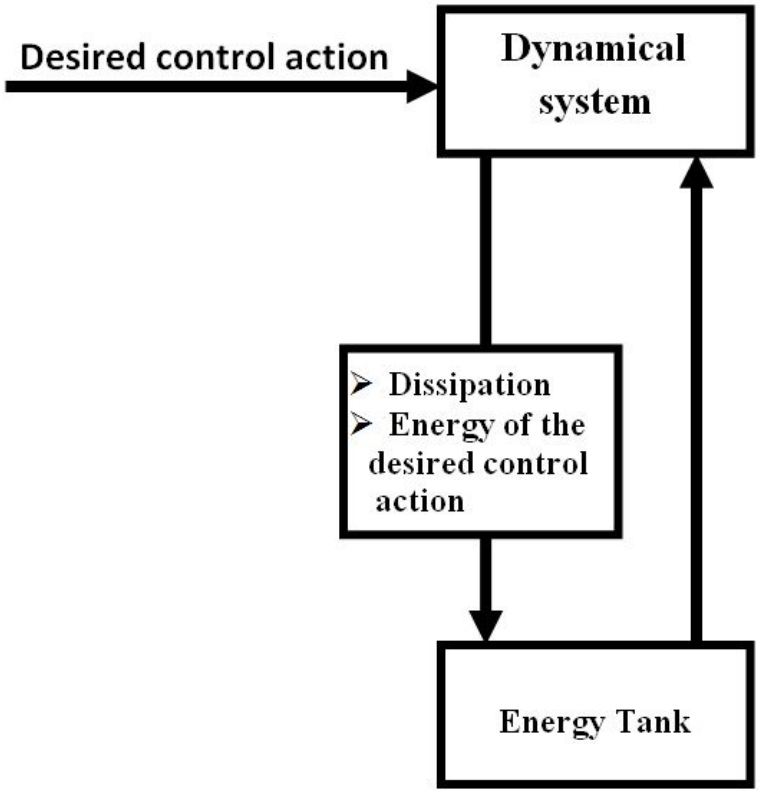

Figure 3.3.2: Energy Tank concept

where $x_t \in R$ is the state associated with the energy storing tank, $T(x) = \frac{1}{2}x_t^2$ is the energy stored in the tank. P_{int} and P_{out} are incoming and outgoing power flows that the tank can exchange with the external world, for example with other tanks, respectively. The control action must be implemented as a lossless energy transfer between the plant and the tank what preserves passivity by construction. Hence, the plant and the tank should be interconnected using the state modulated power preserving interconnection, as follows:

$$\begin{bmatrix} u \\ u_t \end{bmatrix} = \begin{bmatrix} 0 & \frac{u}{x_t} \\ -\frac{u^T}{x_t} & 0 \end{bmatrix} \begin{bmatrix} y \\ y_t \end{bmatrix} \tag{3.12}$$

$D(x)$ represents the dissipated energy of the system, consequently, the larger $D(x)$, the higher the passivity of the system.

$$D(x) = \frac{\partial^T H}{\partial x} R(x) \frac{\partial H}{\partial x} \geq 0 \tag{3.13}$$

The pair (u_t , y_t) is a power port that the tank can use to exchange energy and $y_t = \partial T/\partial x_t = x_t$. The parameter $\sigma \in 0, 1$ is used for bounding the amount of energy that can be stored into the tank.
To check if the tank stores energy we use the following power balance equation:

$$\dot{T} = \sigma D(x) + \sigma P_{in} - P_{out} + u_t^T y_t \tag{3.14}$$

To avoid singularities in (3.11), some energy must always be present in the tank (i.e., $x_t \neq 0$). Thus, the tank has to be initialized and managed in such a way that $(x_t(0)) > \epsilon$ and energy extraction is prevented if $T(x_t) \leq \epsilon$, where ϵ is an arbitrarily small threshold $\epsilon > 0$.
To avoid that the available energy can become very large as time increases, and even if the system remains passive, it is necessary to set an upper bound on the amount of energy that can be stored in the tank.Thus, σ is set using the following policy:

$$\sigma = \begin{cases} 1, & if \quad T(x_t) \leq \bar{T} \\ 0, & otherwise \end{cases} \tag{3.15}$$

where: $\bar{T} > 0$ is a suitable application-dependent upper bound on the energy that can be stored in the tank. Hence, the tank behaves as a virtual storage unit, and it is possible to introduce a tank State of Charge $SoC = T(x_t)/\bar{T}$.

Example 3.3.1 ***Energy-Tank based controller for a 1-DOF system [116]***
The Energy Tank is assimilated to a spring due to its energy-storage nature, such that the controller force output is applied to the system only when there is available stored energy.
The physical interpretation is given in figure (3.3.3). H(s) represents the energy of the spring, so, the internal energy of the tank. The computational unit (CU) calculates the transmission ratio u through which it acts on the transmission element (MT) which ensures the connection between the controller and the plan by delivering the power flow from the controller as long as there is energy left in the tank $(H(s) > \epsilon)$.

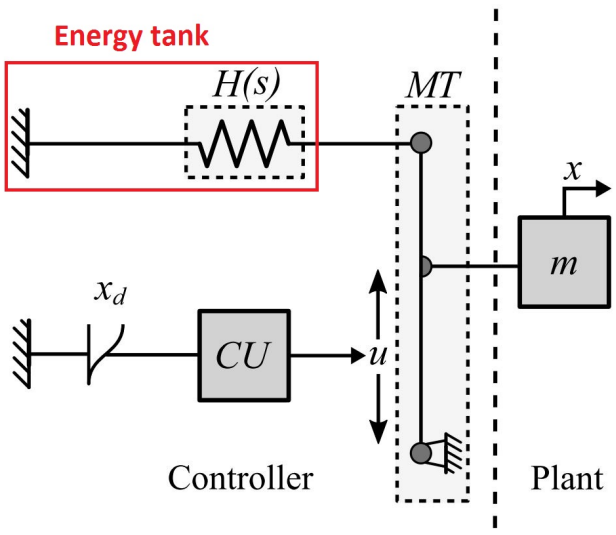

Figure 3.3.3: 1-DOF energy-tank based controller

The port-Hamiltonian configuration of the system in figure (3.3.3), is given in

(3.16) *for a stiffness constant* $k = 1$ *and* s *is the spring state of* $H(s)$.

$$\begin{pmatrix} \dot{s} \\ F_{out} \end{pmatrix} = \begin{pmatrix} 0 & u \\ -u & 0 \end{pmatrix} \begin{pmatrix} s \\ \dot{x} \end{pmatrix} \tag{3.16}$$

The desired transmission ratio u *is defined as:*

$$u = \frac{-F_c}{s} \tag{3.17}$$

where $F_c = k(x_d - x) - b\dot{x} = (x_d - x) - b\dot{x}$ *is the elemental impedance controller. As the transmission ratio should ensure isolation between plant and controller when the Energy Tank is depleted,* u *is chosen as follows:*

$$u = \begin{cases} \frac{-F_c}{s} & if \quad H(s) > \varepsilon \vee P_c < 0 \\ 0, & otherwise \end{cases} \tag{3.18}$$

where, $H(s) = \frac{1}{2}s^2$ *is the potential energy in the tank model designated by* $k = 1$*;* ϵ *the minimum amount of energy allowed in the tank, before plant and controller isolation.*

One the transmission ratio is tuned, the output force command sent to the system plant is given as follows:

$$F_c = -u.s = \begin{cases} F_c & if \quad (H(s) > \varepsilon) \vee (P_c < 0) \\ 0, & otherwise \end{cases} \tag{3.19}$$

where the spring state s *by integrating the following expression:*

$$\dot{s} = u.\dot{x} \tag{3.20}$$

The developed results for 1 *degree of freedom (DOF) and* n *DOF are summarized in figure* (3.3.4).

1-DOF	**Multi-DOF**
$\begin{pmatrix} \dot{s} \\ F_{\text{out}} \end{pmatrix} = \begin{pmatrix} 0 & u \\ -u & 0 \end{pmatrix} \begin{pmatrix} s \\ \dot{x} \end{pmatrix}$	$\begin{pmatrix} \dot{s}_n \\ \tau_{n\text{out}} \end{pmatrix} = \begin{pmatrix} 0 & u_n \\ -u_n & 0 \end{pmatrix} \begin{pmatrix} s_n \\ \dot{q}_n \end{pmatrix}$
$u = \begin{cases} \frac{-F_c}{s}, & \text{if } (H(s) > \epsilon) \vee (P_c < 0)) \\ 0, & \text{otherwise} \end{cases}$	$u_n = \begin{cases} \frac{-\tau_{c_n}}{s_n}, & \text{if } (H_n(s_n) > \epsilon) \\ \frac{-\tau_{c_n}}{\gamma^2} s_n, & \text{otherwise} \end{cases}$
$F_{\text{out}} = -u \cdot s$ $\dot{s} = u \cdot \dot{x}$	$\tau_{n\text{out}} = -u_n \cdot s_n$ $\dot{s}_n = u_n \cdot \dot{q}_n$

Figure 3.3.4: Safety-Aware Intrinsically Passive Controller

For the $n-DOF$ *case (see figure* (3.3.5)*), each joint of the system is considered as a subsystem and analyzed based on this. Thus, each subsystem is described by*

the energy storage phenomenon illustrated in figure (3.3.3). The controller output in n-DOF is the torque τ while in 1-DOF is the force F_c.

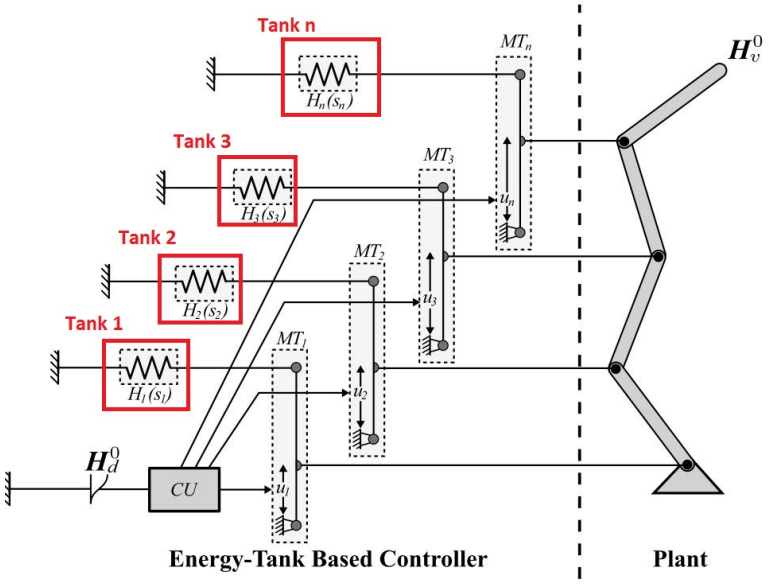

Figure 3.3.5: Physical depiction of the energy-tank based controller for multi-DOF manipulators

Remark 3.2 *The inputs are the motion profile of the robot with the initial internal energy. To get the output, namely, the torque, limitations on energy and power are imposed and the conditions relative to this must be satisfied. These energy and power limitations concern the metrics safety. Finally, an other constraint on the passivity of the system, interpreted by the Energy Tank, must be considered to ensure the stability of the system.*

Example 3.3.2 ***Electrical circuit***
Given the RL circuits of figure (3.3.6)

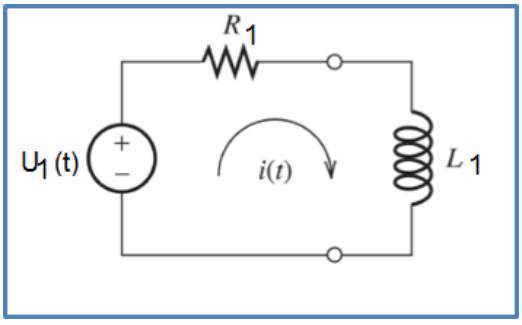

Figure 3.3.6: RL circuits in series

and in application of the Kirchhoff's circuit laws, we get:

$$U_1(t) = R_1 i(t) + L_1 \frac{di(t)}{dt}$$

as $i(t) = \frac{\phi_1}{L_1}$, $\frac{d\phi_1}{dt} = u_{L1}(t)$ *and* $u_{L1}(t) = \dot{\phi} = -R_1\frac{\phi}{L_1} + U_1(t)$, *the port-Hamiltonian representation of the RL circuits can be given in the following form:*

$$\begin{cases} \dot{\phi}_1 = -R_1\frac{\phi}{L_1} + U_1(t) = -R_1\frac{\partial H_1(\phi)}{\partial L_1} + U_1(t) \\ y_1 = \frac{\partial H(\phi_1)}{\partial L_1} = \frac{\phi_1}{L_1} \end{cases} \tag{3.21}$$

where:

- *The internal energy of the system:*

$$H_1(\phi_1) = \frac{1}{2L_1}\phi^2 \tag{3.22}$$

- *The dissipated power:*

$$D_1(\phi_1) = \frac{\partial H_1^T(\phi_1)}{\partial(\phi_1)} R_1 \frac{\partial H_1(\phi_1)}{\partial(\phi_1)} = \left(\frac{\phi_1}{L_1}\right) R_1 \left(\frac{\phi_1}{L_1}\right) = R_1\left(\frac{\phi_1}{L_1}\right)^2 \tag{3.23}$$

1. ***Passivity of the system:*** *The RL circuits system is passive with respect to (w.r.t) (U_1,y_1) since we have:*

$$\begin{aligned} \dot{H}_1(\phi_1) &= \frac{\partial H_1(\phi_1)}{\partial \phi_1} g_1(x) U_1 - \frac{\partial H_1^T(\phi_1)}{\partial \phi_1} R_1 \frac{\partial H_1(\phi_1)}{\partial \phi_1} \\ &= \frac{\phi_1}{L_1} U_1 - \frac{\phi_1}{L_1} R_1 \frac{\phi}{L_1} = \frac{\phi}{L_1} U_1 - R_1\left(\frac{\phi_1}{L_1}\right)^2 \leq \frac{\phi_1}{L_1} U_1 \end{aligned} \tag{3.24}$$

2. ***Extension of the PH systems with a Tank:*** *To store the dissipated energy of the system, we use an Energy Tank in the following form:*

$$\begin{cases} \dot{x}_{t1} = u_{t1} = \frac{1}{x_{t1}} D_1(\phi_1) + \tilde{u}_{t1} \\ y_{t1} = \frac{\partial T_1(x_{t1})}{\partial x_{t1}} = x_{t1} \end{cases} \tag{3.25}$$

where $T_1(x_{t1}) = \frac{1}{2}x_{t1}^2$ *is the internal energy of the tank.*
The PHS system of the RL circuits is interconnected with the Energy Tank using an interconnecting Dirac structure as follows:

$$\begin{bmatrix} U_1 \\ \tilde{u}_{t_1} \end{bmatrix} = \begin{bmatrix} 0 & \frac{\omega}{x_{t1}} \\ -\frac{\omega^T}{x_{t1}} & 0 \end{bmatrix} \begin{bmatrix} y_1 \\ y_{t1} \end{bmatrix} \tag{3.26}$$

By replacing (3.26) in (3.25) we obtain:

$$\begin{aligned} \dot{x}_{t1} &= \frac{1}{x_{t1}} D_1(\phi_1) - \frac{\omega_1}{x_{t1}} g^T(\phi_1) \frac{\partial H_1(\phi_1)}{\partial \phi_1} \\ &= \frac{1}{y_{t1}} R_1 \left(\frac{\phi_1}{L_1}\right)^2 - \frac{\omega_1}{y_{t1}} \left(\frac{\phi_1}{L_1}\right) \\ &= \frac{1}{y_{t1}} R_1 (y_1)^2 - \frac{\omega_1}{y_{t1}} y_1 \end{aligned} \tag{3.27}$$

Then, by replacing (3.26) in (3.21) we get

$$\begin{cases} \dot{\phi}_1 = -R_1\frac{\phi}{L_1} + U_1(t) = -R_1\frac{\partial H_1(\phi)}{\partial L_1} + \omega_1(t) \end{cases} \tag{3.28}$$

Finally, the PH representation of the RL circuits system with the Energy Tank is given in the following form:

$$\begin{aligned}\begin{bmatrix} \dot{p} \\ \dot{x}_{t1} \end{bmatrix} &= \left(\begin{bmatrix} 0 & \frac{\omega_1}{x_{t1}} \\ -\frac{\omega_1}{x_{t1}} & 0 \end{bmatrix} - \begin{bmatrix} R_1 & 0 \\ -\frac{1}{x_{t1}} \frac{\partial H}{\partial(\phi_1)} R_1 & 0 \end{bmatrix} \right) \begin{bmatrix} \frac{\partial \mathcal{H}(\phi_1, x_{t1})}{\partial(\phi_1)} \\ \frac{\partial \mathcal{H}(\phi_1, x_{t1})}{\partial(x_{t1})} \end{bmatrix} \\ &= \left(\begin{bmatrix} 0 & \frac{\omega_1}{x_{t1}} \\ -\frac{\omega_1}{x_{t1}} & 0 \end{bmatrix} - \begin{bmatrix} R_1 & 0 \\ -\frac{1}{x_{t1}} \frac{\phi_1}{L_1} R_1 & 0 \end{bmatrix} \right) \begin{bmatrix} \frac{\partial \mathcal{H}(\phi_1, x_{t1})}{\partial(\phi_1)} \\ \frac{\partial \mathcal{H}(\phi_1, x_{t1})}{\partial(x_{t1})} \end{bmatrix}\end{aligned} \tag{3.29}$$

where ω_1 is the desired action to implement and $\mathcal{H} = T_1(x_{t1}) + H_1(\phi_1)$ the internal energy of the RL circuits system with the Energy Tank. For safety reasons and in order to ensure a passive implementation of the desired action ω_2 we add a switching parameter σ, with:

$$\begin{cases} \sigma = 1 \quad if \quad T_1(x_{t1}) \geq \varepsilon_1 > 0 \\ \sigma = 0 \quad if \quad T_1(x_{t1}) < 0 \end{cases} \tag{3.30}$$

and the system RL with the Energy Tank becomes:

$$\begin{bmatrix} \dot{p} \\ \dot{x}_{t1} \end{bmatrix} = \left(\begin{bmatrix} 0 & \frac{\sigma\omega_1}{x_{t1}} \\ -\frac{\sigma\omega_1}{x_{t1}} & 0 \end{bmatrix} - \begin{bmatrix} R_1 & 0 \\ -\frac{1}{x_{t1}} \frac{\phi_1}{L_1} R_1 & 0 \end{bmatrix} \right) \begin{bmatrix} \frac{\partial \mathrm{H}(\phi_1, x_{t1})}{\partial(\phi_1)} \\ \frac{\partial \mathrm{H}(\phi_1, x_{t1})}{\partial(x_{t1})} \end{bmatrix} \tag{3.31}$$

3.4 Passivity margins estimation via Energy Tanks

Passivation consists of rendering a system passive with respect to its inputs and outputs. The dissipation energy term $D(x)$ margin is a quantitative way to check the excess or shortage of passivity in dynamical systems. Hence, a system is in excess of passivity for a non zero and positive dissipation value ($D(x) > 0$).
In the framework of interconnected port-Hamiltonian systems, the passivity of the subsystems implies the passivity of the whole system [2]. Therefore, a decentralized passivation of the subsystems must be ensured.
To illustrate the concept we studied the case of two interconnected RLC systems in series. The port-Hamiltonian representation of the RLC system in series is given as follows:

$$\begin{cases} \begin{bmatrix} \dot{q} \\ \dot{p} \end{bmatrix} = \begin{bmatrix} 0 & 1 \\ -1 & -R \end{bmatrix} \begin{bmatrix} \frac{q}{C} \\ \frac{\phi}{L} \end{bmatrix} + \begin{bmatrix} 0 \\ 1 \end{bmatrix} V \\ y(t) = \begin{bmatrix} 0 & 1 \end{bmatrix} \begin{bmatrix} \frac{q}{C} \\ \frac{\phi}{L} \end{bmatrix} = \frac{\phi}{L} = i(t = \end{cases} \tag{3.32}$$

The internal energy of the system is given in equation (3.33).

$$H(\phi, q) = \frac{1}{2L}\phi^2 + \frac{1}{2C}q^2 \tag{3.33}$$

The power of the system is given in equation (3.34):

$$\begin{aligned}\dot{H}(\phi,q) &= \frac{\partial H^T(x)}{\partial x} R(x) \frac{\partial H(x)}{\partial x} + y^T(t)u(t) \\ &= -\begin{bmatrix} \frac{q}{C} & \frac{\phi}{L} \end{bmatrix} \begin{bmatrix} 0 & 0 \\ 0 & R \end{bmatrix} \begin{bmatrix} \frac{q}{C} \\ \frac{\phi}{L} \end{bmatrix} + \frac{\phi}{L} V \\ &= \frac{\phi}{L}(V - R\frac{\phi}{L})\end{aligned} \tag{3.34}$$

The simulation results are obtained with zero initial value using the following numerical data:

1. For system 1: R=10 Ω, L=0.6 H, C=10 F
2. For system 2: R=5 Ω; L=0.6 H; C=10 F;

The total power including power in system 1, system 2, tank 1 and tank 2 we get the power figure in figure (3.4.1).

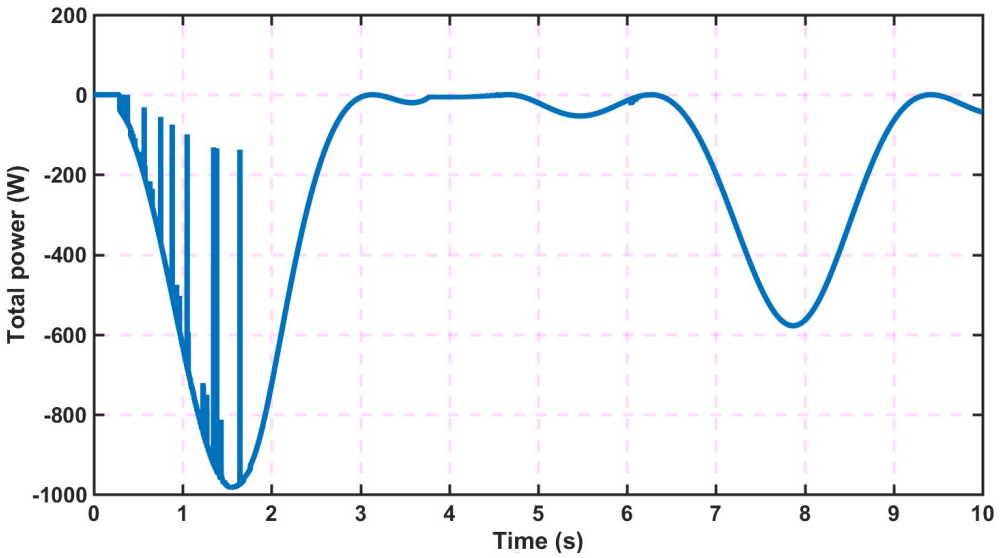

Figure 3.4.1: Total power of the systems plus tanks

The energy exchange between the two tanks is reported in figure (3.4.2).

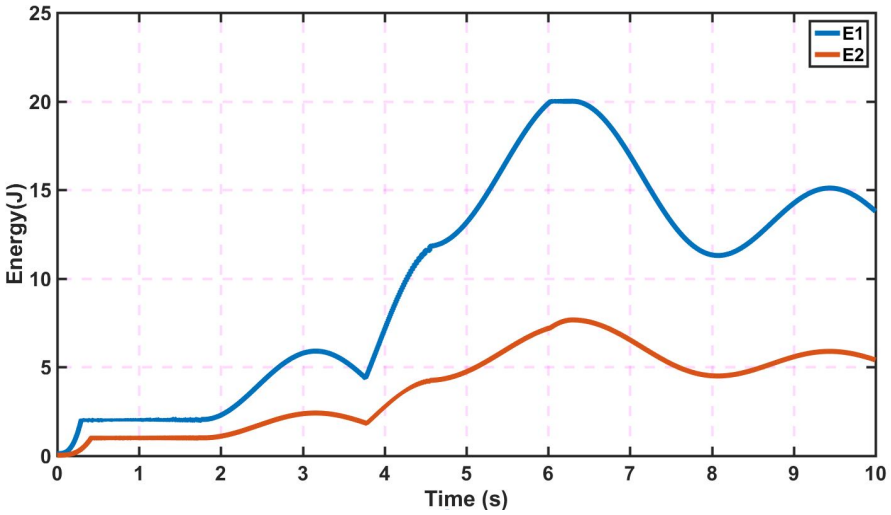

Figure 3.4.2: Energy exchange between T_1 and T_2

The energy exchange between the two systems is reported in figure (3.4.3).

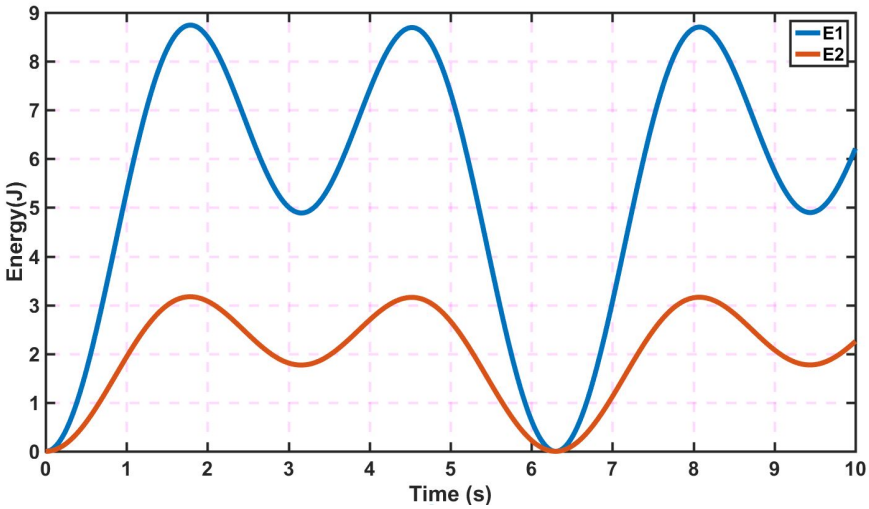

Figure 3.4.3: Energy exchange between system 1 and system 2

The visualization of the energy of the system 1 with the tank 2 is reported in figure (3.4.4).

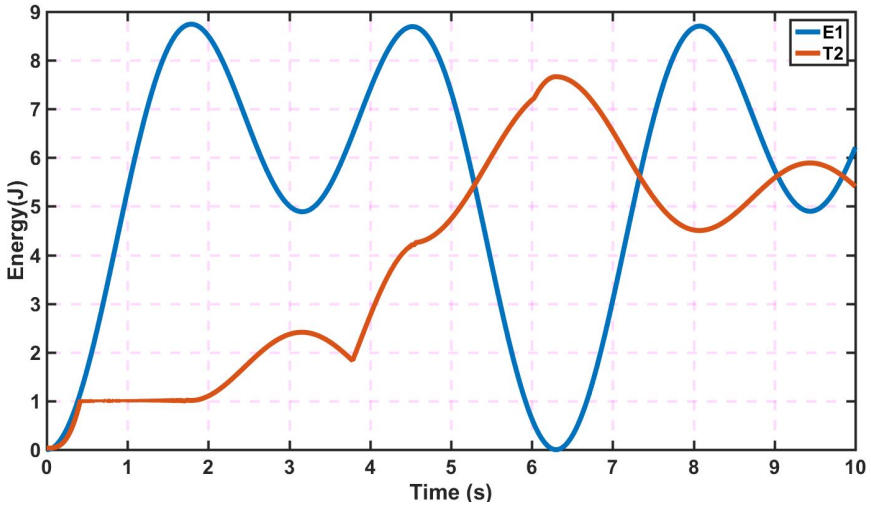

Figure 3.4.4: Energy exchange between system 1 and tank 2

The energy exchange between the system 2 and the tank 1 is shown in figure (3.4.5).

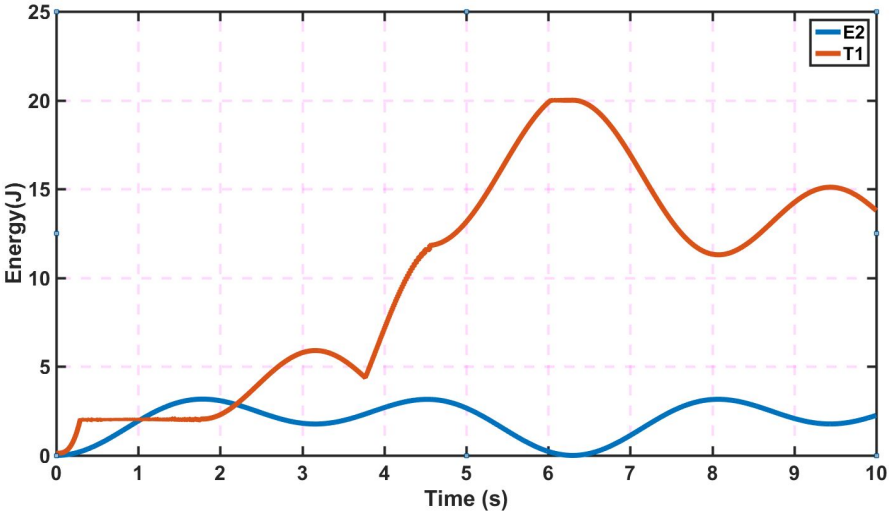

Figure 3.4.5: Energy exchange between system 2 and tank 1

The P_{int} and P_{out} of the system 1 are shown in figure(3.4.6). The available output power of the system is zero in this case which means that the system can not transfer energy to other systems and as the curve of the ingoing power shows, the system is receiving energy from the system 2 for a short period at 6 s.

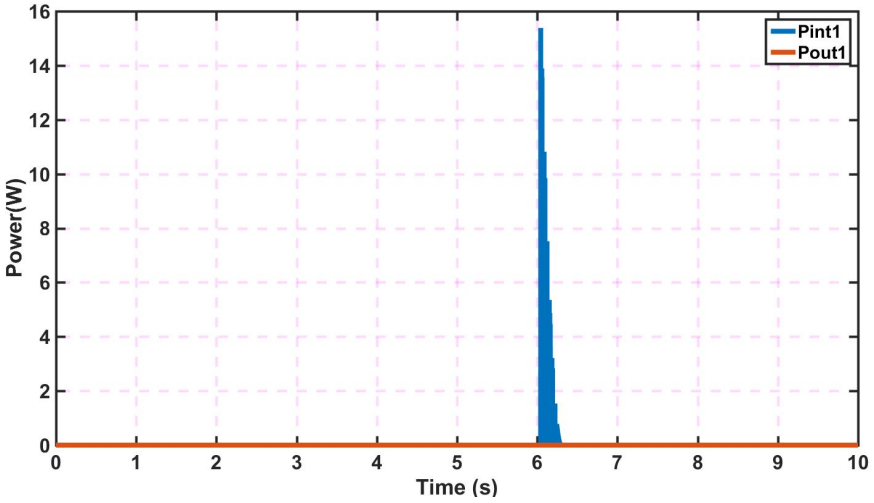

Figure 3.4.6: Pint 1 and Pout 1

3.5 Energy Tanks to guarantee the passivity margins

The energy saved in the virtual Energy Tanks can be exchanged with other systems equipped with tanks to help keep the passivity margins and implement the control actions for the different systems interconnected together in order to achieve different tasks. In what follows the energy exchange process between two or more systems is explained and impartial and preferential distribution strategies are exposed.

3.5.1 Systems power exchange via Energy Tanks

In case of two tanks that exchanges energy, as showed in figure (3.5.1), we compute the incoming P_{int} and outgoing P_{out} powers for each tank. This power quantities are the external power ports through which the systems can exchange energy passing through their respective Energy Tanks and they are defined as follows:

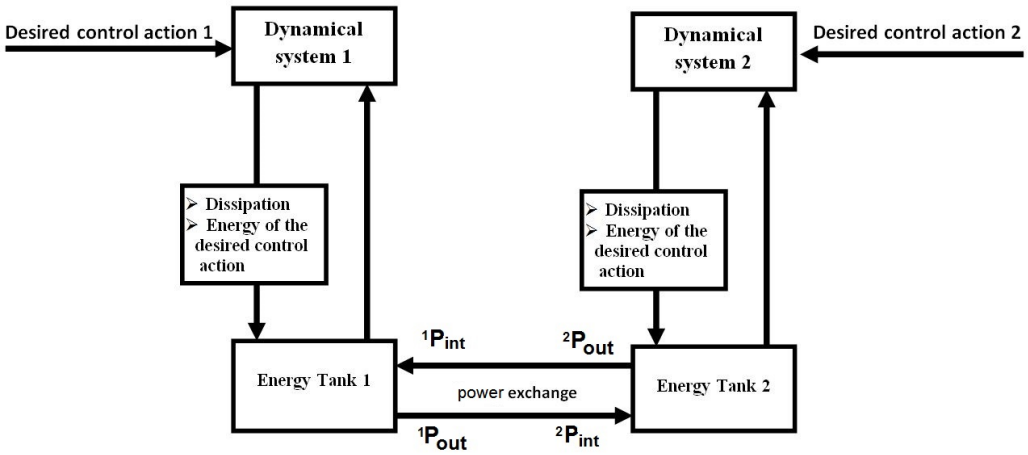

Figure 3.5.1: Energy Tank exchange with two systems

$$\begin{array}{l} {}^1P_{out} = (1-\sigma_1)D_1 + {}^2E_{req}\beta_1\bar{P}_1 = {}^2P_{\text{int}} \\ {}^2P_{\text{out}} = (1-\sigma_2)D_2 + {}^1E_{req}\beta_2\bar{P}_2 = {}^1P_{\text{int}} \end{array} \tag{3.35}$$

the power balance can be written in the matrix form:

$$\begin{bmatrix} {}^1P_{\text{int}} \\ {}^2P_{\text{int}} \end{bmatrix} = \begin{bmatrix} 0 & 1 \\ 1 & 0 \end{bmatrix} \begin{bmatrix} {}^1P_{out} \\ {}^2P_{out} \end{bmatrix} \tag{3.36}$$

The first term of the output energy equation $(1-\sigma_i)D_i$ means that, when the upper threshold (${}^iT_{max}$) is reached, each system (i) transfers the dissipated energy of the system to the other system.

$${}^iE_{req} = \begin{cases} 1 & if \quad {}^iT(x_{t_i}) < {}^iT_{req} \\ 0 & otherwise \end{cases} \tag{3.37}$$

where $T_i(x_{t_i})$ is the tank energy and ${}^iT_{req}$ is an energy threshold below which the tank i requests energy from the other tanks, selected by the control designer. $\bar{P}_i$ is the rate of energy flowing from one tank to an other. β_i enables/disables the transfer of energy from tank i to the other tanks and it is defined as follows:

$$\beta_i = \begin{cases} 1 & if \quad {}^iT(x_{t_i}) < {}^iT_{ava} \\ 0 & otherwise \end{cases} \tag{3.38}$$

where ${}^iT_{ava}$ is the available energy threshold (selected and tuned by the control designer) in tank i that can be transferred to the other tanks, such that we have $e_i <^i T_{req} <^i T_{ava} <^i T_{\max}$ where $e_i > 0$ is the minimal energy of the tank and ${}^iT_{\max}$ is the upper threshold of the tank. When there is a transfer of energy between tanks, this can be achieved through the interconnection with P_{in} and P_{out}. Of course, for one tank, if $P_{in} \neq 0$, $P_{out} = 0$ and vice versa. These thresholds prevent the tanks from being overloaded or under loaded. Figure (3.5.2) shows the main energy levels in the tank; the available energy (T_{ava}) in the tank corresponds to the difference between the Energy Tank State of Charge and the Energy Tank request (${}^iT_{ava} =^i T(x_{t_i}) - {}^iT_{req}$). Hence, the energy request level is the the energy level at which an energy request in sent to the other tank in order to get energy. The energy request level is specific to each tank and it is the lower safety energy level of the tank.

3.5.2 Power exchange strategies between Energy Tanks

There are different ways of exchanging power between tanks; for example, the Duindam-Stramiglioli Energy Router provides a way (which can be implemented as a hardware circuit) to exchange power, but it does not control energy. Exchanging power between tanks corresponds to a power flow between the passivity reserves (or virtual storage units) of the systems. Hence, this exchange takes care

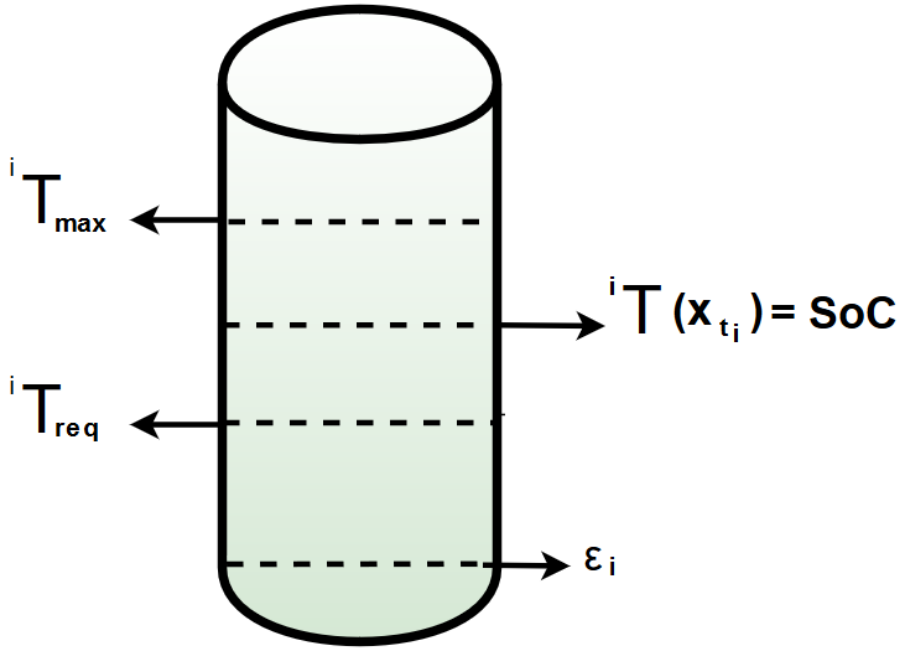

Figure 3.5.2: Energy Tank main levels

of power and energy limitations while preserving the passivity of the systems. Consider n systems with their corresponding tanks. The Boolean ${}^{j}E_{req}$ defines whether there exists a power request from system j, the Boolean β_i defines whether the system i is allowed to supply energy, and $\bar{P}_{ij}$ is the possible exchange rate between these two systems. The idea is to share power as follows:

$$\begin{cases} {}^{i}P_{out} = \beta_i \left(\sum_{j=1, j\neq i}^{n} {}^{j}E_{req}((1-\sigma_j)D_j(x) + \bar{P}_{ij}) \right) \\ {}^{i}P_{\text{int}} = \sum_{j\neq i} {}^{j}P_{out} \end{cases} \tag{3.39}$$

The ${}^{i}P_{int}$ and ${}^{i}P_{out}$ power are linked by a hollow square matrix whose diagonal elements are all equal to zero while the rest are equal to 1, namely:

$$\begin{bmatrix} {}^{1}P_{\text{int}} \\ \vdots \\ \vdots \\ \vdots \\ {}^{n-1}P_{\text{int}} \\ {}^{n}P_{\text{int}} \end{bmatrix} = \begin{bmatrix} 0 & 1 & \dots & \dots & \dots & 1 \\ \vdots & 0 & \dots & \dots & \dots & \dots \\ \vdots & \dots & 0 & \dots & \dots & \dots \\ \vdots & \dots & \dots & \dots & \dots & \dots \\ 1 & \dots & \dots & \dots & 0 & 1 \\ 1 & 1 & \dots & \dots & 1 & 0 \end{bmatrix} \begin{bmatrix} {}^{1}P_{out} \\ \vdots \\ \vdots \\ \vdots \\ {}^{n-1}P_{\text{int}} \\ {}^{n}P_{out} \end{bmatrix} \tag{3.40}$$

From the previous equation, the overall power balance is ensured. As said before, for each tank, there exist an upper power limit of the tank $\bar{T}_i$ above which the tank is full (there is too much energy), and a lower bound ϵ_i (the virtual storage unit should not be depleted). In the case of exchange between tanks, there are

different important parameters to be tuned, that is ${}^{j}E_{req}$ and β_i. For example, ${}^{j}E_{req} = (T_i < {}^{i}T_{req})OR(T_i > {}^{i}T_{ava})$. ${}^{i}T_{req} \geq \epsilon_i$ is a lower bound under which the tank i requests assistance from the others to maintain a State of Charge before it decreases until full depletion. ${}^{i}T_{ava} \leq \bar{T}_i$ is an upper bound over which the tank i tries to discharge excess energy to other tanks before being full. In the contrary, parameter β_i can be set to zero if the tank is requested to supply energy but its state of charge is below a prescribed threshold T_i^{min}, or if the tank is requested to receive energy but its state of charge is above a prescribed threshold T_i^{max}. As an example, if $T_i^{min} > T_i > {}^{i}T_{req}$, the tank may not be sufficiently depleted to request assistance but not sufficiently full to supply power to other tanks.
Moreover, the rates $\bar{P}_{ij}$ can be adapted using different strategies, two of them are described next; for the sake of simplicity, consider only one request ${}^{i}\bar{P}_{in}$ from system i and assume that $\beta_j = 1, j = 1 \cdots I, j \neq i$.

1. **Preferential sharing:** One may want to get some help preferably from system 1 and next system 2, and so on. In this case one will have $\bar{P}_{i(j+1)} = min({}^{i}\bar{P}_{in} - \sum_{k=1}^{j} \beta_i \bar{P}_{ki}, 0)$. Whenever the first j systems are able to supply the power requested by system i, the assistance of other systems is not required. This can change of course if some of the other systems are no more able to supply power and their authorization variable β is zero. Such a hierarchy can be set for example under economical considerations. This can be also set to minimize pollution (CO2 emissions). For example, one will prefer using renewable sources than clean hydrogen, and clean hydrogen than conventional batteries or generators.

2. **Impartial sharing:** In this case, the power rate of each of the J systems would be proportional to the capacity of their tanks, that is $\bar{P}_{ij} = {}^{i}\bar{P}_{in}\frac{\bar{T}_j}{\sum_{k=1,k\neq j}^{J} \bar{T}_k}$.

   This other strategy allows any system to contribute according to its maximal capacity. We called it impartial because every system is requested with respect to the size of its possible reserves. Of course there would be many other strategies, such as impartial sharing according the actual State of Charge, etc. Instead of using heuristics, another way to share power could be based on a criterion which can be economical for instance. Such a criterion could include maintenance, pollution (CO2 emissions), operational costs, penalties for not respecting power references, etc.

In these cases, the rate of power exchange between the systems and their energy level are fully controlled, with many parameters being as many degrees of freedom to control power request and supply authorizations. Whenever the tanks are not

empty, the passivity is preserved, and when this is not the case, energy can be requested from other systems. In the same way, when a system has an excess of passivity, then it may request other systems to supply its extra energy.
Another interesting aspect is that the strategy is very close to that of a real storage unit (a conventional battery). Hence, it is possible to share a common power sharing strategy between different energy storage units, either virtual Energy Tanks or real batteries. For the latter elements, there is no need to ensure passivity, but the State of Charge has to remain between prescribed bounds, and power exchange is allowed if the batteries are not depleted.

3.5.3 Power exchange for closed loop uncertain systems

In this paper, the above methodology is used to ensure a guaranteed passivity margin for N uncertain closed loop systems, for which a IDA-PBC control u^i has been defined:

$$\dot{x}^i = [J_d^i(x) - R_d^i(x)]\frac{\partial^i H_d^i}{\partial^i x^i} + g^i v^i + \zeta^i v^i = -K_d {g^i}^T \frac{\partial H_d^i}{\partial x^i} \tag{3.41}$$

where $i = 1 \cdots N$, v^i is an additional output feedback term that ensures asymptotic convergence - which should be implemented with the help of the Energy Tank. The main problem is that, according to the values of $\zeta^i = R_{\zeta^i}\frac{\partial H_d^i}{\partial x^i}$, the passivity margin $D_{R_d^i}$ can be lost because R_{ζ^i} may not be positive definite.
In this case, one will try to ensure a minimum passivity margin $D_{\bar{R}_d^i}$ with $\bar{R}_d^i R_d^i \succ 0$. Hence, the Energy Tank will be filled only if $D_{\bar{R}_d^i} > 0$, that is when $R_d^i + R_{\zeta^i} - \bar{R}_d^i \succ 0$. Then, the power sharing policy described in the previous section applies.

3.6 Conclusion

The dynamic energy transfer between multi-ports of different physical systems is a challenging task and different strategies are developed in the literature to solve partially the problem.
The Duindam Stramigioli dynamic energy router is an available solution for non dissipative systems that uses standard switched power electronic devices as a solution for power routing.
After a review on power routing techniques using the Port-Hamiltonian formalism, we have extended the Energy Tank design for power routing. The interesting thing is that we can link the States of Charge of the tanks with power reserves in the system, in order to ensure the switch between the different operating modes based on the state of charge as an internal parameter to the system.
The virtual Energy Tank concept allows to recover the dissipated energy of the

physical systems and use it to implement passively the desired control actions and ensure a dynamic energy transfer between interconnected systems through their respective Energy Tanks. The main interest of using Energy Tank is that it behaves as a virtual battery (or as a virtual flywheel). This enables not only to control the level of power flows but also the energy level (equivalent to a State of Charge) of the tank.

The energy transfer between the tanks can be released based on the user expectations and objectives. For example, in our situation we proposed to study the case of preferential and impartial repartition as an illustrative way to proceed, but there are many other possibilities, that could be based on optimal or economical criteria.

When addressing the management of a system with multiple operating modes, it is possible to trigger the switching based on the state of charge of the tanks. This is more interesting than relying only on decision variables for which the switching domains are arbitrary. As the virtual tank state of charge accounts for power reserves of the system, it allows to know whether a system, requested to share power, is able to supply it or not without affecting its passivity.

Chapter 4

Application: Energy Tank power exchange in multi-source renewable systems

4.1 Introduction

The port-Hamiltonian representation of multi-physics systems is an energetic modeling formalism that in addition to the energy aspect as in bond graph owns, the state space form of the model that allows to design control techniques in a generic fashion for linear and non-linear systems.
Different port-Hamiltonian models can be interconnected together in an easy way and disconnected whenever we want it, depending of the cases studied. The use of an automaton where the switches are triggered by a set of variables (internal or external to the system) which is independent from the system dynamics would allow to easily generate and handle different operating modes.
The management of the different operating modes in a multi-physics system through an automaton can be achieved through the thresholds of Energy Tanks as explained in chapter 3, which also allows to consider parameter uncertainties.
To illustrate the use of Energy Tanks in renewable energy systems, we will consider a sub-part of the multi-source renewable energy platform for hydrogen production, modeled in chapter 3. The graphical results are obtained using Matlab/Simulink.

4.2 Estimation of the passivity margins via Energy Tanks in a multi-source renewable system

The Energy Tanks offer a good estimation of the passivity margins and the power reserves of the systems. They tell us about the amount of power available to exchange with other systems which will help them to guarantee their passivity rate necessary for their power stability while enabling them to share power.
The proposed technique is applied to the multi-source renewable energy platform

for hydrogen production. To recall, the multi-physical platform is composed of two renewable energy resources, namely, a PMSG wind turbine and a solar panel, a proton exchange membrane electrolyser and a proton exchange membrane fuel cell, with two storage units, using a conventional lead-acid battery and a hydrogen storage tank. The wind turbine system, the PEM fuel cell and the electrolyser are augmented with an Energy Tank system through which we can deduce the passivity margins of the three systems. The whole system is simulated under the Matlab/Simulink software, as displayed in figure (4.2.1)

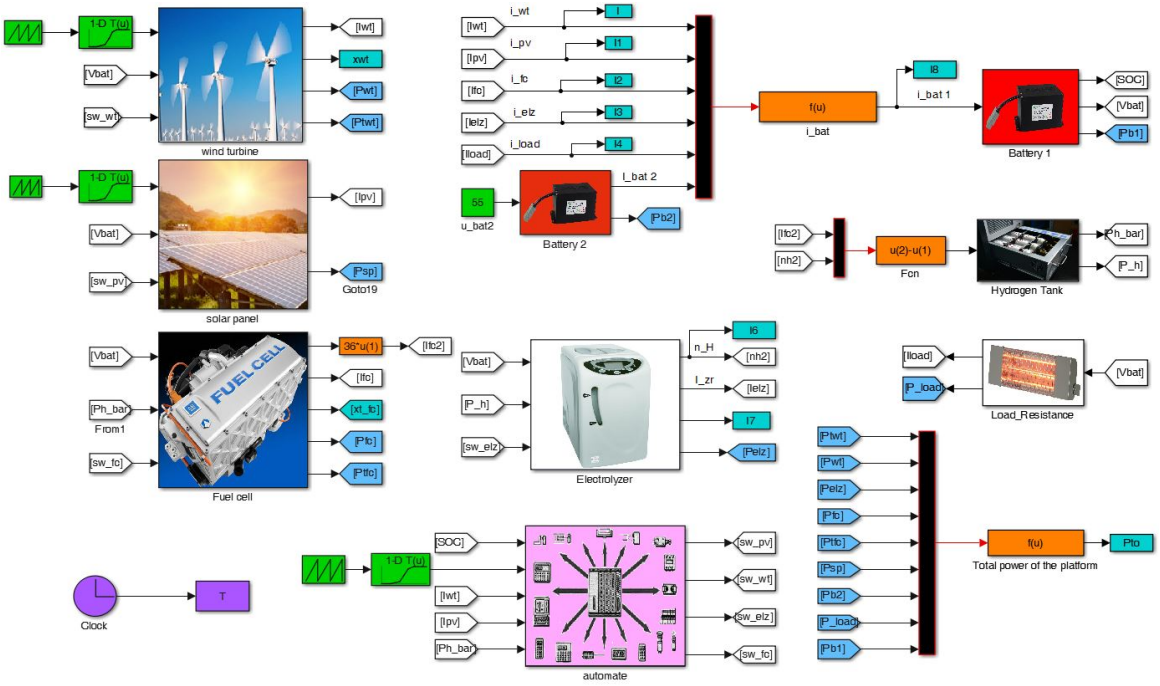

Figure 4.2.1: Simulink model of the platform with Energy Tanks

Otherwise, as already explained in the previous chapter, the energy exchange between the different tanks is achieved depending on power and energy control objectives and depending on the number of the Energy Tanks involved in the power exchange process. Preferential and impartial distribution of energy may be considered.

The simulation results are obtained by respecting the switches between three operating modes: Low power (OM_1), High power (OM_2) and safe power (OM_3) operating mode. Hence, OM_1 is accessed when the generated power by the sources (P_r) is less than 100 W. The system maintains in this mode until the generated power reaches 200W. Then, the OM_2 is triggered when the generated power by the sources is strictly greater than 200W. The system maintains in OM_2 until the generated power drops to 100W.

When the OM_1 is no more available due to component failure or due to power shortage $(P_r < 100W) \wedge (SoC < 30\%) \wedge (P_{H2} < 1bars)$ the safe mode OM_3 is

triggered. Otherwise, the OM_3 is activated when the OM_2 mode is not available due to a fault or due to the saturation of all the storage units $(P_r > 200W) \wedge (SoC > 95\%) \wedge (P_{H2} > 10bars)$. In this chapter, we will show with an example how one can manage an operating mode, not with an external variable but using the systems Energy Tanks.

4.2.1 Wind turbine system

The dynamic model of the PMSG wind turbine (see chapter 2) is given in the following form,

$$\begin{cases} \dot{p} = -\left(f_r + \frac{K^2}{d}\right)\frac{p}{m_r} + r_{Gy}v_w + \frac{K}{d}V_{bat} + \eta \\ y = r_{Gy}\frac{p}{m_r} \end{cases} \tag{4.1}$$

where η is the external disturbance that can be due to the wind speed estimation error or parameter uncertainties.
For the wind turbine system a Maximum power point tracking (MPPT) is used to maximize power extraction under all conditions. The system is augmented with an Energy Tank system which feeds the system with the desired energy in case of shortage of energy while it saves the excess of energy due to the dissipation energy of the system and to external disturbances guaranteeing by this way the passivity of the system.

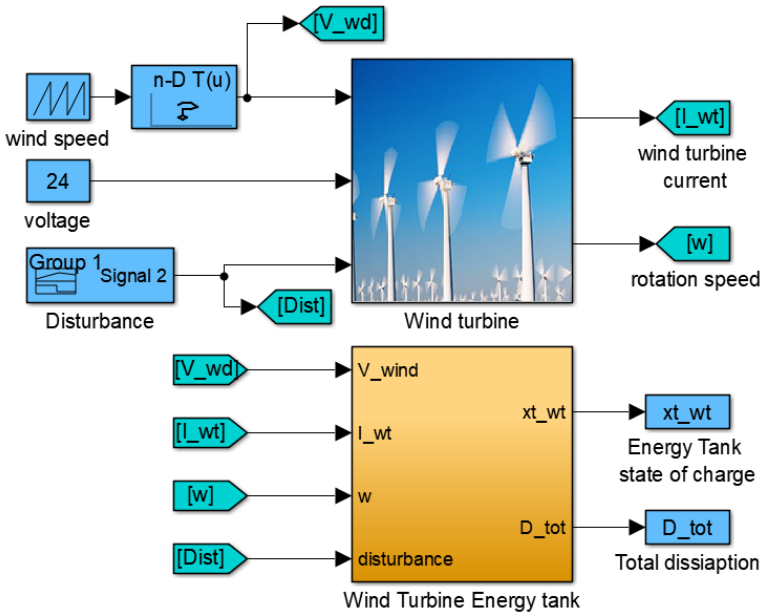

Figure 4.2.2: Wind turbine with its virtual Energy Tank

From the simulation given in figure (4.2.2) of the wind turbine system with the disturbance profile in figure (4.2.4), we obtain the following rotation speed of the rotor and the produced current as reported in figure (4.2.3).

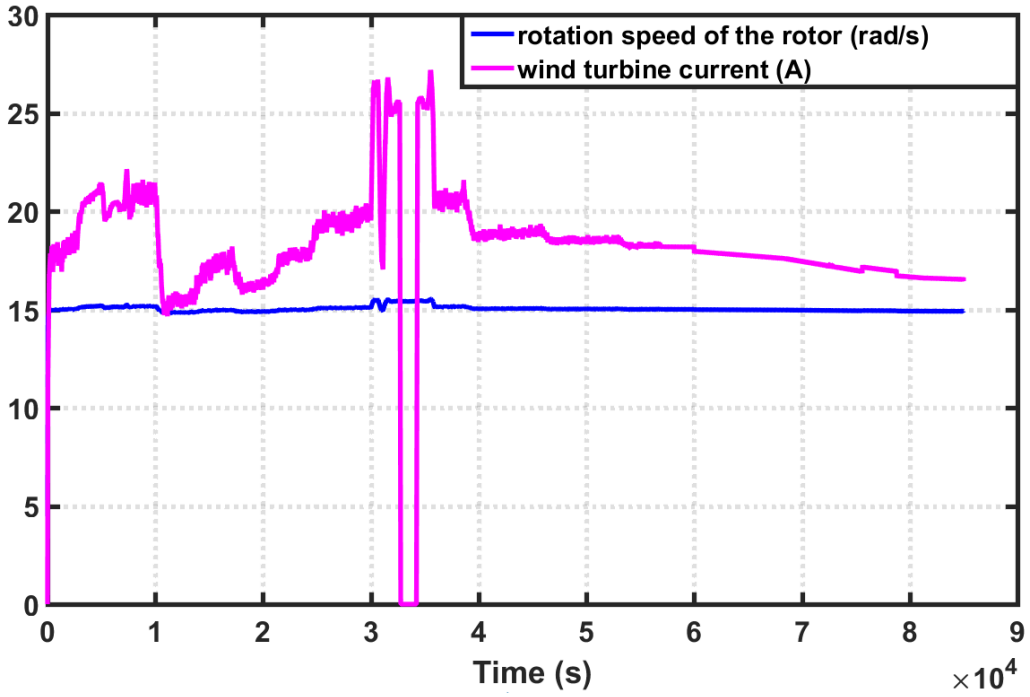

Figure 4.2.3: Rotation speed of the rotor and the wind turbine current

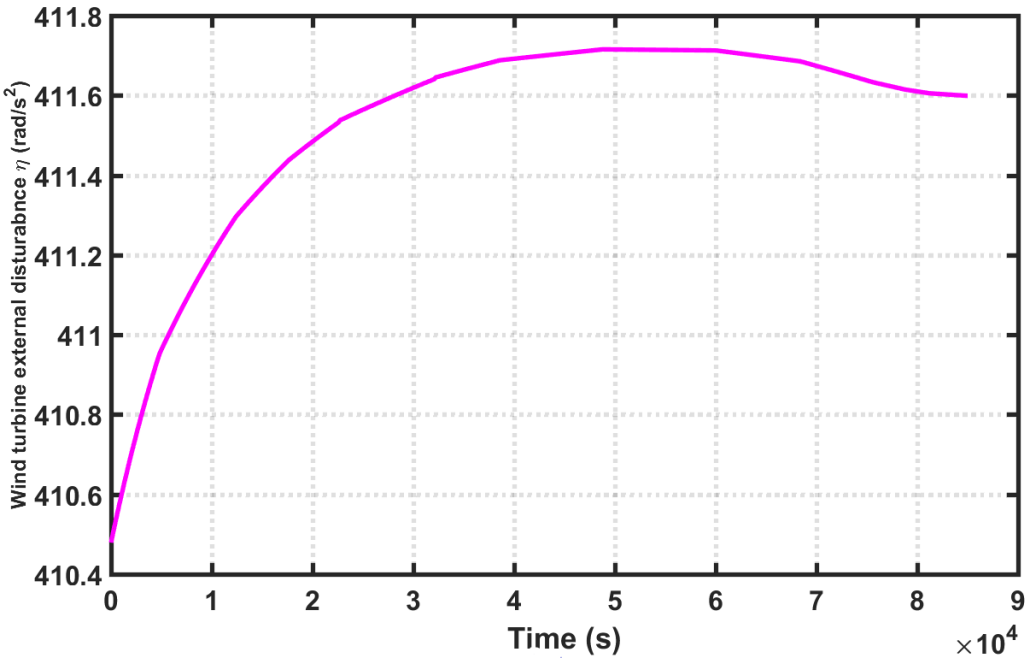

Figure 4.2.4: Wind turbine system's external disturbance (rd/s^2)

The curve of the dissipated power of the wind turbine system with the percentage rate of the energy state of charge of the Energy Tank that informs us about the passivity of the whole system comprising the wind turbine system and its Energy Tank are reported in figure (4.2.5). We notice that the rate of energy stored in the Energy Tank decreases after 3.2×10^4 s due to the external disturbance.

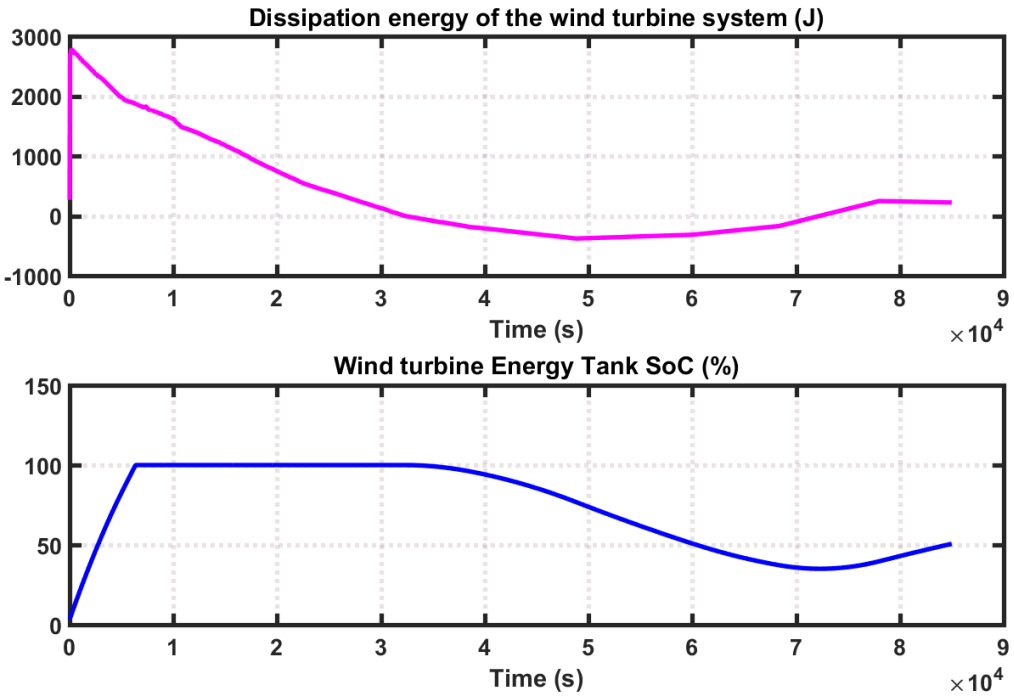

Figure 4.2.5: Wind turbine dissipation and its Energy Tank state of charge

The changes observed on the wind turbine Energy Tank level correspond to the behavior of the parameter $\sigma(t)$ of the wind turbine tank (see figure (4.2.6)) which allows or not the storage of energy in the tank, depending on the tank load rate. For the period $[0 - 1.2 \times 10^4]$ (s) and $[1.2 \times 10^4 - 3.2 \times 10^4]$ (s), $\sigma(t) = 1$ therefore, the tank is not sufficiently loaded and storage is authorized unlike period $[1.2 \times 10^4 - 3.2 \times 10^4]$(s), where the tank is fully loaded and therefore it is no longer possible to store additional power.

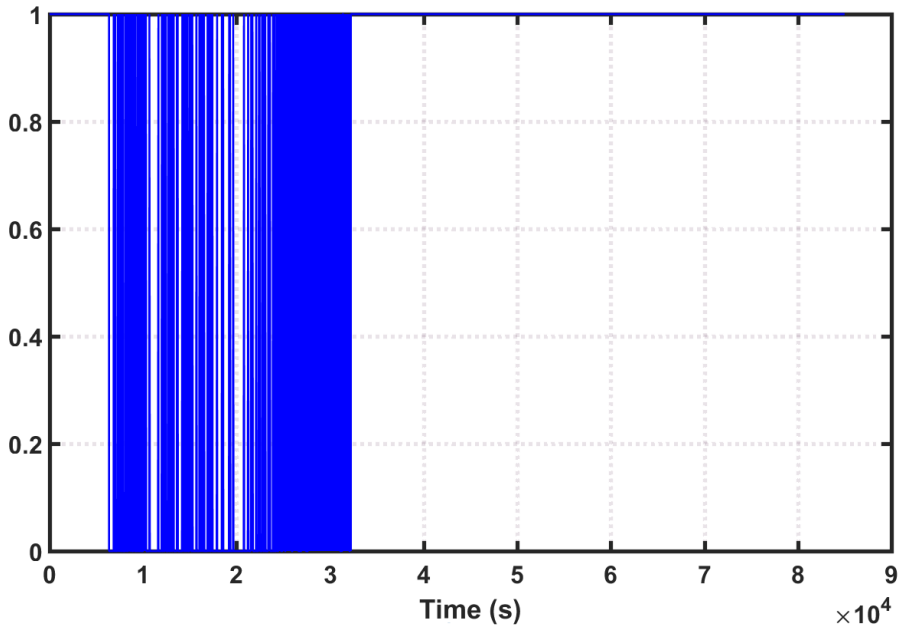

Figure 4.2.6: Wind turbine parameter $\sigma(t)$

4.2.2 PEM fuel cell system

The PH model of the PEM fuel cell model (see chapter 2) is given by:

$$\begin{bmatrix} \dot{q}_{mb} \\ \dot{q}_{cal} \end{bmatrix} = \begin{bmatrix} -\frac{1}{\mathrm{R_{ohm}}} & 0 \\ 0 & \frac{1}{\mathrm{R_{th}}} \end{bmatrix} \begin{bmatrix} \frac{\mathrm{q_{mb}}}{\mathrm{C_{mb}}} \\ \frac{\mathrm{q_{cal}}}{\mathrm{C_{cal}}} \end{bmatrix} + \begin{bmatrix} 1 & 0 \\ h & \frac{1}{\mathrm{R_{th}}} \end{bmatrix} \begin{bmatrix} I_{AC} \\ T \end{bmatrix} \tag{4.2}$$

The PEM fuel cell system produces a nominal current of 11.2 (A).
The profile of the dissipated power of the PEM fuel cell system and the SoC (%) of the Energy Tank that provides information on the passivity system are shown in the figure (4.2.7).

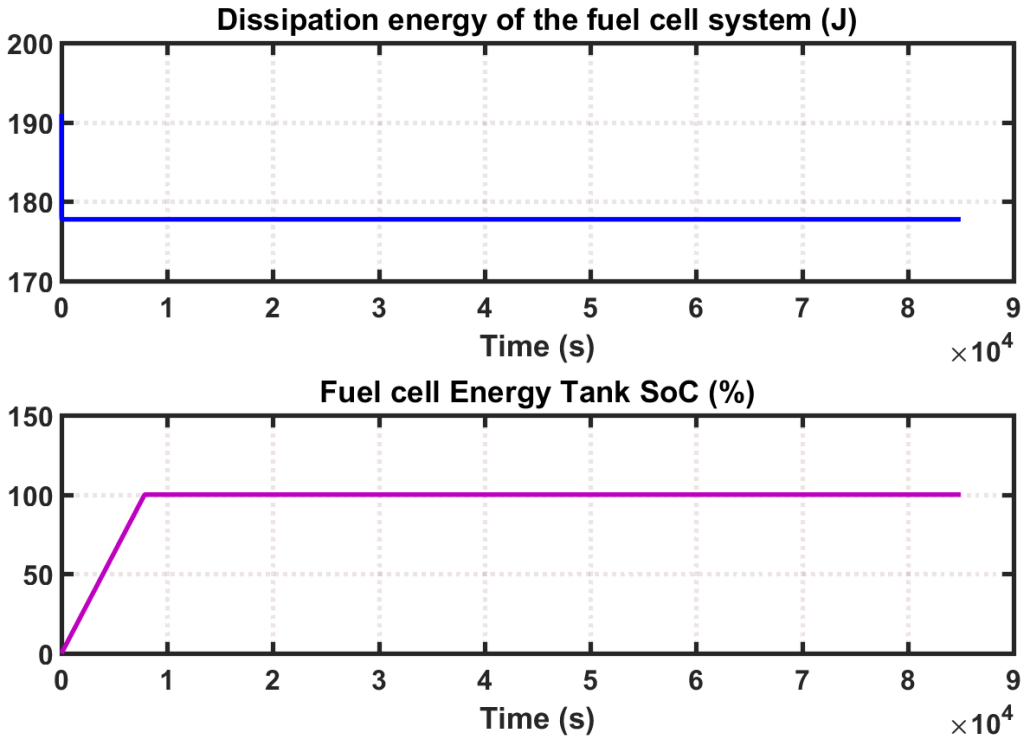

Figure 4.2.7: PEM Fuel Cell dissipation and its Energy Tank state of charge

Figure (4.2.8) represents the curve of the PEM fuel cell current which remains constant at 11.2 A .

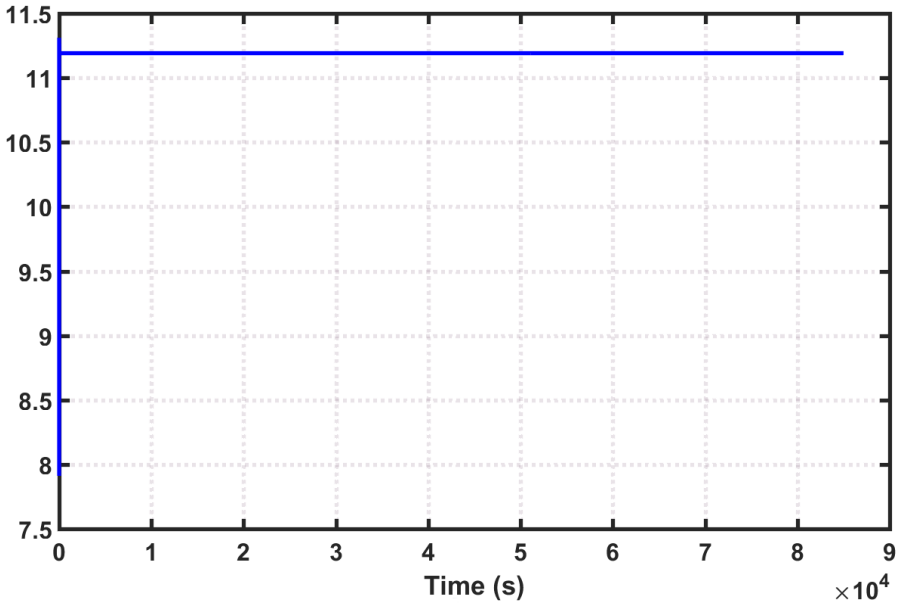

Figure 4.2.8: PEM fuel cell current curve (A)

The hydrogen (H2) and oxygen (O2) molar flow which represents the PEM fuel cell input is given in figure (4.2.9) under a constant pressure of 35 (Bar) and a temperature of $296K$.

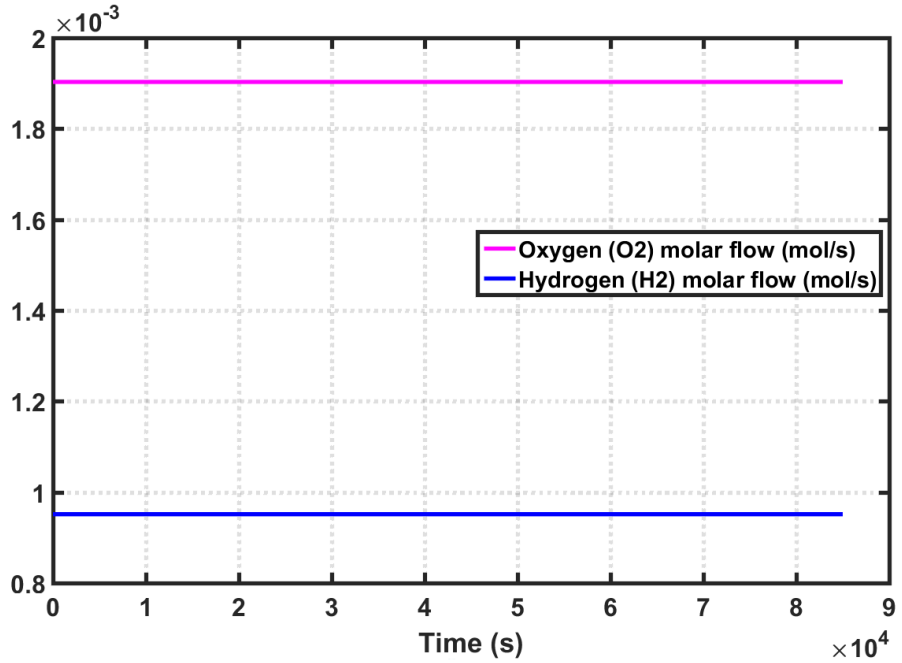

Figure 4.2.9: Hydrogen and oxygen molar flow to the PEM fuel cell (mol/sec)

Otherwise, figure (4.2.10) represents the curve of the fuel cell $\sigma(t)$ that decides whether energy can be stored or not in the fuel cell tank.

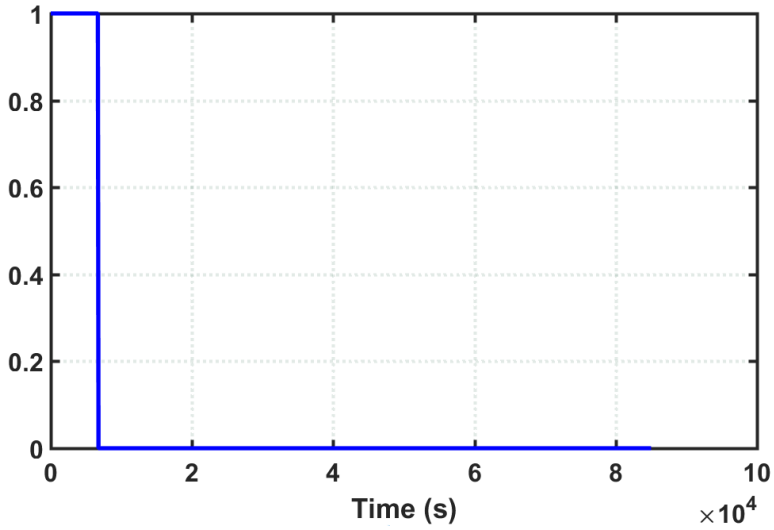

Figure 4.2.10: The curve describing the behavior of the fuel cell $\sigma(t)$

4.3 Power exchange between the wind turbine and fuel cell system via Energy Tanks

The main goal of the port-Hamiltonian representation of the multi-source renewable platform and the use of the Energy Tank concept is to ensure a power exchange between the different sub-systems of the platform, indirectly, by using the Energy Tanks linked to each sub-system whenever this is possible. The use of Energy Tanks to feed systems with the desired energy comes as an other solution equivalent to the Virtual Power Plants (VPP).
To illustrate the case of preferential repartition on the energy between Energy Tanks, we consider the configuration of two tanks linked to the wind turbine system and PEM fuel cell respectively, and an additional conventional battery.

4.3.1 Preferential power distribution between the wind turbine and the fuel cell systems Energy Tanks

In what follows, a preferential distribution of energy between the Energy Tanks of the fuel cell and the wind turbine is studied in presence of an external battery, see figure (4.3.1). Hence, an external battery serving as a physical Energy Tank is used in the context of a depleted operating mode, where the wind turbine Energy Tank is the concerned system by the energy depletion.
The external battery supplies energy to the tanks of the wind turbine and the PEM fuel cell according to the energy exchange policy between the Energy Tanks. The dynamic of the battery is described in the following equation,

$$SoC = 70 - \frac{100}{C_{bat}} \left(\int_{t_0}^{t} i dt + \int_{t_0}^{t} \frac{{}^{bat}P_{\text{int}} - {}^{bat}P_{out}}{24} dt \right) \tag{4.3}$$

where $SoC_0 = 70\%$ is the initial state of charge of the battery, C_{bat} is the battery capacity, ${}^{bat}P_{in}$ and ${}^{bat}P_{out}$ are respectively the ingoing and outgoing power to/from the battery.

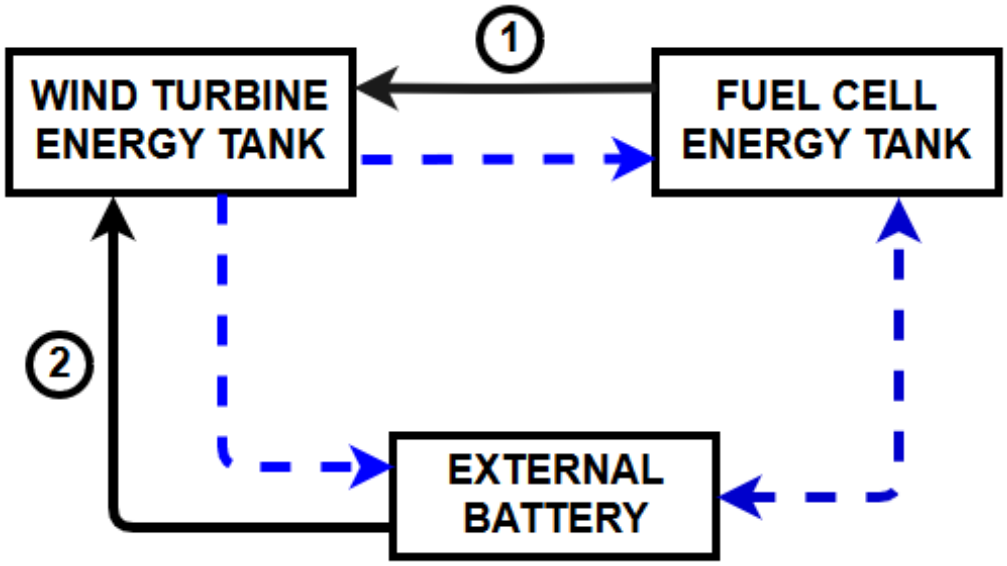

Figure 4.3.1: Energy exchange priority between the wind turbine Energy Tank, fuel cell Energy Tank and the external battery

For this specific study case, we consider that the wind turbine system subject to external disturbances or parameter uncertainties causes a discharge of its Energy Tank below the energy request threshold (${}^{wt}T_{req}$). To prevent the situation from getting worse, the wind turbine Energy Tank sends an energy request (${}^{wt}E_{req}$), to the fuel cell Energy Tank first, which is supposed to be full enough such that it can help by transferring energy to the wind turbine Energy Tank. The fuel cell Energy Tank keeps feeding the wind turbine Energy Tank until it reaches its limits($T_{fc} \approx {}^{fc}T_{req}$) fixed around 75%. When the fuel cell Energy Tank is not anymore able to feed the wind turbine Energy Tank, the external battery takes over, in a second position. The blacks arrows in figure (4.3.1) shows the energy exchange priority between the three storage elements (Wind turbine Energy Tank, fuel cell Energy Tank and external battery) while the discontinued blue arrows shows the secondary energy transfer possibilities in this situation, where the wind turbine and the fuel cell Energy Tanks can transfer their excess of energy to the external battery and the fuel cell Energy Tank also can be supplied by the wind turbine Energy Tank or/and the external battery in case of need.

Figure (4.3.2) represents the Energy Tank State of Charge for both the wind turbine and the PEM fuel cell systems as well as the State of Charge of the battery (70% in this case) are shown. The wind turbine Energy Tank SoC starts

to decrease after 3.5×10^4 (s) getting below the 60% at 5.5×10^4 (s) without ever going up and this due the external disturbance given in figure (4.2.4). In this situation, it is important to send an energy request to the fuel cell Energy Tank for help then for the external battery.

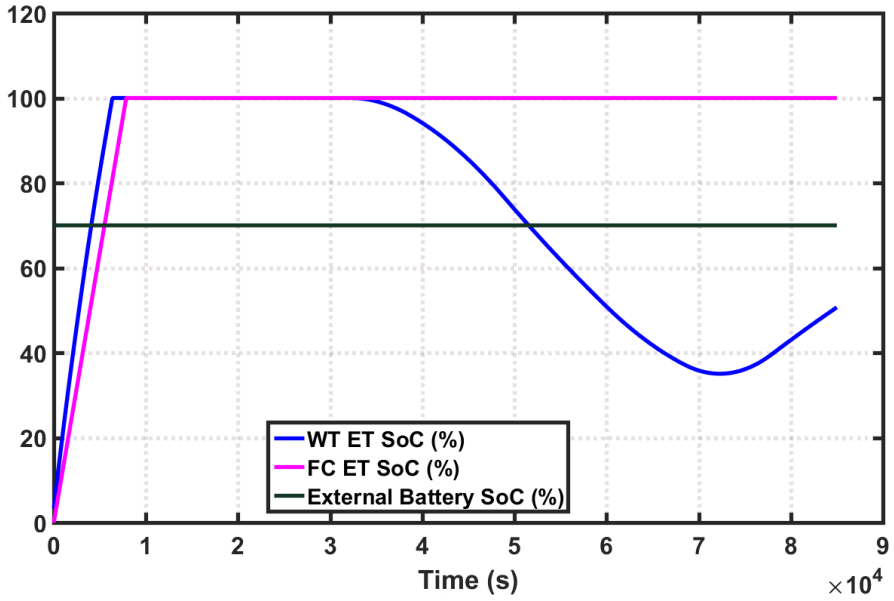

Figure 4.3.2: Energy Tank of the wind turbine and fuel cell state of charge and the state of charge of the external battery

For this study case it is specified that the wind turbine Energy Tank should be fed by the Fuel cell Energy Tank and the external battery if the fuel cell Energy Tank is not able to completely feed it, preventing it from going below 60% of its SoC.
In figure (4.3.3), after an exchange of energy between the two Energy Tanks linked to the wind turbine and fuel cell systems with the external battery, the state of charge of the three storage elements have changed compared to the figure (4.3.2). Hence, the fuel cell Energy Tank transfers energy to the wind turbine Energy Tank at 5.1×10^4 (s), until it reaches 75% nearly of its SoC at 6.5×10^4 (s) the moment from which the external battery takes over and transfers energy to the wind turbine Energy tank. Thanks to energy exchange the wind turbine Energy Tank SoC is stabilized at 60% as desired.

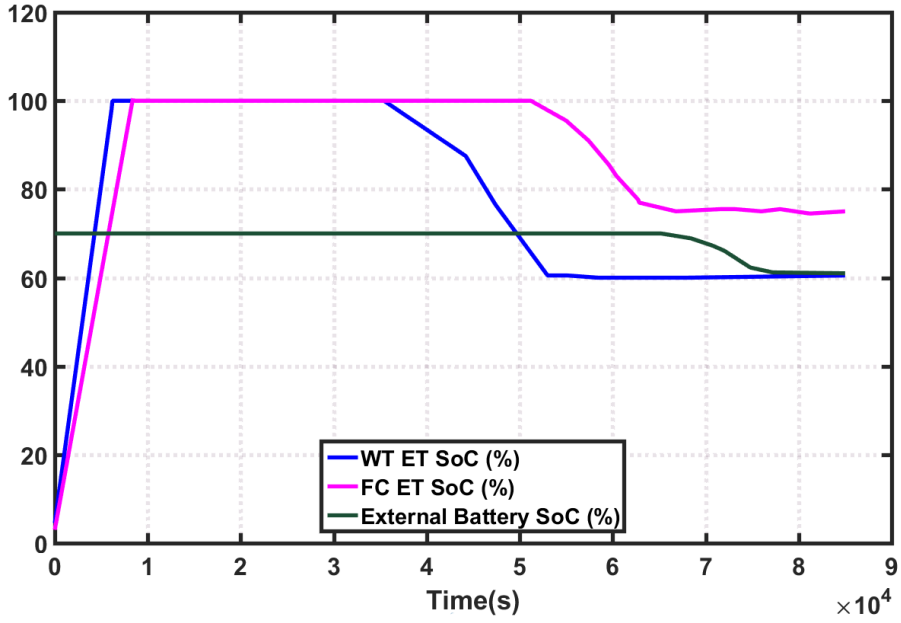

Figure 4.3.3: Energy exchange between the tanks and the battery

The external battery current behavior is given in figure (4.3.4) where the battery current is equal to 0 during the time interval $[0 - 6.5 \times 10^4]$ s, but because of the energy transferred to the wind turbine Energy Tank it starts to increase which corresponds to a discharge of the battery.

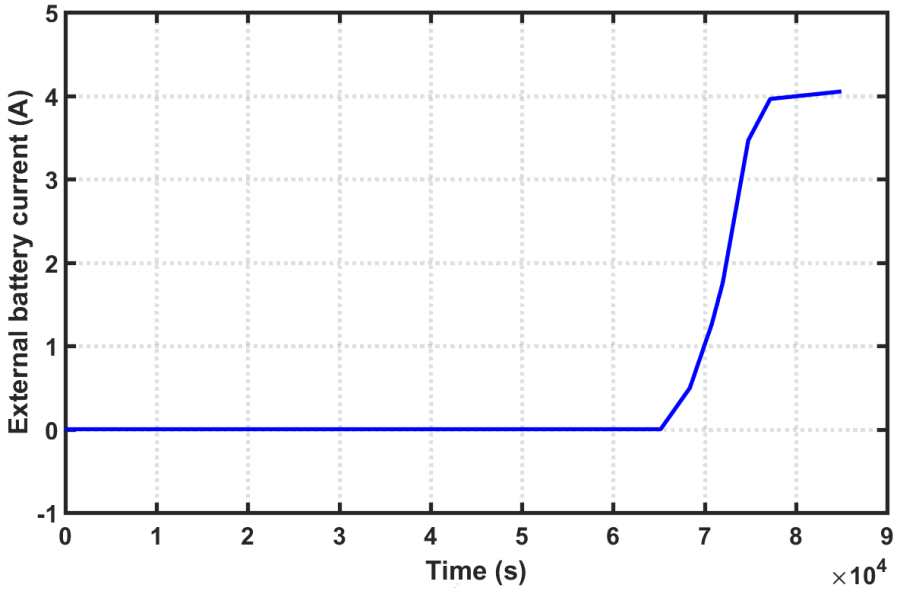

Figure 4.3.4: External battery current curve (A)

Figure (4.3.5) represents the curve of the PEM fuel cell current which around 5.1×10^4 s is increasing which corresponds to the energy transfer period from the fuel cell Energy Tank to the wind turbine Energy Tank.

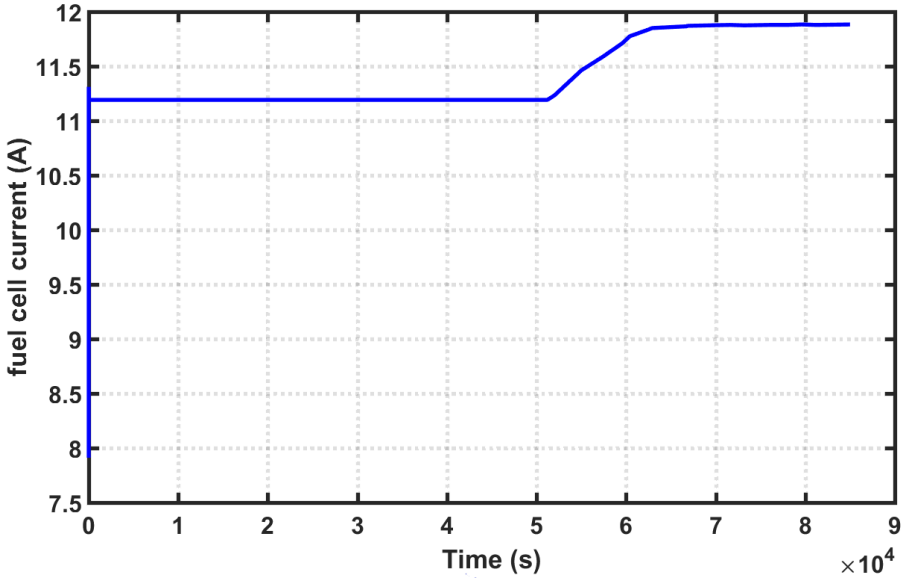

Figure 4.3.5: PEM fuel cell current curve (A)

4.3.2 The ingoing and outgoing power of the systems Energy Tanks

The ingoing (P_{in}) and outgoing (P_{out}) power quantities are the power flows through which the Energy Tanks can exchange energy with the external world and between each other.
The available power at the Energy Tank of the wind turbine ready to be exchanged with the other systems through their respective Energy Tanks is given in figure (4.3.6).

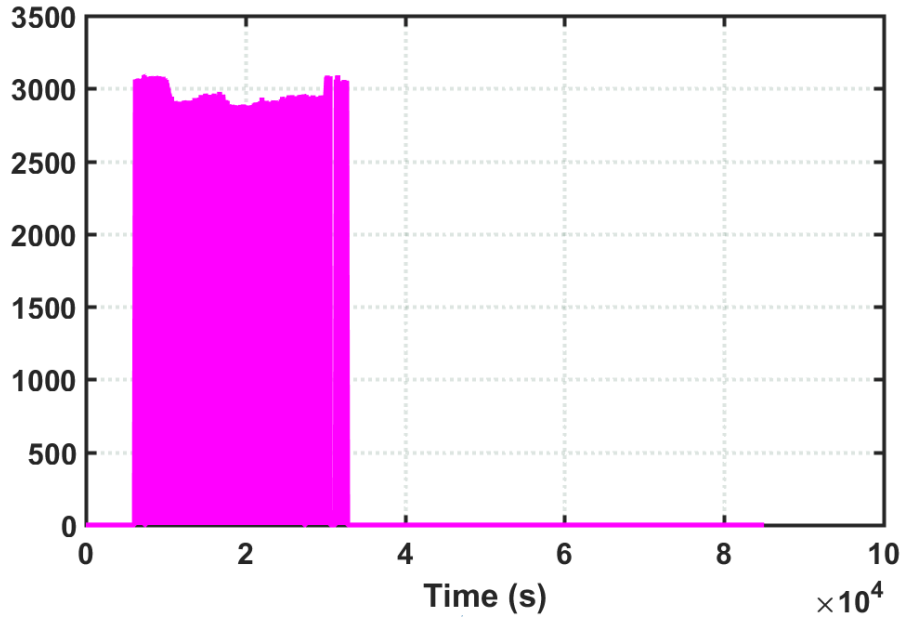

Figure 4.3.6: Wind turbine available outgoing power (W)

The available power to be exchanged with the external world in equal to zero

after (3.6×10^4 s) which means that the Energy Tank of the wind turbine has no enough energy and this is confirmed by the behavior of the wind turbine energy request parameter E_{req} given in figure (4.3.7) where around 5.5×10^4 (s) goes from 0 to 1, what means that the wind turbine Energy Tank is asking for energy since it reached its lowest limit of 60%.

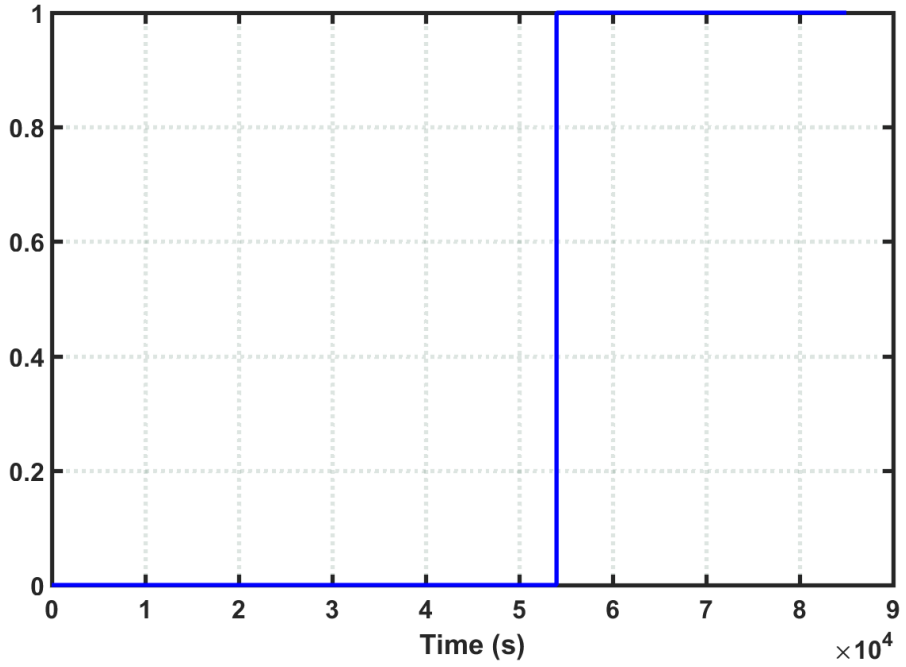

Figure 4.3.7: Wind turbine energy request parameter E_{req}

In the other side, the available power at the Energy Tank of the PEM fuel cell is shown in figure (4.3.8), where we can see that it contains enough energy ready to be transferred to the wind turbine Energy Tank for help.

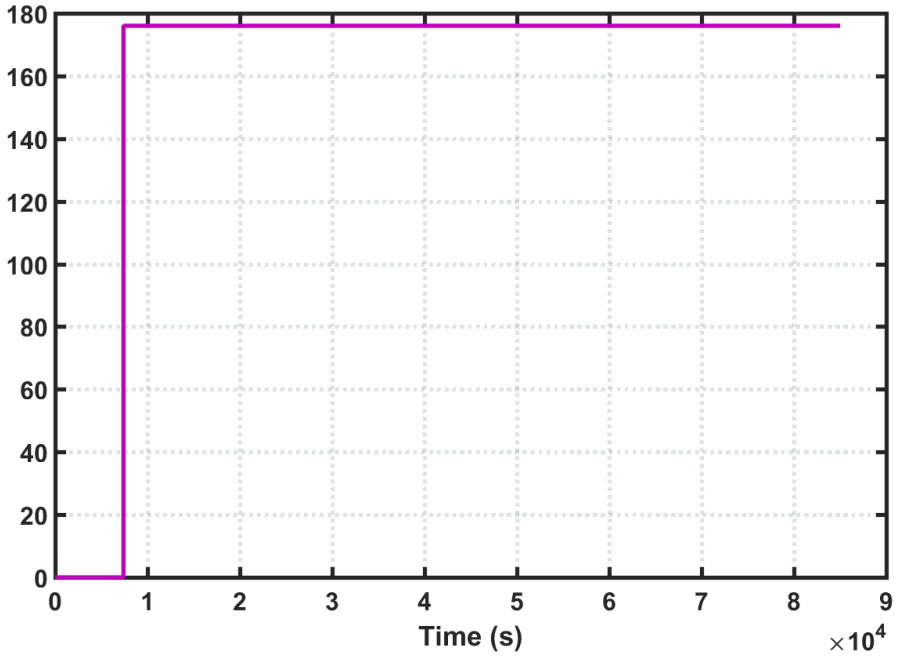

Figure 4.3.8: PEM fuel cell available outgoing power (W)

4.4 Conclusion

The port-Hamiltonian representation of the hydrogen-based power cell with an automaton for the triggering of the switches between the operating modes among the platform is equivalent to the Event-Driven Hybrid Bond Graph system presented in [5]. Hence, the port-Hamiltonian tool allows to explore different operating modes of the platform and describe the discrete and continuous dynamic of the system.However, it can allow a tight control of the power flows and energy reserves.

The virtual Energy Tanks store the excess of energy related to the passivity of a system, or is depleted whenever the system is no more passive. They have an external power input and power output which allow them to be used in different ways, for power and energy management. In a first time, we used the virtual Energy Tanks to estimate the reserves of energy in systems and also as an intermediate power routing system, which helps to troubleshoot systems in terms of power. In fact, Energy Tanks are systems linked to physical systems, they can not operate on their own, on the other hand, they can be interconnected together in order to help each other to guarantee the power stability of the global system. The State of Charge and the maximum and minimum threshold of each Energy Tank can be used by an automaton to trigger the switching between the different OM.

The use of port-Hamiltonian formalism for modeling the elements of the multi-source power cell for hydrogen production has shown that this formalism largely

meets the requirements required for the modeling of these multi-physics systems and that this representation can therefore be used reliably for various model-based applications.

General conclusion and perspectives

Summary and discussion of the thesis

Green electrical energy production and storage is a challenging topic nowadays. Electrical energy production using the renewable energy resources includes more and more new systems (Electrolyzer, Fuel cell, ..etc) and these different subsystems should be interconnected together and work simultaneously depending on the weather conditions and grid load. The use of hydrogen tanks to store the electrical energy is a promising alternative solutions to the classical chemical batteries.

Power routing with control of energy reserves within hydrogen-based power cells was the fundamental objective of this thesis.In this context, we selected modeling tools which allowed us to estimate the energy reserves in multi-physical systems. We exploited in a first time the bond graph formalism to represent these systems graphically and then used the port-Hamiltonian state space representation. We extended the concept of passivity margins, which represents the rate of energy available in a system allowing it to guarantee its stability and a power margin as a safety measure, to systems with known disturbances. The passivity reserves can be stored in a so-called Energy Tank. These virtual tanks are an image of the energy reserves of a system. One of the main interest of energy tanks is that they behave as a conventional storage unit, with input and output power ports in addition to their input/output connections. Hence, we have introduced in these tanks a concept of State of Charge likewise a battery, which defined the ratio between the available and maximum energies in the tank.

Next, our contribution was to use the energy tank connected to a system as a medium for power routing and exchange with other systems. An Energy Tank is interconnected in a first time through its input and output with a system. Instead of exchanging directly power between different systems, the power exchange is carried out between their energy tanks using their power ports. The main interest is to control not only the power exchange while keeping the systems passive, but also the level of energy in the tanks. We designed different policies for power routing between the tanks. For example, we have thought of a preferential strategy, or a fair sharing of the effort between the tanks. Any kind of strategy based

on power or energy levels can be imagined.
We have used these concepts for the power routing in a hydrogen power cell. First, we have designed a simplified port-Hamiltonian model of the power cell, and in particular, of the electrolyser and the fuel cell. These modeling works represent a major part in the contribution made in this thesis. Through the designed models, we have shown that changing interconnection ports or the type of input does not affect the passivity of the systems.Therefore, the general model generated, allows us to learn about the level of passivity and therefore of the energy in each system. Furthermore, the concept of exchange between energy tanks has been demonstrated for a simple power cell consisting of a fuel cell, a wind turbine and a battery. We have shown that one can control the passivity and energy level in the wind turbine and the fuel cell under the scenario of a wind speed disturbance. A preferential strategy was used, that is the fuel cell should be requested when the passivity margin of the wind turbine falls under a prescribed threshold, and then the battery complements when the fuel cell passivity is not sufficient enough. This means that the management of the operating modes is not triggered by an external variable but by the level of energy in the tanks. What is interesting is that, since the Energy Tanks behave as Virtual Storage Units, one can team them with a real battery. Hence, the work in this thesis is a promising way to handle both power and energy routing for power systems.
The obtained results at the end of this research work show that the port-Hamiltonian modeling tool is an interesting tool for the modeling of multi-physical systems. The state space representation offered by this tool makes possible the use of several linear and nonlinear control techniques, cover the discrete and continuous behavior in the systems and test different OMM in a flexible way without the need to reconfigure the model representation. Then, the virtual energy tanks for energy storage and exchange seems to be a promising power exchange concept.

Perspectives and future work

The results obtained within the framework of this thesis open promising perspectives, on the modeling, control and diagnostic level of multi-physical systems. At the end of this research work, we have tried, in what follows, to list some of the points that remain to be developed as research, internship or doctoral project.

1. **Investigation of different operating modes and energy distribution strategies for better power routing:** A single operating mode with a preferential exchange of energy including two virtual energy tanks, namely, a wind turbine and fuel cell virtual energy tank with a real storage battery has been tested in this thesis work. Different operating modes and energy

distributions strategies can be investigated in future to optimize power routing in HRES.

2. **Test different energy distribution strategies and compare:** The energy transfer between the systems can be performed based on different criteria. Preferential and impartial strategies can be adopted for different operating modes, that is why it is suitable to test the different strategies and compare them to select the good strategy for each studied case.

3. **Explore other internal switching parameters**: The operating modes are triggered based on the energy tanks state of charge and their minimum and maximum thresholds. Hence, other parameters can be used to trigger the switches between the different operating modes.

4. **Use Energy Tanks in diagnosis:** Diagnosis of HRES has not been studied in this thesis. However, the use of the Energy Tanks in diagnosis can be investigated to compensate for the effects of defaults in the system based on power and energy in the system.
   In fault detection and isolation [117], Energy Tanks can be used to adapt the OMM, namely, to get out from a degraded operating mode or to switch from an OMM to another. The prediction of power and energy related failures in the system can be avoided by using Energy Tanks that work as a power plant which makes it possible to supply and/or store energy.
   Otherwise, Energy Tanks can be used to ensure the operation of a system in the presence of faults, within the framework of a Fault Tolerant Control (FTC). Indeed, with the possibility of exchanging power between the Energy Tanks, we are not obliged to change the operating mode in the event of faults, but we can continue to operate the system in FTC mode as long as the reserves in energy from the Tanks allow it.

5. **Economic triggering criteria:** For the switching between the different operating modes we only focused on the state of charge of the virtual Energy Tanks and their minimum and maximum thresholds. Economic criteria can be investigated in presence of Energy Tanks.

6. **Physical implementation:** Only simulated results using Matlab/Simulink simulations have been presented in this work, so a real application of the developed theories and operating modes for the multi-source renewable energy platform for hydrogen production remains to be done.

Appendices

.1 Tables

Parameter	Description	Value
Solar panel		
$MR : R_d$	Modulated non-linear resistance	
R_{Sh}, R_S	Shunt and series resistances	
$K[m^2kgs^{-2}K^{-1}]$	Boltzmann constant	$1.38064852x10^{-23}$
Hydrogen storage tank		
$C : h_2$	Storage capacity	
T_{tank}	Tank temperature	298
V_{tank}	Tank volume	3
P	Storage pressure	
$R : r_v$	Leak resistance	1×10^10
$N[kmol\ s^{-1}]$	hydrogen moles	
K	Gain to get pressure from pascal to bar	1×10^{-5}
Electrolyzer and fuel cell		
$E_{rev(T,P)}$	Open circuit electrical potential	
$\Delta G^0_{(T)}$	Gibbs free energy	
E_0	standard potential	-1.23 $[V]$
TF : Electrolyzer		1
TF : Fuel cell		1.1
$C : Cal$	Thermal capacity of the water	
T_{out}	External temperature	
P_{h_2}	Hydrogen pressure	
P_{O_2}	Oxygen pressure	
$R : R_{ohm}$	ohmic resistance	
$RS : R_{trans}$	Transition resistance	
$RS : R_{act}$	Activation resistance	
$R : r_{th}$	thermal resistance (conductivity)	
$C : C_{mb}$	Electrical capacitor	
$\alpha_{rec}\ [J.mol^{-1}.K^{-1}]$		-11.5575
$\beta_{rec}\ [J.mol^{-1}.K^{-1}]$		3.9582×10^{-3}
$\gamma_{rec}\ [J.mol^{-1}.K^{-1}]$		3.9582×10^{-6}
Wind turbine		
C_p	Power coefficient	0.585
$I : m_r$	inertia of the rotor	4.5
λ	Tip speed ratio	
W_r	Wind turbine rotation speed	
r	Rotating radius	
v_w	wind speed	
β	Pitch angle	
A, ρ	Swept erea, Air density	
T_{mech}	Mechanical torque	
f_{wind}	speed flow	
Ng	Gear transformation ratio	1
K	DC generator transformation	
r_{GY}	Gyrator transformation ratio	
$R : f_r$	Viscous friction of the bearing	0.002
$R : d$	stator resistance	0.1
phi		1.721

Table 1: Bond graphs parameters

Solar panel characteristics	
$STC : G = 1000[W/m^2], T = 25C^\circ, I_{ph} = 1.5[AM]$	$U_{OC} = 33.77V$
$P_{MPP} = 220Wp(\pm 2.5Wp)$	$I_{SC} = 8.62A$
$U_{MPP} = 27.54V$	$\delta I_{SC} = 0.05\%/^\circ K \left[4.335.10^{-3} A/^\circ K\right]$
$I_{MPP} = 8.08A$	$\delta U_{OC} = -0.32\%/^\circ K \left[0.108V/^\circ K\right]$
Wind turbine characteristics	
Rotor diameter	1.17m
Wind speed	$3.1 - 22m/s$
Alternator	PM brushless
Startup Wind Speed	3.1 m/s
Voltage	24 VDC
Fuel cell characteristics	
FC model	NEXA 1.2 KW
H2 pressure	0.3-0.5 bar
Power	1200 W
Output voltage	40-20 V/DC
Electrolyzer characteristics	
Hydrogen flow rate STP	$20C, 1bar$
Model NMH2 plus 500	0-500 cc/min at STP
Max outlet pressure	11 bar
Power consumption	350 W
Input voltage	$110 - 230V/50 - 60HzMax$

Table 2: Characteristics of the system elements

Bibliography

[1] A. K. Samantaray and B. Ould Bouamama, *Model-based process supervision: a bond graph approach*. Springer Science & Business Media, 2008.

[2] V. Duindam, A. Macchelli, S. Stramigioli, and H. Bruyninckx, *Modeling and control of complex physical systems: the port-Hamiltonian approach*. Springer Science & Business Media, 2009.

[3] A. Donaire and S. Junco, "Derivation of input-state-output port-Hamiltonian systems from bond graphs," *Simulation Modelling Practice and Theory*, vol. 17, no. 1, pp. 137–151, 2009.

[4] J. Bao and P. L. Lee, *Process control: the passive systems approach*. Springer Science & Business Media, 2007.

[5] I. Abdallah, A.-L. Gehin, and B. Ould Bouamama, "Event driven hybrid bond graph for hybrid renewable energy systems part I: modelling and operating mode management," *International Journal of Hydrogen Energy*, vol. 43, no. 49, pp. 22088–22107, 2018.

[6] "Battery basics." https://www.progressivedyn.com/service/battery-basics/. Accessed: 2017-10-16.

[7] A. Sanchez-Squella, R. Ortega, R. Grino, and S. Malo, "Dynamic energy router," *IEEE Control Systems Magazine*, vol. 30, no. 6, pp. 72–80, 2010.

[8] M. J. Moran, H. N. Shapiro, D. D. Boettner, and M. B. Bailey, *Fundamentals of Engineering Thermodynamics*. John Wiley & Sons, 2010.

[9] J. Lygeros, K. H. Johansson, S. N. Simic, J. Zhang, and S. S. Sastry, "Dynamical properties of hybrid automata," *IEEE Transactions on Automatic Control*, vol. 48, no. 1, pp. 2–17, 2003.

[10] A. Schwarze, M. Buntins, J. Schicke-Uffmann, U. Goltz, and F. Eggert, "Modeling driving behaviour using hybrid automata," *IET Intelligent Transport Systems*, vol. 7, no. 2, pp. 251–256, 2013.

[11] L. Ghomri and A. Hassane, "Continuous Petri Nets and Hybrid Automata for the analysis of manufacturing systems," *IFAC-PapersOnLine*, vol. 48, no. 3, pp. 1024–1029, 2015.

[12] R. David and H. Alla, *Discrete, continuous, and hybrid Petri Nets*, vol. 1. Springer, 2005.

[13] P. J. Mosterman and G. Biswas, "Modeling discontinuous behavior with hybrid bond graphs," in *Proc. of the Intl. Conference on Qualitative Reasoning, Amsterdam, the Netherlands*, pp. 139–147, 1995.

[14] J.-Y. Dieulot, F. Colas, L. Chalal, and G. Dauphin-Tanguy, "Economic supervisory predictive control of a hybrid power generation plant," *Electric Power Systems Research*, vol. 127, pp. 221–229, 2015.

[15] L. Chalal, J.-Y. Dieulot, G. Dauphin-Tanguy, and F. Colas, "Supervisory predictive control of a hybrid solar panels, micro turbine and battery power generation plant," *IFAC Proceedings Volumes*, vol. 45, no. 21, pp. 375–380, 2012.

[16] M. Legry, F. Colas, J. Y. Dieulot, C. Saudemont, and Y. Pankow, "Improved real-time operation of microgrids with integrated economic constraints," *CIREDL Ljubljana Workshop, Slovenia*, 2018.

[17] M. Legry, J.-Y. Dieulot, F. Colas, C. Saudemont, and O. Ducarme, "Nonlinear primary control mapping for droop-like behavior of microgrid systems," *IEEE Transactions on Smart Grid*, 2020.

[18] S. Awerbuch and A. Preston, *The virtual utility: Accounting, technology & competitive aspects of the emerging industry*, vol. 26. Springer Science & Business Media, 2012.

[19] O. Palizban, K. Kauhaniemi, and J. M. Guerrero, "Micro-grids in active network management—Part I: Hierarchical control, energy storage, virtual power plants, and market participation," *Renewable and Sustainable Energy Reviews*, vol. 36, pp. 428–439, 2014.

[20] S. SenGupta, A. F. Zobaa, K. S. Sherpa, and A. K. Bhoi, *Advances in smart grid and renewable energy*. Springer, 2018.

[21] A.-L. Allègre, A. Bouscayrol, P. Delarue, P. Barrade, E. Chattot, and S. El-Fassi, "Energy storage system with super-capacitor for an innovative subway," *IEEE Transactions on Industrial Electronics*, vol. 57, no. 12, pp. 4001–4012, 2010.

[22] C. Mayet, P. Delarue, A. Bouscayrol, E. Chattot, and J.-N. Verhille, "Comparison of different EMR-based models of traction power substations for energetic studies of subway lines," *IEEE transactions on Vehicular Technology*, vol. 65, no. 3, pp. 1021–1029, 2015.

[23] T. Zhou and B. François, "Modeling and control design of hydrogen production process for an active hydrogen/wind hybrid power system," *International Journal of Hydrogen Energy*, vol. 34, no. 1, pp. 21–30, 2009.

[24] A. Bouscayrol, X. Guillaud, P. Delarue, and B. Lemaire-Semail, "Energetic macroscopic representation and inversion-based control illustrated on a wind-energy-conversion system using hardware-in-the-loop simulation," *IEEE Transactions on Industrial Electronics*, vol. 56, no. 12, pp. 4826–4835, 2009.

[25] E. Bilbao, P. Barrade, I. Etxeberria-Otadui, A. Rufer, S. Luri, and I. Gil, "Optimal energy management strategy of an improved elevator with energy storage capacity based on dynamic programming," *IEEE Transactions on Industry Applications*, vol. 50, no. 2, pp. 1233–1244, 2013.

[26] L. Boulon, K. Agbossou, D. Hissel, P. Sicard, A. Bouscayrol, and M.-C. Péra, "A macroscopic PEM fuel cell model including water phenomena for vehicle simulation," *Renewable Energy*, vol. 46, pp. 81–91, 2012.

[27] K. Agbli, M. Péra, D. Hissel, O. Rallières, C. Turpin, and I. Doumbia, "Multiphysics simulation of a PEM electrolyser: Energetic Macroscopic Representation approach," *International Journal of Hydrogen Energy*, vol. 36, no. 2, pp. 1382–1398, 2011.

[28] L. Boulon, D. Hissel, A. Bouscayrol, and M.-C. Péra, "From modeling to control of a PEM fuel cell using energetic macroscopic representation," *IEEE Transactions on Industrial Electronics*, vol. 57, no. 6, pp. 1882–1891, 2009.

[29] D. Chrenko, M.-C. Péra, and D. Hissel, "Fuel cell system modeling and control with energetic macroscopic representation," in *IEEE International Symposium on Industrial Electronics*, pp. 169–174, IEEE, 2007.

[30] H. M. Paynter, *Analysis and design of engineering systems*. MIT press, 1961.

[31] D. Karnopp, "Power-conserving transformations: physical interpretations and applications using bond graphs," *Journal of the Franklin Institute*, vol. 288, no. 3, pp. 175–201, 1969.

[32] W. Borutzky, *Bond graph methodology: development and analysis of multidisciplinary dynamic system models*. Springer Science & Business Media, 2009.

[33] W. Borutzky, *Bond graph modeling of engineering systems*, vol. 103. Springer, 2011.

[34] L. N. Khanh, J.-J. Seo, Y.-S. Kim, and D.-J. Won, "Power-management strategies for a grid-connected PV-FC hybrid system," *IEEE Transactions on Power Delivery*, vol. 25, no. 3, pp. 1874–1882, 2010.

[35] N. Bigdeli, "Optimal management of hybrid PV/fuel cell/battery power system: a comparison of optimal hybrid approaches," *Renewable and Sustainable Energy Reviews*, vol. 42, pp. 377–393, 2015.

[36] A. Yilanci, I. Dincer, and H. K. Ozturk, "A review on solar-hydrogen/fuel cell hybrid energy systems for stationary applications," *Progress in Energy and Combustion Science*, vol. 35, no. 3, pp. 231–244, 2009.

[37] D. Lu, T. Zhou, H. Fakham, and B. François, "Design of a power management system for an active PV station including various storage technologies," in 13^{th} *International Power Electronics and Motion Control Conference*, pp. 2142–2149, IEEE, 2008.

[38] P. Bajpai and V. Dash, "Hybrid renewable energy systems for power generation in stand-alone applications: A review," *Renewable and Sustainable Energy Reviews*, vol. 16, no. 5, pp. 2926–2939, 2012.

[39] S. Nasri, B. S. Sami, and A. Cherif, "Power management strategy for hybrid autonomous power system using hydrogen storage," *International Journal of Hydrogen Energy*, vol. 41, no. 2, pp. 857–865, 2016.

[40] L. M. Halabi, S. Mekhilef, L. Olatomiwa, and J. Hazelton, "Performance analysis of hybrid PV/diesel/battery system using HOMER: A case study Sabah, Malaysia," *Energy Conversion and Management*, vol. 144, pp. 322–339, 2017.

[41] Z. Jiang, "Power management of hybrid photovoltaic-fuel cell power systems," in *Power Engineering Society General Meeting*, pp. 6–pp, IEEE, 2006.

[42] S. Kong, M. Hilairet, and R. Roche, "Passivity-based control for a PV/Battery/Fuel Cell/Electrolyser Hybrid Power System," in *IEEE Milan PowerTech*, pp. 1–6, IEEE, 2019.

[43] T. Zhou, B. François, M. El Hadi Lebbal, and S. Lecoeuche, "Modeling and control design of hydrogen production process by using a causal ordering graph for wind energy conversion system," in *International Symposium on Industrial Electronics*, pp. 3192–3197, IEEE, 2007.

[44] T. Bakka and H. R. Karimi, "Bond graph modeling and simulation of wind turbine systems," *Journal of Mechanical Science and Technology*, vol. 27, no. 6, pp. 1843–1852, 2013.

[45] D. Mezghanni, R. Andoulsi, A. Mami, and G. Dauphin-Tanguy, "Bond graph modelling of a photovoltaic system feeding an induction motor-pump," *Simulation Modelling Practice and Theory*, vol. 15, no. 10, pp. 1224–1238, 2007.

[46] A. E. Badoud, M. Khemliche, B. Ould Bouamama, S. Bacha, and L. F. L. Villa, "Bond graph modeling and optimization of photovoltaic pumping system: Simulation and experimental results," *Simulation Modelling Practice and Theory*, vol. 36, pp. 84–103, 2013.

[47] R. Saisset, G. Fontes, C. Turpin, and S. Astier, "Bond graph model of a PEM fuel cell," *Journal of Power Sources*, vol. 156, no. 1, pp. 100–107, 2006.

[48] M. Bressel, M. Hilairet, D. Hissel, and B. Ould-Bouamama, "Dynamical modeling of proton exchange membrane fuel cell and parameters identification," in *6th International Conference on Fundamentals and Development of Fuel Cells (FDFC), Toulouse, France, Feb*, pp. 3–5, 2015.

[49] P. Olivier, C. Bourasseau, and B. Bouamama, "Dynamic and multiphysic PEM electrolysis system modelling: A bond graph approach," *International Journal of Hydrogen Energy*, vol. 42, no. 22, pp. 14872–14904, 2017.

[50] X. Roboam, S. Astier, H. Foch, G. Fontes, G. Gandanegara, H. Piquet, R. Saïsset, B. Sareni, and C. Turpin, *Graphes de liens causaux pour systèmes à énergie renouvelable (partie 1).* Editions Techniques Ingénieur, 2006.

[51] X. Roboam and S. Astier, *Graphes de liens causaux pour systèmes à énergie renouvelable (partie 2).* Editions Techniques Ingénieur, 2006.

[52] A. Van Der Schaft, *L2-gain and passivity techniques in nonlinear control.* Springer, 2017.

[53] A. Van Der Schaft and D. Jeltsema, "Port-Hamiltonian systems theory: An introductory overview," *Foundations and Trends in Systems and Control*, vol. 1, no. 2-3, pp. 173–378, 2014.

[54] O. Hamdous, *Mise en œuvre d'une commande par interconnexion basée sur la passivité.* PhD thesis, Université Mouloud Maameri de Tizi Ouzou, 2013.

[55] A. Van Der Schaft and B. Maschke, "Port-Hamiltonian systems on graphs," *SIAM Journal on Control and Optimization*, vol. 51, no. 2, pp. 906–937, 2013.

[56] G. Golo, A. Van Der Schaft, P. C. Breedveld, and B. M. Maschke, "Hamiltonian formulation of bond graphs," *Nonlinear and hybrid systems in automotive control*, pp. 351–372, 2003.

[57] T. H. Pham, I. Prodan, D. Genon-Catalot, and L. Lefevre, "Port-Hamiltonian model for DC-microgrid lift systems," *IFAC-PapersOnLine*, vol. 48, no. 13, pp. 117–122, 2015.

[58] A. Donaire and S. Junco, "Energy shaping, interconnection and damping assignment, and integral control in the bond graph domain," *Simulation Modelling Practice and Theory*, vol. 17, no. 1, pp. 152–174, 2009.

[59] J.-E. Strömberg, J. Top, and U. Söderman, "Variable causality in bond graphs caused by discrete effects," *CiteSeerX*, 1993.

[60] L. Umanand, "Switched junctions in bond graph for modelling power electronic systems," *Journal of the Indian Institute of Science*, vol. 80, no. 4, p. 327, 2013.

[61] A. C. Umarikar and L. Umanand, "Modelling of switching systems in bond graphs using the concept of switched power junctions," *Journal of the Franklin Institute*, vol. 342, no. 2, pp. 131–147, 2005.

[62] J. C. Willems, "Dissipative dynamical systems part I: General theory," *Archive for Rational Mechanics and Analysis*, vol. 45, no. 5, pp. 321–351, 1972.

[63] R. Sepulchre, M. Jankovic, and P. V. Kokotovic, *Constructive nonlinear control*. Springer Science & Business Media, 2012.

[64] C. I. Byrnes, A. Isidori, and J. C. Willems, "Passivity, feedback equivalence, and the global stabilization of minimum phase nonlinear systems," *IEEE Transactions on Automatic Control*, vol. 36, no. 11, pp. 1228–1240, 1991.

[65] S. Boyd, L. El Ghaoui, E. Feron, and V. Balakrishnan, *Linear matrix inequalities in system and control theory*. SIAM, 1994.

[66] R. Ortega, A. Van Der Schaft, B. Maschke, and G. Escobar, "Interconnection and damping assignment passivity-based control of port-controlled Hamiltonian systems," *Automatica*, vol. 38, no. 4, pp. 585–596, 2002.

[67] S. H. Chaabna and J.-Y. Dieulot, "Bond Graph Modeling and Energetic Control of a PEM Electrolyzer," 13^{th} *International Conference on Bond Graph Modeling (ICBGM), Bordeaux, France*, 2018.

[68] I. Shchur, A. Rusek, and Y. Biletskyi, "Energy-shaping optimal load control of PMSG in a stand-alone wind turbine as a port-controlled Hamiltonian system," *Przegląd Elektrotechniczny (Electrical review)*, vol. 5, pp. 50–55, 2014.

[69] C. Batlle and A. Doria-Cerezo, "Energy-based modelling and simulation of the interconnection of a back-to-back converter and a doubly-fed induction machine," in *American Control Conference*, IEEE, 2006.

[70] M. Hilairet, O. Bethoux, T. Azib, and R. Talj, "Interconnection and damping assignment passivity-based control of a fuel cell system," in *International Symposium on Industrial Electronics*, pp. 219–224, IEEE, 2010.

[71] C. Colson and M. Nehrir, "A review of challenges to real-time power management of microgrids," in *Power & Energy Society General Meeting*, pp. 1–8, IEEE, 2009.

[72] A. Ghazanfari, M. Hamzeh, H. Mokhtari, and H. Karimi, "Active power management of multihybrid fuel cell/super-capacitor power conversion system in a medium voltage microgrid," *IEEE Transactions on Smart Grid*, vol. 3, no. 4, pp. 1903–1910, 2012.

[73] A. Etxeberria, I. Vechiu, H. Camblong, and J.-M. Vinassa, "Hybrid energy storage systems for renewable energy sources integration in microgrids: A review," in *Conference Proceedings IPEC*, pp. 532–537, IEEE, 2010.

[74] R. H. Lasseter, "Microgrids and distributed generation," *Journal of Energy Engineering*, vol. 133, no. 3, pp. 144–149, 2007.

[75] V. Prema and K. U. Rao, "Predictive models for power management of a hybrid microgrid—A review," in *International Conference on Advances in Energy Conversion Technologies (ICAECT)*, pp. 7–12, IEEE, 2014.

[76] C. Sandoval, V. M. Alvarado, J.-C. Carmona, G. L. Lopez, and J. Gomez-Aguilar, "Energy management control strategy to improve the FC/SC dynamic behavior on hybrid electric vehicles: A frequency based distribution," *Renewable Energy*, vol. 105, pp. 407–418, 2017.

[77] S. H. Chaabna and J.-Y. Dieulot, "Port-Hamiltonian Formulation of the Bond Graph model of a Hybrid Renewable Energy System," 13^{th} *International Conference on Bond Graph Modeling (ICBGM), Bordeaux, France*, 2018.

[78] M.-C. Pera, D. Hissel, H. Gualous, and C. Turpin, *Electrochemical components*. John Wiley & Sons, 2013.

[79] H. Zhang, S. Su, G. Lin, and J. Chen, "Efficiency calculation and configuration design of a PEM electrolyzer system for hydrogen production," *International Journal of Electrochemical Science*, vol. 7, no. 4, pp. 4143–4157, 2012.

[80] S. Rabih, *Contribution à la modélisation de systèmes réversibles de types électrolyseur et pile à hydrogène en vue de leur couplage aux générateurs photovoltaïques*. PhD thesis, INPT, 2008.

[81] O. Rallieres, *Modélisation et caractérisation de piles à combustible et électrolyseurs PEM*. PhD thesis, Institut National Polytechnique de Toulouse-INPT, 2011.

[82] T. Zhou, *Commande et supervision energétique d'un générateur hybride actif eolien incluant du stockage sous forme d'hydrogène et des supercondensateurs pour l'Intégration dans le Système electrique d'un micro réseau*. PhD thesis, Ecole Centrale de Lille, 2009.

[83] K. Agbli, D. Hissel, M.-C. Péra, and I. Doumbia, "EMR modelling of a hydrogen-based electrical energy storage," *The European Physical Journal Applied Physics*, vol. 54, no. 2, p. 23404, 2011.

[84] T. Yigit and O. F. Selamet, "Mathematical modeling and dynamic Simulink simulation of high-pressure PEM electrolyzer system," *International Journal of Hydrogen Energy*, vol. 41, no. 32, pp. 13901–13914, 2016.

[85] A. Awasthi, K. Scott, and S. Basu, "Dynamic modeling and simulation of a proton exchange membrane electrolyzer for hydrogen production," *International Journal of Hydrogen Energy*, vol. 36, no. 22, pp. 14779–14786, 2011.

[86] S. Busquet, C.-E. Hubert, J. Labbe, D. Mayer, and R. Metkemeijer, "A new approach to empirical electrical modelling of a fuel cell, an electrolyser or a regenerative fuel cell," *Journal of Power Sources*, vol. 134, no. 1, pp. 41–48, 2004.

[87] M. Khan and M. Iqbal, "Dynamic modeling and simulation of a small wind-fuel cell hybrid energy system," *Renewable Energy*, vol. 30, no. 3, pp. 421–439, 2005.

[88] O. Ulleberg, "Modeling of advanced alkaline electrolyzers: a system simulation approach," *International Journal of Hydrogen Energy*, vol. 28, no. 1, pp. 21–33, 2003.

[89] H. Görgün, "Dynamic modelling of a proton exchange membrane (PEM) electrolyzer," *International Journal of Hydrogen Energy*, vol. 31, no. 1, pp. 29–38, 2006.

[90] B. Lee, K. Park, and H.-M. Kim, "Dynamic simulation of PEM water electrolysis and comparison with experiments," *International Journal of Electrochemical Science*, vol. 8, no. 1, pp. 235–248, 2013.

[91] R. García-Valverde, N. Espinosa, and A. Urbina, "Simple pem water electrolyser model and experimental validation," *International Journal of Hydrogen Energy*, vol. 37, no. 2, pp. 1927–1938, 2012.

[92] Heliocentris, *MHS – Metal Hydride Storage Canisters*. https://www.heliocentris.com, 2016.

[93] F. Gonzatti and F. Farret, "Mathematical and experimental basis to model energy storage systems composed of electrolyzer, metal hydrides and fuel cells," *Energy Conversion and Management*, vol. 132, pp. 241–250, 2017.

[94] G. Lucas and W. Richards, "Mathematical modelling of hydrogen storage systems," *International Journal of Hydrogen Energy*, vol. 9, no. 3, pp. 225–231, 1984.

[95] S. Mohammadshahi, Shahrzad, E. M. Gray, and C. J. Webb, "A review of mathematical modelling of metal-hydride systems for hydrogen storage applications," *International Journal of Hydrogen Energy*, vol. 41, no. 5, pp. 3470–3484, 2016.

[96] S. Mohammadshahi, Shahrzad, T. Gould, E. M. Gray, and C. J. Webb, "An improved model for metal-hydrogen storage tanks-Part 1: Model development," *International Journal of Hydrogen Energy*, vol. 41, no. 5, pp. 3537–3550, 2016.

[97] U. Mayer, M. Groll, and W. Supper, "Heat and mass transfer in metal hydride reaction beds: experimental and theoretical results," *Journal of the Less Common Metals*, vol. 131, no. 1-2, pp. 235–244, 1987.

[98] I. El Osery, "Theory of the computer code RET 1 for the calculation of space-time dependent temperature and composition properties of metal hydride hydrogen storage beds," *International Journal of Hydrogen Energy*, vol. 8, no. 3, pp. 191–198, 1983.

[99] D.-W. Sun and S.-J. Deng, "Study of the heat and mass transfer characteristics of metal hydride beds," *Journal of the Less-common Metals*, vol. 141, no. 1, pp. 37–43, 1988.

[100] B. J. Hardy and D. L. Anton, "Hierarchical methodology for modeling hydrogen storage systems. part II: Detailed models," *International Journal of Hydrogen Energy*, vol. 34, no. 7, pp. 2992–3004, 2009.

[101] H. Choi and A. Mills, "Heat and mass transfer in metal hydride beds for heat pump applications," *International Journal of Heat and Mass Transfer*, vol. 33, no. 6, pp. 1281–1288, 1990.

[102] A. Jemni, S. B. Nasrallah, and J. Lamloumi, "Experimental and theoretical study of a metal-hydrogen reactor," *International Journal of Hydrogen Energy*, vol. 24, no. 7, pp. 631–644, 1999.

[103] A. Jemni and S. B. Nasrallah, "Study of two-dimensional heat and mass transfer during absorption in a metal-hydrogen reactor," *International Journal of Hydrogen Energy*, vol. 20, no. 1, pp. 43–52, 1995.

[104] S. B. Nasrallah and A. Jemni, "Heat and mass transfer models in metal-hydrogen reactor," *International Journal of Hydrogen Energy*, vol. 22, no. 1, pp. 67–76, 1997.

[105] B. Sakintuna, F. Lamari-Darkrim, and M. Hirscher, "Metal hydride materials for solid hydrogen storage: a review," *International Journal of Hydrogen Energy*, 2007.

[106] D. Rekioua and E. Matagne, *Optimization of photovoltaic power systems: modelization, simulation and control*. Springer Science & Business Media, 2012.

[107] N. Derbel and Q. Zhu, *Modeling, Identification and Control Methods in Renewable Energy Systems*. Springer, 2018.

[108] O. C. Onar, M. Uzunoglu, and M. S. Alam, "Modeling, control and simulation of an autonomous wind turbine/photovoltaic/fuel cell/ultra-capacitor hybrid power system," *Journal of Power Sources*, vol. 185, no. 2, pp. 1273–1283, 2008.

[109] K. C. Kong, M. Z. Ibrahim, and A. M. Muzathik, "New approach on mathematical modeling of photovoltaic solar panel," *Applied Mathematical Sciences*, vol. 6, no. 8, pp. 381–401, 2012.

[110] R. Perez, "Lead-acid battery state of charge vs. voltage," *Home Power*, vol. 36, pp. 66–69, 1993.

[111] V. Ramirez, R. Ortega, O. Bethoux, and A. Sánchez-Squella, "A dynamic router for microgrid applications: Theory and experimental results," *Control Engineering Practice*, vol. 27, pp. 23–31, 2014.

[112] F. Ferraguti, N. Preda, A. Manurung, M. Bonfe, O. Lambercy, R. Gassert, R. Muradore, P. Fiorini, and C. Secchi, "An energy tank-based interactive control architecture for autonomous and tele-operated robotic surgery," *IEEE Transactions on Robotics*, vol. 31, no. 5, pp. 1073–1088, 2015.

[113] G. Raiola, C. A. Cardenas, T. S. Tadele, T. De Vries, and S. Stramigioli, "Development of a Safety-and Energy-Aware Impedance Controller for Collaborative Robots," *IEEE Robotics and Automation Letters*, vol. 3, no. 2, pp. 1237–1244, 2018.

[114] M. Franken, S. Stramigioli, S. Misra, C. Secchi, and A. Macchelli, "Bilateral tele-manipulation with time delays: A two-layer approach combining passivity and transparency," *IEEE Transactions on Robotics*, vol. 27, no. 4, pp. 741–756, 2011.

[115] P. Robuffo Giordano, A. Franchi, C. Secchi, and H. H. Bülthoff, "A passivity-based decentralized strategy for generalized connectivity maintenance," *The International Journal of Robotics Research*, vol. 32, no. 3, pp. 299–323, 2013.

[116] C. A. Cardenas, "Development of a safety-aware intrinsically passive controller for a multi-DOF manipulator," Master's thesis, University of Twente, 2017.

[117] A. K. Samantaray, K. Medjaher, B. Ould Bouamama, M. Staroswiecki, and G. Dauphin-Tanguy, "Diagnostic bond graphs for online fault detection and isolation," *Simulation Modelling Practice and Theory*, vol. 14, no. 3, pp. 237–262, 2006.